1-1-2021

A VALENCE-BOND OPERATOR ALGEBRA FOR QUANTUM SPIN MODELS AND ITS APPLICATIONS

HUU TRAN DO
University of Mississippi

A VALENCE-BOND OPERATOR ALGEBRA FOR QUANTUM SPIN MODELS AND ITS APPLICATIONS

A Dissertation
presented in partial fulfillment of requirements
for the degree of Doctor of Philosophy
in the Department of Physics and Astronomy,
The University of Mississippi

by

HUU T. DO

August 2021

ABSTRACT

The Heisenberg Hamiltonian is the prototype model for quantum magnetism. The Hamiltonian includes exchange couplings between vector spins, which are the intrinsic magnetic moments of localized electrons. The classical energy between any pair of interacting spins can be minimized by aligning them parallel (ferromagnetic case) or antiparallel (antiferromagnetic), depending on the sign of the coupling. But quantum fluctuations play a key role, and a full quantum mechanical treatment of the many-body system is generally required. Finding the exact ground-state energy and wave function of isotropic antiferromagnetic (AFM) systems for an arbitrary spin-S and lattice morphology is still a challenging and hotly debated topic. A questions arises: Which is the best quantum representation (fermion, boson, or other) in which to describe the spin model when the charge component of an electron is quenched at the atomic limit? For example, physicists often formulate a half-odd spin chain in the fermionic basis; while the integer spin chain is more typically treated with bosonic auxiliary particles. In my dissertation, I propose a bond-operator algebra for entangled spin pairs which are constructed using hard-core bosons as a book-keeping trick. I show how this bond operator formalism can be used to express the Hamiltonians for generic quantum spin systems, but especially Affleck, Kennedy, Lieb, and Tasaki (AKLT) and AKLT-like models. The AKLT class of models is an extension of the AFM Heisenberg paradigm, with localized quantum spins on a lattice directly coupled to their neighbors on adjacent sites. While the ground-state energy and wave function of most AFM Heisenberg Hamiltonians are unknown, they are known explicitly in the fixed-point AKLT Hamiltonian for the standard cases of the spin-1 chain, spin-3/2 honeycomb lattice, and spin-2 in a chain and square lattice. We confirm that our bond-operator approach reproduces the original results of Affleck *et al*. [Phys. Rev. Lett. **59**, 799, 1987]. Furthermore, we use the bond operator framework to construct an "update projector" which is the main

ingredient for valence-bond quantum Monte Carlo sampling. We derive a valence-bond "coherent state" as a superposition of bond creation operators and show that its energy expectation value can be evaluated exactly for a broad class of quantum antiferromagnets.

LIST OF ABBREVIATIONS AND SYMBOLS

AFM	antiferromagnetic state
AKLT	Affleck–Kennedy–Lieb–Tasaki
BCS	Bardeen–Cooper–Schrieffer
BZ	Brillouin zone
FM	ferromagnetic state
FT	Fourier transform
FQHE	fractional quantum Hall effect
HDD	hard disk drive
PM	paramagnetic state
QCP	quantum critical phase transition
QPT	quantum phase transition
QSL	quantum spin liquid
RVB	resonating valence bond
SBMFT	Schwinger boson mean field theory
SPT	symmetry-protected topological phase
VBS	valence-bond solid
1D	one dimension
2D	two dimension
M	magnetization
B	magnetic field
$\sigma^{x,y,z}$	Pauli spin matrices
χ_{m}	magnetic susceptibility

T_c	critical temperature
T_C	Curie temperature
T_N	Néel temperature

ACKNOWLEDGEMENTS

As long as I have been working at The University of Mississippi, I take this golden chance to acknowledge my advisor, our department, committee members, colleagues and my family.

I greatly appreciate my supervisor, Dr. Kevin S. D. Beach who has faithfully guided to do research on one of the most exciting but very challenging topics in condensed matter physics. Working in many quantum spin models shows me a zoo of interesting knowledge in quantum mechanics but hard-achievable problems in the quantum many-body physics. Although I have failed a thousand times to get the correct paths, through helpful discussions and dedicating guidances with Dr. Beach, I have overcome and improved my problem-solving skill. Therefore, several horizons in quantum physics have opened for me to explore in the future. He has also helped me unlimited times during my work at the department.

Let me say many thanks to my committee members, Dr. Leo Stein, Dr. Samuel Lisi and Dr. Breese Quinn. They took their precious time to read my dissertation and gave many useful comments. Furthermore, they challenged me in a lot of interesting questions which are different point of views about my work. Without their dedicated comments and corrections, my story would be incomplete. I also appreciate Mr. Thomas and Dr. Cremaldi for their help in my TA work, and Dr. Sanders for research discussions.

I would like to thank Department of Physics and Astronomy, University of Mississippi for generous support to me to do research for the whole time. I would say thank to the Graduate School and Graduate Student Council for providing me a student research grant 2019–2020.

Last but not least, I am indebted to my family, my daughter and wife. Without their support, I would not have remained motivated to complete this work.

TABLE OF CONTENTS

LIST OF FIGURES

LIST OF TABLES

CHAPTER 1

GENERAL INTRODUCTION TO QUANTUM MAGNETISM AND SPIN MODELS

1.1 Overview of quantum magnetism

Investigating the properties and behaviors of electrons in materials has been an important focus of condensed matter physics. A lone electron in free space has well-defined values of charge ($e = -1.62\times10^{-19}$ C), intrinsic angular momentum ($\hbar/2$), and mass ($m_e = 9.11\times10^{-31}$ kg), but in a material environment the effective low-energy excitations can be quasiparticles with renormalized values for these quantities — or the various degrees of freedom can decouple completely (e.g. spin-charge separation).

Electrons behave very differently in the presence of a crystalline background (a periodic arrangement of ions) and in mutual interaction with other electrons. Consequently, the electric, thermal, and magnetic properties of materials may vary widely. For example, if we consider a system of noninteracting electrons (or one in which electron-electron interactions are weak), the presence of the background lattice transforms the carriers into band electrons. The *band theory* is like a "standard model" in condensed matter physics. This allows us to categorize materials into *conductors*, in which an electric current is carried by low-lying current-carrying excitations, and *insulators*, where the current motion is prevented by a band gap (and electrons are localized on individual atoms) [1, 2]. However, many other strange behaviors are possible when interactions are significant, e.g. Mott insulators where conventional band theory would have predicted conducting behavior [3]. Stranger still, in correlated electron systems, the charge component of an electron can be paired to result in a doubly-charged particle (the Cooper pair with $q_C = 2e$) in superconductors or "fractionalize" into quasiparticles with only a fraction of the electron charge ($q_f = e/3$), as in the fractional quantum Hall effect (FQHE) [2, 4].

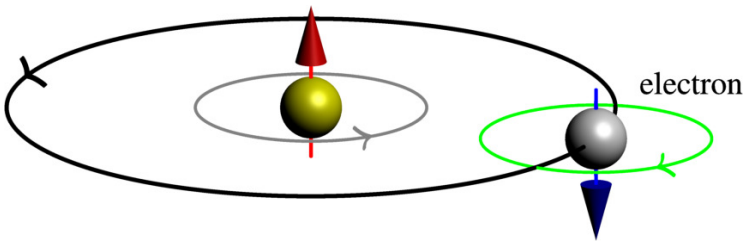

Figure 1.1: Schematic visualization of the spin and orbital of an electron in a hydrogen atom, and up and down arrows represent spin-up and spin-down of its electron and proton, respectively.

Spin, or intrinsic angular momentum, is an especially interesting property of the electron. From the classical point of view, the spin component of an electron is analogous to the Earth rotating around its axis. It is an intrinsic quantum property of an electron and a *vector quantity* (or recent definition: a two-vector quantity), denoted by **S**. The z-component of a spin-half particle is given by $S_z = m_s\hbar$ with $m_s = \pm 1/2$. The projection of **S** onto the z-axis is quantized: "spin-up" with an eigenvalue $m_s = +1/2$ and "spin-down" with an eigenvalue $m_s = -1/2$ [5]. For example, in the ground state of the hydrogen atom, the magnetic moments of the proton and electron are oppositely directed (Fig. 1.1).

The spin degree of freedom is extremely important in both physics and chemistry. First, it is one of the fundamental quantum numbers (n, ℓ, m_ℓ and m_s) that determine how we arrange the chemical elements in the periodic table. For example, hydrogen and helium are in the first row because they are filled in the 1s orbital with one and two electrons, respectively. Electrons are fermionic particles, so we cannot put two identical particles in the same quantum state because of the Pauli exclusion principle and Fermi-Dirac statistics. However, in a helium atom or hydrogen molecule we can put two electrons in the same orbital by populating with two different spin states. So, when we properly account for the spin component, the exclusion principle is effectively softened, allowing us to place more than one fermionic particle per orbital. Multiple spin-half objects can combine to produce large, composite moments; and conversely large spin S objects can be decomposed into $2S$ spin half particles, which is the idea at the heart of the formalism detailed in this dissertation.

Spin is the key parameter to determine the *magnetic properties* of materials. In experiments,

we measure the effective magnetic moment of elements or ions rather than the spin value, with formula $\mu_{\text{eff}} = n_{\text{eff}}\mu_B$ [6]. Here, the spin-only formula is defined as $n_{\text{eff}} = g\sqrt{S(S+1)}$; where $g \approx 2$ is the spectroscopic splitting factor, or g-factor, and S is the magnitude of a spin $\mathbf{S}$. $\mu_B = \frac{e\hbar}{2m_e}$ is the Bohr magneton. In that way, we can determine the actual value of spin (1/2, 1, 3/2, etc) in materials. For example, the very large magnetic moment of Ho^{3+} in a spin-ice compound $Ho_2Ti_2O_3$ is about $\mu_{\text{eff}} = 10\mu_{\text{B}}$ [7]. Here, the spin value $\mathbf{S}$ in the above spin-only-formula is replaced by the total angular momentum $\mathbf{J} = \mathbf{L} + \mathbf{S}$ ($\mathbf{L}$: orbital angular momentum). More details are referred to Appendix A.

1.2 Introduction to quantum spin liquid

Similar to how scientists categorize ordinary phases of matter as gas, liquid, and solid, we often classify magnetic materials into three types.

First, a **spin gas** describes the random orientation of spin magnetic moments inside materials. These materials show very weak response (with positive or negative sign) of the magnetization $\mathbf{M}$ even to high applied magnetic field. For example, the paramagnetic (PM) state offers a weak, positive response in many open-shelled simple metals, such as alkaline elements (e.g. Li, Na and K) or magnetic materials at high temperature [Fig. 1.2(a)]. They are also characterized by the inverse susceptibility going to zero value (top panel in Fig. 1.3). Diamagnetic state is the weakest effect and respond negative in an applied magnetic field. This state is shown in some closed-shell atoms, such as He, Ar and superconducting materials below the critical value T_{c} [6].

When we consider the magnetic properties of materials, we usually think about the **spin solid state**, such as ferromagnetic (FM: means a magnet containing iron) and long-range antiferromagnetic (AFM) orders, e.g. Néel state. In these kinds of materials, the vector spins are arranged in a definite pattern [Fig. 1.2(b)]. In these systems, the magnetic moments of neighboring atoms may mutually align each other in some directions because the interaction between magnetic moments — the quantum mechanical exchange — is sufficiently strong on the scale of thermal energies. For example, in a system with FM order, all spins point predominantly in the same direction (z-axis

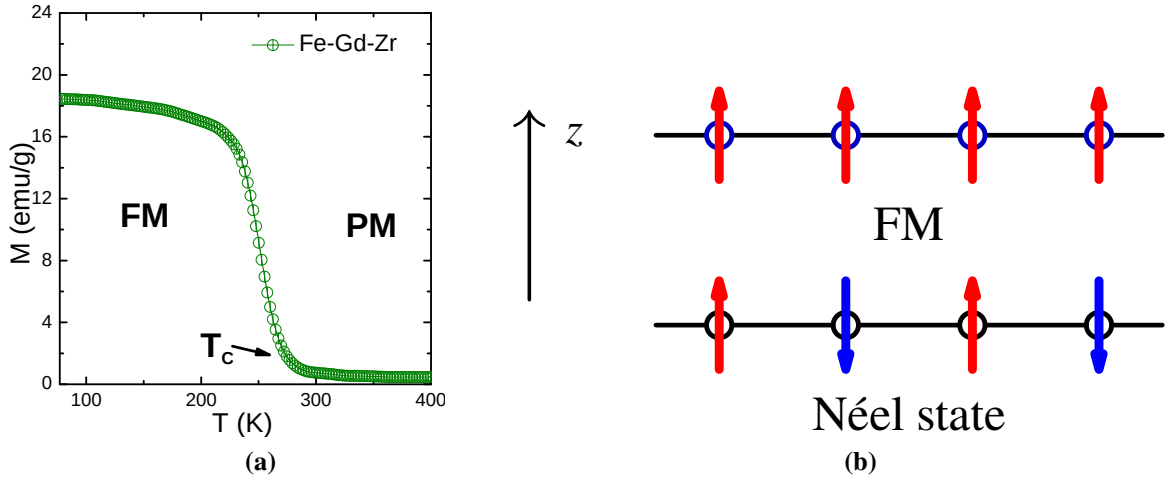

Figure 1.2: (a) Phase transition between FM and PM phase in a Fe-Gd-Zr compound is detected by a thermomagnetization measurement with the applied magnetic field **B** = 100 Oe (1 Oe = 10^{-4} T). (b) Visualization of spin-half FM and Néel states (long-range AFM) in a chain.

in Fig. 1.5). A net-spontaneous magnetization (M) is generated and these materials exhibit strong magnetic properties even without an applied magnetic field. The magnetization in FM materials serves as a *local order parameter* which is used to detect a phase transition between an ordered FM state and a disordered state (PM). On the temperature axis, the two phases are separated by the Curie temperature T_C [Fig. 1.2(a)], and the behavior at the critical point follows *Landau-Ginzburg phase transition theory*, a cornerstone theory in condensed matter and statistical mechanics. There are many popular ferromagnetic elements, such as Fe, Co, Gd and their intermetallic compounds (e.g. Nd-Fe-B hard magnet used in electric rotors, hybrid cars; Fe-Pt compound in fabricating hard disk drives (HDD) for data storage in a computer). As shown in [Fig. 1.2(a)], with a small magnetic field $H = 10^{-2}$ T applied to a Fe-Gd-Zr compound, the magnetization value M in the FM phase is many times larger than in the PM phase.

The classical AFM state was first proposed by L. Néel in 1932. It exhibits an alternating alignment of localized magnetic moments with *zero* net magnetization [2]. This is simply because half the magnetic moments point in one direction and the other half point in the opposite direction [Fig. 1.2(b)]. But the spin-rotation symmetry of the system in broken because the ordering picks out a preferred direction in spin space. There are plenty of elements and compounds that exhibit

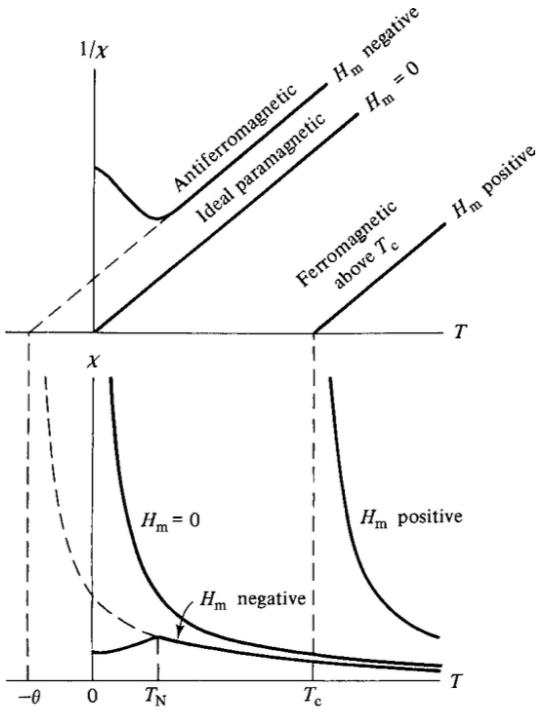

Figure 1.3: Magnetic susceptibility and inverse susceptibility for FM, PM and AFM (Néel) materials.

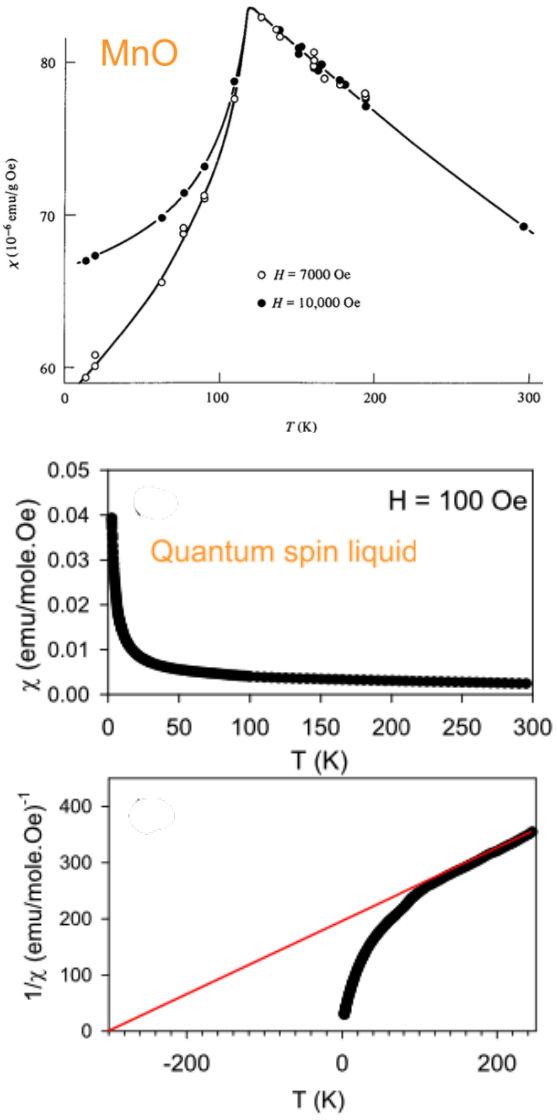

Figure 1.4: Magnetic susceptibility of the Néel state in MnO (above) [6] and a QSL state in $ZnCu_3(OH)_6Cl_2$ compound – a kagome lattice [8]. The susceptibility χ of the Néel order shows a cusp, which is a sign of a phase transition (top figure); while the χ of the QSL is a smooth curve like a PM state in Fig. 1.3 (middle graph). However, the inverse susceptibility of QSL looks like a Néel state (bottom plot).

Néel order, including Cr, Mn, FeO, and MnO. Because of the weak response to an apply magnetic field, the susceptibility is a good measurement to detect the Néel order. The susceptibility of that state is shown in Fig. 1.3 (label "antiferromangetic" plot) with a cusp at the Néel temperature T_N, which is comparable to the Curie temperature in the FM case. Physicists initially thought these materials were PM, but it was found that the inverse susceptibility (top panel in Fig. 1.3) cuts the temperature axis at some negative points θ, compared with positive and zero point for FM and PM cases, respectively. According to the Curie-Weiss theorem [6], this is an evidence of a strong interaction between spins. Ideally, the $-\theta$ is equal to the T_N. More advanced measurements, e.g. neutron diffraction, eventually directly confirmed the existence of the staggered spin order [2, 6].

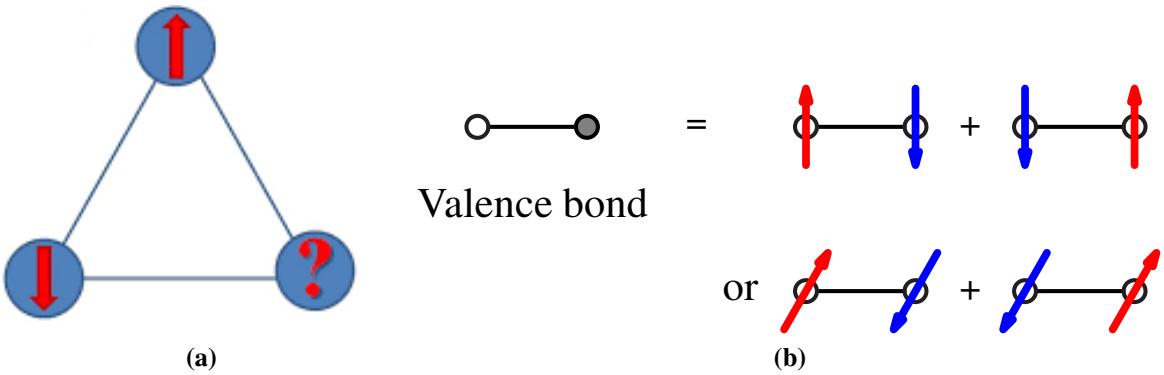

Figure 1.5: (a) Three Ising spins are interacted antiferromagnetically on the vertices of a triangular lattice. (b) The valence bond

However, the newest and most unusual form of spin system is a **quantum spin liquid** (QSL). It is defined as a "quantum disordered state" (like an ordinary liquid), and it remains in that state even down to the lowest temperatures because of strong quantum fluctuations and high entanglement between spins. The QSL is a key motivation for the formalism developed in this dissertation. Philip W. Anderson first proposed this kind of state in 1973 as a possible ground state of the "frustrated" spin-half AFM system on a triangle lattice [9, 10]. On every triangular plaquet, three spins are arranged on the three vertices [Fig. 1.5(a)]. If they couple antiferromagnetically, the first spin can be pointed upward (arbitrarily), the second spin can be pointed downward (to satisfy the Heisenberg interaction preference), but the direction of third spin cannot be determined to obtain a unique lowest-energy configuration [9, 10]. So classical Néel order fails in this situation,

and the true behavior is governed entirely by the quantum fluctuations. Anderson proposed a new ground state consisting of the superposition of singlet bonds or *valence-bond state* [i.e. short-range AFM coupling illustrated in Fig. 1.5(a)]. It was the first proposal for a QSL.

The QSL is significant for both fundamental research and practical applications, e.g. topological phase transition (transition without any symmetry breaking or local order parameter detection) [11–14], understanding the superconducting mechanism of high-T_c cuprate (considered as a hole-doped QSL) [15–18] or recently topological computation (capacity to protect quantum information from decoherence) [19]. This interesting quantum liquid state is long-sought but hotly debated because it is very hard to detect in real materials. However, there have been credible reports of possible QSL candidates, such as κ-$(ET)_2Cu_2(CN)_3$ (an organic solid), $ZnCu_3(OH)_6Cl_2$ (kagomé lattice) and $Na_4Ir_3O_8$ (3D hyperkagome lattice) [10, 16].

In experiments, physicists have tried to construct different measurements to characterize the differences between long-range AFM and QSL in materials. These include magnetic susceptibility, nuclear magnetic resonance, Raman scattering, and inelastic neutron scattering [8, 20]. In Figs 1.3 and 1.4, we show the susceptibility of $ZnCu_3(OH)_6Cl_2$ (a QSL material), which was provisionally termed a quantum PM state, because there was no any sign of a phase transition. However, the inverse susceptibility is similar to the AFM case rather than the PM case (lower part of Fig. 1.4). Moreover, no phase transition is detected from heat capacity measurements, even though the AFM coupling between the spin-1/2 Cu^{2+} ions arranged on the kagomé lattice [16, 20] are estimated to be very strong.

An exact theoretical construction for the QSL states remains ellusive. In the one dimensional (1D) case, the strong quantum fluctuation destroys the long-range order which easily shows QSL, but in dimension $d > 1$, it is difficult to stabilize because a long-range AFM often intervenes. The canonical models for demonstrating QSL states are extensions of the Heisenberg model, such as the Affleck–Kennedy–Lieb–Tasaki (AKLT) model, or the Kitaev model. The properties of the AFM Heisenberg model depend sensitively on the morphology of lattices, so we can separate into two kinds: bipartite lattices (e.g. 1D chain, square and hexagonal lattice) and frustrated lattices such

as triangular, kagome (2D), and tetragonal (3D) lattices. The main approaches for solving AFM models are (i) approximate methods which are based on mean-field theory, large-N, or large-S calculations [18, 21–27] and (ii) computational approaches such as quantum Monte Carlo [16] and density matrix renormalization group (DMRG) [28]. For each calculation, there are some advantages and limitations, which are stated in detail below.

For analytic calculations, one technique is to solve the spin model by proposing a Néel ordered ground state, then adding quantum fluctuations around that reference point. This is essentially a semiclassical approximation to the Feynman path integral. This method only works for systems with dimension $d > 1$ on a bipartite lattice and where an ordered ground state can be established, e.g. a spin-half square lattice. It is similar to the magnon approximation, which is a method to characterize the excited states in a FM system [27, 29]. However, this method fails on highly frustrated lattices or in 1D.

Another popular approach is to reformulate the spin model into a problem of interacting fermions or bosons, construct the partition functions, and then apply a mean-field approach around a saddle point via the Hubbard-Stratonovich transformation [18, 21–23, 30]. Unfortunately, this method artificially enlarges the Hilbert space of the system, and unphysical states must be projected out. Since this is hard to carry out, the solution is simply restricted using an additional mean-field, Lagrange-multiplier-like constraint. The bosonic approach (Schwinger bosons) works well enough for bipartite lattices with $d > 1$. For the fermionic formalism, Liu and coworkers [30] have shown how to treat cases up to spin-2. However, they needed to construct very complicated, idiosyncratic tensors case-by-case, and they are not able to obtain a general representation for a spin-S and higher powers of the Heisenberg term. It is harder to obtain AFM order within the fermionic approach, but it appears to be useful for the frustrated-lattice cases [31]. A question that we consider in later chapters is how to construct a general basis for spin-S models that is in 1–1 correspondence with the true Hilbert space (i.e. no artificial Hilbert space enlargement and no artificially introduced bosonic or fermionic statistics).

Currently, investigating properties of quantum spin models relies heavily on computational

approaches. For very small spin size, we can use exact diagonalization to find the energy for spin systems because the size of the matrix increased as 2^N, where N is the number of spins. For large systems, the growing resource requirements demand other approaches. For example, quantum Monte Carlo simulation works well in bipartite lattices but not in frustrated lattices because of suffering a famous "sign problem" [16, 32]. DMRG is very good in 1D cases but is less reliable in higher dimension [28]. For 2D examples, they need to twist the boundary conditions similar to the 1D situation. Our goal is to construct a fundamental language to described spin systems and to introduce operators for spins that are analogous to the second quantization operators for the Fock basis of bosons and fermions.

1.3 Heitler-London theory and the Heisenberg model for magnetic insulators

In some interacting systems, we can even interpret their physical properties without considering the intrinsic spin component of an electron (e.g. Fermi liquid and FQHE [4]). However, in many cases, spin properties exhibit strongly, particularly in explaining the strong magnetic properties of transition metals – d-orbital electron systems, rare-earth elements – f-orbital electron metals and their compounds. We cannot understand them by the "band theory". A new theory needs to explain the strong correlation phenomenon in partly filled orbitals called atomic or Heitler-London picture[33]. This theory is so important to interpret the chemical molecules by the orbital wave functions.

In real materials, there are three general microscopic mechanisms about the magnetic formation: *direct exchange*, *indirect exchange* and *superexchange*. The *direct exchange* is the coupling between two spins on the nearest-neighbor atoms of which their wave functions are overlapped strong enough to result in an exchange energy between two magnetic moments. This is the main theme of our work which we will carefully address in the next sections. When two atoms are far apart and the system contains available free electrons, two localized spins interact via itinerant electrons. This is the *indirect exchange*. It is the typical interaction in intermetallic compounds of Mn, and rare-earth elements in which their atomic radii are too large for overlapping

wave function. Third, when two atoms are far apart, and there are no mobile electrons available, they can interact indirectly via other ions, usually non-metallic elements (e. g: MnO, MnF_2). We call that the *superexchange* interaction. [2].

We will focus on the *direct exchange* which forms the Heisenberg model. The derivation of the Heisenberg model starts with the Heitler-London approximation for a simple hydrogen molecule (applicable for ordinary insulating systems) or the Hubbard model with a limit of $U/t \gg 1$ (i.e. strongly correlated interaction or atomic limit) for the Mott insulators. Here, I show in detail the Heitler-London calculation.

Heitler-London theory: Following the discussion of Chapter 32, "*Solid State Physics*", by Ashcroft and Mermin [1], we illustrate how the Pauli exclusion principle results in magnetic effects even though there is no any spin-dependent term in the Hamiltonian by simply considering a two-electron system with a *spin-independent* Hamiltonian [like the hydrogen molecule in Fig. 1.6(a)]. Because $\hat{H}$ does not depend on spin, the general stationary state ψ will be the product of a purely orbital stationary state whose wave function $\psi(\mathbf{r}_1, \mathbf{r}_2)$ satisfies the orbital Schrödinger equation,

$$\hat{H}\psi = \big[-(\nabla_1^2 + \nabla_2^2) + V(\mathbf{r}_1, \mathbf{r}_2)\big]\psi(\mathbf{r}_1, \mathbf{r}_2) = E\psi(\mathbf{r}_1, \mathbf{r}_2), \tag{1.1}$$

with any linear combination of the four spin states: $|\uparrow\uparrow\rangle$, $|\uparrow\downarrow\rangle$, $|\downarrow\uparrow\rangle$, $|\downarrow\downarrow\rangle$. Here, these symbols denote spin states with both electrons in levels of definite s_z. In the state $|\uparrow\downarrow\rangle$, for example, the electron 1 has the spin value $s_z = 1/2$, and the electron 2 with $s_z = -1/2$. We can choose these linear combinations to have definite values of the total spin S, and its component S_z along an axis. We have in total four linear combinations of spin states: spin $S = 0$ (singlet state) $|S = 0, S_z = 0\rangle = \frac{1}{\sqrt{2}}\big(|\uparrow\downarrow\rangle - |\downarrow\uparrow\rangle\big)$ and three spin-1 states (triplet states) with same eigenenergy $|S = 1, S_z = 1\rangle = |\uparrow\uparrow\rangle$, $|S = 1, S_z = 0\rangle = \frac{1}{\sqrt{2}}\big(|\uparrow\downarrow\rangle + |\downarrow\uparrow\rangle\big)$, and $|S = 1, S_z = -1\rangle = |\downarrow\downarrow\rangle$. The singlet changes its sign when the positions of two electrons are interchanged, whereas the triplet states ($S = 1$) remain unchanged during that action.

Because an electron is a fermionic particle, the Pauli exclusion principle requires that

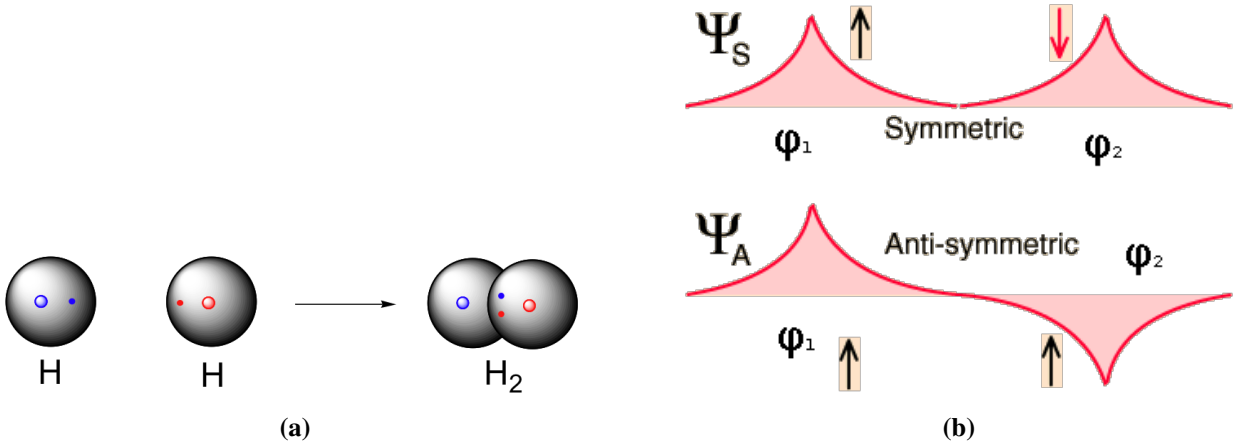

Figure 1.6: (a) The formation of two hydrogen atoms into a molecule based on the Lewis covalent bond theory as an example of the Heitler-London model. (b) Overlapping two separate wave functions into a symmetric orbital state with AFM coupling of spins and antisymmetric state with FM coupling of spins. That is the main result of Heitler-London theory.

the *total* wave function ψ changes sign under simultaneous interchange of both space and spin coordinates. We call the atomic orbital wave functions for two electrons: ϕ_1 and ϕ_2 which only depend on the space coordinates of electrons. The "symmetric" in space with corresponding *singlet* ψ_s and "anti-symmetric" in space with *triplet* ψ_t states of the molecule composing two electrons are trial wave functions of the Hamiltonian $\hat{H}$ [illustrated in Fig. 1.6(b)]

$$\psi_s = \phi_1(\mathbf{r}_1)\phi_2(\mathbf{r}_2) + \phi_1(\mathbf{r}_2)\phi_2(\mathbf{r}_1), \tag{1.2}$$

$$\psi_t = 2[\phi_1(\mathbf{r}_1)\phi_2(\mathbf{r}_2) - \phi_1(\mathbf{r}_2)\phi_2(\mathbf{r}_1)]. \tag{1.3}$$

The singlet-triplet energetic splitting is:

$$E_t - E_s = \frac{(\psi_t, H\psi_t)}{(\psi_t, \psi_t)} - \frac{(\psi_s, H\psi_s)}{(\psi_s, \psi_s)}. \tag{1.4}$$

Here, the E_s and E_t are the energies of singlet and triplet states, respectively. The energy difference between singlet and triplet states is called the "*exchange interaction*" or $J = E_t - E_s$. The exchange energy J originates from the electrostatic repulsion between two electrons, the $V(\mathbf{r}_1, \mathbf{r}_2)$ term in

Eq. (1.1), and it falls rapidly with respect to the distance between two atoms.

So, we can rewrite the spin Hamiltonian of two electrons in close atoms:

$$\hat{\mathcal{H}}^{\text{spin}} = J\mathbf{S}_1 \cdot \mathbf{S}_2. \tag{1.5}$$

Since $\mathcal{H}^{\text{spin}}$ is the scalar product of the two vector spin operators $\mathbf{S}_1$ and $\mathbf{S}_2$, and it will favor parallel spins – FM case if $J < 0$ and antiparallel ones – AFM state if $J > 0$. In other words, the J is positive or negative depending on whether the E_{s} or E_{t} level is lower. The above Hamiltonian is applied to the two-spin system. We can generalize for N-spin systems with:

$$\hat{\mathcal{H}}_{\text{Heis}} = \sum_{\langle i,j \rangle} J_{ij}\mathbf{S}_i \cdot \mathbf{S}_j \qquad \textbf{Heisenberg Hamiltonian}. \tag{1.6}$$

Here, the J_{ij} is known as the *exchange coupling constant* (or parameter or coefficient). There are general remarks about the Heisenberg Hamiltonian in Eq. (1.6):

- In order to include the products of spin pairs in Eq. (1.6), the condition is that all magnetic ions are far enough apart. That happens in magnetic insulators in which the overlap of their electronic wave function is very small or magnetic ions superexchange through an anion (e.g. Mn^{2+} ions exchange through anion O^{2-} in MnO oxide). It is true for AFM cases because most of them are insulators or semiconductors [6]

- The angular momentum of each ion contains both orbital and spin components which may lead to a spin-orbit coupling (e.g. some heavy atomic elements and their compounds [7, 34, 35]). Therefore the *coupling* in the spin Hamiltonian may depend on the absolute and the relative spin orientations.

- In general, extracting information from the Heisenberg Hamiltonian is a difficult task. It is itself as a starting point for many profound investigations of magnetism in solids [1]. We will discuss in detail below.

Analyzing the Heisenberg model: From the Heisenberg Hamiltonian, we can separate into two cases: ferromagnetic interaction or $J_{ij} < 0$, and antiferromagnetic interaction or $J_{ij} > 0$ (Fig. 1.5). For a ferromagnetic coupling, $J_{ij} = J < 0$ which is invariant under a translation vector, the exact ground-state energy and corresponding wave function are derived exactly. Furthermore, the properties of low-lying excited states of the FM Heisenberg model are extracted by using the "spin-wave theory" [1, 2]. However, the ground-state energy and wave function of the AFM Heisenberg model are not derived analytically except in the special case of 1D spin-half chain only considering the nearest-neighbor interaction [1]. The properties of the Heisenberg model in low dimensions are described by the Mermin-Wagner theorem.

Theorem 1. ***(Mermin–Wagner theorem)****: It is rigorously proved that at any nonzero temperature, a one- or two-dimensional isotropic spin-S Heisenberg model with finite-range exchange interaction can be neither ferromagnetic or antiferromagnetic orders [36].*

The theorem, which was originally formulated to describe the Heisenberg Hamiltonian, stated that in $d \leq 2$ dimensions no long-range ordered state may exist at any finite temperature that breaks a continuous symmetry of the Hamiltonian. This clearly applies for the isotropic Heisenberg model in which the rotational symmetry is preserved.

The problem of the ground state is even more interesting. The ordered FM ground state may exist at $T = 0$ K in arbitrary dimensions because it is an eigenstate of the Hamiltonian, and the order parameter of the FM state, magnetization is a conserved quantity. For AFM , the situation is different because the Néel state is not an eigenstate. The long-range order may exist at $T = 0$ K in 2D systems, but it is destroyed by quantum fluctuations even at $T = 0$ for $d = 1$ [2].

1.4 Some possible ways to solve the AFM Heisenberg model

Although the quantum AFM Heisenberg model is hard to solve, a wide range of concepts and techniques can be learned from studies of its ground state, excitation and thermodynamic phases.

1.4.1 Break into anisotropic models

The Hamiltonian [Eq. (1.6)] for a lattice of N spins of magnitude S can break into Ising and XY-models:

$$\hat{\mathcal{H}}_{\text{Heis}} = \mathcal{H}^{zz} + \mathcal{H}^{xy}, \tag{1.7}$$

$$\hat{\mathcal{H}}^{zz} = \frac{1}{2}\sum_{\langle ij\rangle} J_{ij} S_i^z S_j^z, \qquad \text{(Ising model)}, \tag{1.8}$$

$$\hat{\mathcal{H}}^{xy} = \frac{1}{2}\sum_{\langle ij\rangle} J_{ij}(S_i^x S_j^x + S_i^y S_j^y) = \frac{1}{4}\sum_{\langle ij\rangle} J_{ij}(S_i^+ S_j^- + S_i^- S_j^+), \qquad (XY-\text{ model}), \tag{1.9}$$

Here, $\langle i, j\rangle$ represents nearest-neighbor pairs and $J_{ij} = J_{ji} = J > 0$ is the exchange interaction and the lattice translational invariant. The Néel state, which is composed of the equal number of spin-up and spin-down (along the z-component of the Pauli matrices) and the alternation of spin-up and spin-down sublattice, was thought to be the ground-state of the Heisenberg Hamiltonian. However, it is just eigenstate of the Ising model but not of the isotropic model because $\hat{\mathcal{H}}^{XY}$ will flip the direction of spins and connect it to other Ising configuration. However, in bipartite lattices such as 1D chain, square, hexagonal lattice and simple cubic lattices, we can define two different sublattices A and B. The rotation of Ising configuration may be considered as a ground state of "*bipartite AFM Hamiltonian*". The properties of the spin system are defined by two Marshall's theorems:

Theorem 2. ***(Marshall's theorem 1)****: Consider the Heisenberg Hamiltonian Eq. (1.7) with antiferromagnetic exchanges $J_{ij} > 0$ which connect between two sublattices A and B, any two sites on the lattice are connected by a sequence of finite exchanges between intermediary sites. The eigenvalues of square of and $z-$component of the total spin $\mathbf{S} = \sum_i \mathbf{s}_i$ are $S(S+1)$ and M, receptively. In any allowed M sector, the lowest energy state Ψ_0^M can be chosen to have positive definite coefficients f_α^M in the rotated Ising basis $\tilde{\Psi}_\alpha^M$: $\Psi_0^M = \sum_\alpha f_\alpha^M \tilde{\Psi}_\alpha^M$ with $f_\alpha^M > 0$, for any α state. The coefficients*

of Ψ_0^M in terms of the unrotated Ising configurations $|\psi_\alpha\rangle$ obey the "Marshall sign criterion":

$$\Psi_0^M = \sum_\alpha (-1)^{\Gamma(\alpha)} f_\alpha^M \Phi_\alpha, \tag{1.10}$$

$$\Gamma_\alpha = \sum_{i\in B} (S + m_i^\alpha). \tag{1.11}$$

Here, α denotes any Ising spin configuration. The second formula is summed of all site i in sublattice B. m_i^α is the eigenvalue of the $z-$component for each spin $\mathbf{s}$ on each site i. Φ_α is the eigenstate of the Ising Hamiltonian [Eq. (1.7)] which has the eigenvalue E_α:

$$\hat{\mathcal{H}}^{zz}\Phi_\alpha = E_\alpha \Phi_\alpha. \tag{1.12}$$

More detail proofs and calculations about this theorem are referred to Refs. [21, 37].

Theorem 3. ***(Marshall's theorem 2):*** *The absolute ground state Ψ_0, for equal size sublattices A and B, is a singlet of total spin.*

We emphasize that not all total singlet states follow the Marshall's sign criterion, and conversely not all states obeying Marshall's sign are singlet of total spin. The ground state in bipartite Heisenberg AFM must satisfy both two theorems [21, 38].

In a **square lattice** (2D case), the Néel state seems to be the ground state of spin-half AFM Heisenberg model [Fig. 1.7(a)] which is proved by some numerical and experimental evidences.

In the theory, the AFM Heisenberg Hamiltonian on a square lattice was solved by "*spin-wave theory*", which is similar to finding the excitation in the FM case. Physically speaking, it starts from the Néel order as the ground state in the classical limit, and includes quantum fluctuations (XY-model) which are expanded as the order of $1/S$ [2, 29, 39] . Although this method is poor in most $S = 1/2$ cases, it seems to work well for the square lattice. The numerical tracks also confirmed that point by calculating the correlation function. The staggered magnetization, the local ordering parameter in AFM, is calculated about $m_s = 0.3$ in the thermodynamic limit [32].

In experiment, many physicists believe the parent phase of cuprate superconductors, e.g.

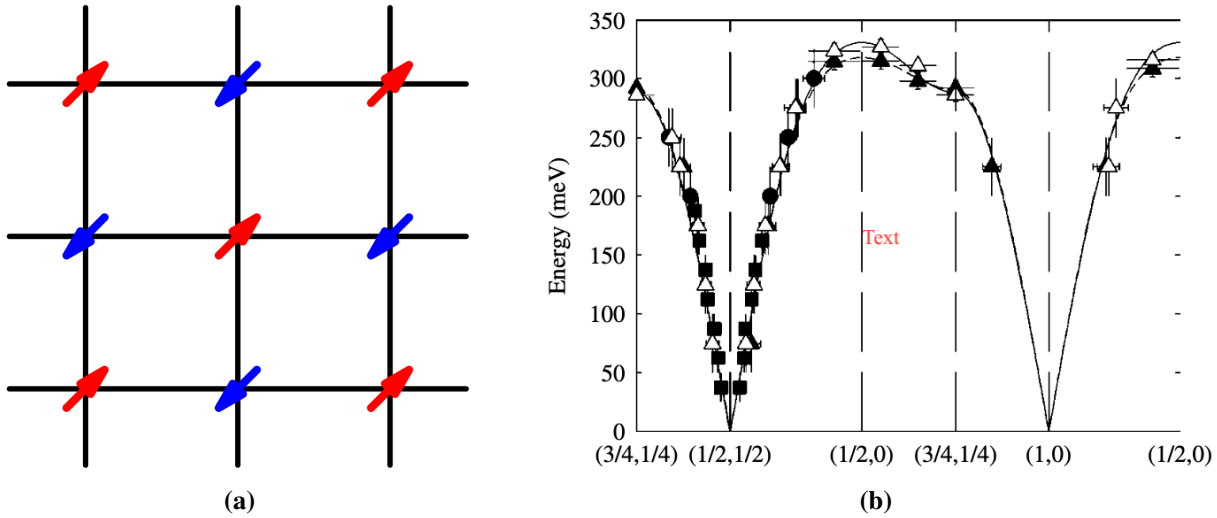

Figure 1.7: (a) Visualization of spin-half square lattice as a Néel state (red arrow is the spin-up, and blue arrow denotes spin-down). (b) Experimental observation of a spin-wave dispersion of the high-T_c parent $LaCuO_4$ by an inelastic neutron diffraction, i.e. a spin-half AFM in square lattice [40]. The horizontal axis is the momentum vector $\mathbf{q}$ in the 2D Brillouin zone, and the π value is simplified.

the La_2CuO_4 compound is an AFM Mott insulator which is true ground state [40]. In this material, the cuprate plane is a perfect CuO_2 plane in which each Cu^{2+} ion exhibits as a $S = 1/2$ unpaired electron, i.e. spin-half on the square lattice. Specifically, spin waves emerge from the wavevector $\mathbf{q} = (1/2, 1/2)$ showing AFM order, and the neutron diffraction data (symbol plots) concur with the theoretical prediction [solid line in Fig. 1.7(b)]. It becomes a superconducting state if the parent phase is doped with mobile holes [40]. The Néel temperature is also measured experimentally in the compound as the $T_N = 350K$ [39].

1.4.2 1D Spin chain

Another possibility is that the quantum fluctuations completely destroy the Néel order even in the ground state. So, the framework of the spin-wave theory becomes invalid. The fruitful examples are 1D spin system or low spin-S on frustrated lattices. The ground state of a quantum AFM without the Néel or any other conventional order is called a *quantum spin liquid* (QSL). We may distinguish two classes of quantum spin liquids: gapful and gapless systems [13].

If there is a continuum of excited states just above the ground state(s) without any finite gap – spin-half chain, the system is said to be *gapless*. When the system is gapful, the ground state is stable against any various small perturbations (e.g. spin-1 chain), unless the gap is closed. In the gapless systems, the ground state is susceptible to perturbations.

Spin-half chain: In this system, particles have an interesting quantum property such that their wave function acquires a minus sign under a rotation of 2π about any spin axis. The system remains disordered because of strong quantum fluctuations. Even in a 1D anisotropic model – Ising spin, there is no ordered state, but in 2D systems there exists some orders such as FM or AFM Ising spin or XY-model with finite critical temperatures [41]. That property follows the **Mermin–Wagner theorem**.

Following the Bethe ansatz, the energy can be calculated exactly in the large-N limit (N is the number of spin sites in chain) [2, 42]:

$$E_0 = -0.443J. \tag{1.13}$$

Here, J is the coupling parameter. This energy is lower than its Néel state, $E_{\mathrm{N}} = -0.25J$. It proves that the ground state of the AFM spin-1/2 chain is disordered phase [2]. Other properties of spin-half chain are: (i) the ground state is nondegenerate and (ii) there is no energy gap above the ground state in the energy spectrum. Figure 1.8(a) shows the energy spectrum of spin-half chain with the excited triplet energy contacting with the ground-state energy at the point $k = 0$ in momentum space. The correlation function, coupling strength between two spins in the system, is decaying in a power law with respect to the distance between two spins. It is called the **Lieb, Schultz and Mattis theorem** [43].

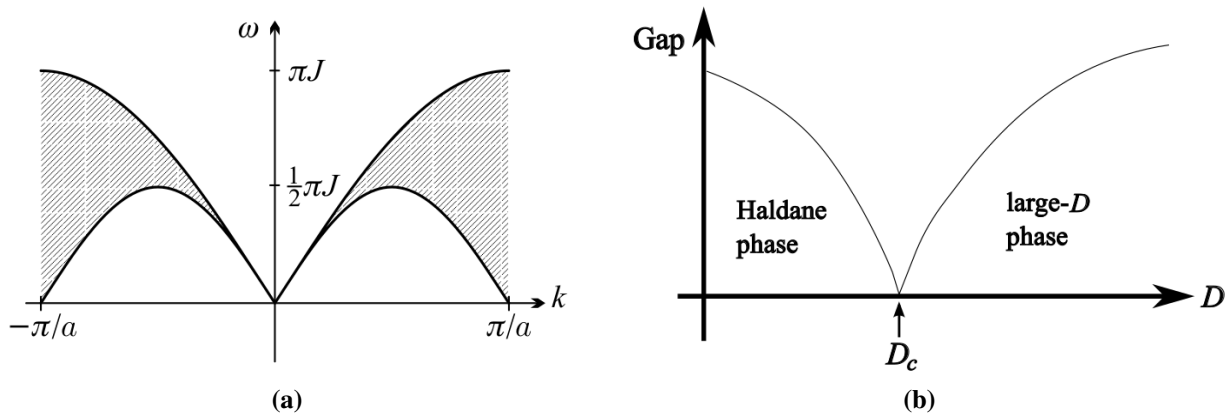

Figure 1.8: (a) The continuum of the triplet excitation in an isotropic AFM spin-half chain. The cross-hatched represents the energetic spectrum. (b) Phase diagram of the excitation gap as a function of the uniaxial anisotropy D, with the value $\lambda = 1$. There is a quantum critical point $D = D_c \approx J$ where the gap closes. Both phases are disordered and examples of topological quantum orders.

Haldane phase in a spin-1 chain: Let us consider an anisotropic generalization of the standard spin-1 Heisenberg chain:

$$\hat{\mathcal{H}}_{\text{Haldane}} = \sum_i \left[J(S_i^x S_{i+1}^x + S_i^y S_{i+1}^y) + \lambda S_i^z S_{j+1}^z + D(S_i^z)^2 \right]. \tag{1.14}$$

In some tetragonal crystals, in addition to the contribution of ion pairs to uniaxial anisotropy, the last term in Eq. (1.14) corresponds to single-ion anisotropy [2]. In the large-D limit ($D \to \infty$), all the spins are restricted to the $S_i^z = 0$ state.

However, a numerical study shows a gapless QCP between the Heisenberg phase and the large-D limit [44]. In the $\lambda - D$ plane [Fig. 1.8(b)], there should be a critical transition connecting the Heisenberg point and the large-D limit which belong to two different phases. The first one is called the *Haldane phase*, a topological non-trivial phase; the second one is the *large-D phase*, topological trivial state. This distinction may be characterized by a *topological definition* (or specifically symmetry protected transition phase) [12–14]. Therefore, a new kind of phase transition should be proposed beyond the Landau phase transition based on the local order parameter and spontaneous broken symmetry (briefly described in Section 1.2).

1.4.3 Valence-Bond State

The idea is that when acting on spin systems, quantum mechanics may lead to exotic ground states and low-energy behaviors that cannot be captured by the traditional semiclassical approaches, especially frustrated lattice models. Therefore, an alternative approach is a variational wave function, in which we must essentially guess the ground state wave function based on experience or physical intuition. The most important one is the resonance valence bond (RVB) concept for spin-half systems suggested by Anderson. The RVB term was first initiated by Pauling in the context of metallic materials. Anderson revised interest in this concept when he constructed a nondegenerate quantum ground state for a $S = 1/2$ AFM system on a triangular lattice [Fig.1.5(a)]. To start finding AFM configurations for frustrated lattices such as triangle and kagomé lattices, instead of the Néel state, he provided a ground state made up of a superposition of singlet pairs that cover the whole lattice [9, 10, 15] . The singlet state is defined as:

$$|\psi_{\text{singlet}}\rangle = \frac{1}{\sqrt{2}}(|\uparrow\downarrow\rangle - |\downarrow\uparrow\rangle). \tag{1.15}$$

It is invariant under any rotation. Here, $\uparrow$ and $\downarrow$ arrows are not meant that they only point out in the z-direction. They can orient in an arbitrary direction such that two spins point in opposite directions (illustrated early in [Fig.1.5(b)]. In contrast to the Néel state, which is not the eigenstate of the two-spin-half AFM Hamiltonian [Eq. (1.5)], the singlet state is its exact eigenstate.

Also, The singlet state of a pair of $S = 1/2$ spins is a typical example of a *quantum entanglement* in which the state cannot be written as a product state of two spins. It is also referred to as a "*valence bond*" state. It is an important theory for solving many AFM models, such as the AKLT model, RVB state and other QSL paradigms as well. The AFM exchange energy between two neighboring sites i and j, is minimized if these sites belong to the same valence bond. However, in this case, the spin j can not form a singlet with the other neighboring spins, and the interaction energy is not minimized for corresponding bonds, (I will describe an example below). Although the Heisenberg AFM on a bipartite lattice is not frustrated in the classical sense, there still exists a

frustration if we consider the next-nearest-neighbor interaction [13]. Solving this model is still a controversial topic [31].

The RVB state is represented by a tensor product of valence-bond basis, whose wave function is given by

$$|\Psi_{\mathrm{RVB}}\rangle = \sum_{i_1 j_1;\ldots;i_n j_n} a(i_1 j_1;\ldots;i_n j_n)\,|(i_1, j_1)\ldots(i_n, j_n)\rangle\,, \tag{1.16}$$

where $(i_1, j_1)\ldots(i_n, j_n)$ are dimer configurations covering the entire lattice. The wave function is summed over all possible choices in which the lattice can be divided into pairs of sites. The quantities $a(i_1 j_1;\ldots;i_n j_n)$ are variational parameters determined by minimizing the ground-state energy of a given Hamiltonian. For a disordered AFM, it was proposed that the valence-bond pairs in the RVB construction are dominated by short-range bonds, resulting in liquid-like states with no long-range order. Depending on the behavior of a spin correlation function $\langle \mathbf{S}_i \cdot \mathbf{S}_j \rangle$, we will call the short-range RVB (sRVB) if it is short-range and a finite correlation length; or algebraic QSL if the correlation function decays with distance following a power law. Another state is called a valence-bond solid (VBS) state if it is strictly connecting bonds between the nearest-neighbor sites. The algebraic QSL is usually invariant under all symmetry operations allowed by the lattice. The RVB state can also be used to describe the Néel state if its correlation function is slow decaying or reaches a constant [16, 32].

Restated again, we do not know the exact ground state and excitation spectrum of most AFM Heisenberg models. Even in the analytical form, such as the Bethe solution in spin-half chain, we still need numerical calculations such as their spin correlations to confirm that point. By adding some other terms to the Hiesenberg Hamiltonian, some models may give exact results (wave function and energy). The two famous Hamiltonians are Majumdar-Ghosh spin-half chain (considering the next-nearest-neighbor coupling) and AKLT model in 1D and 2D lattices [21].

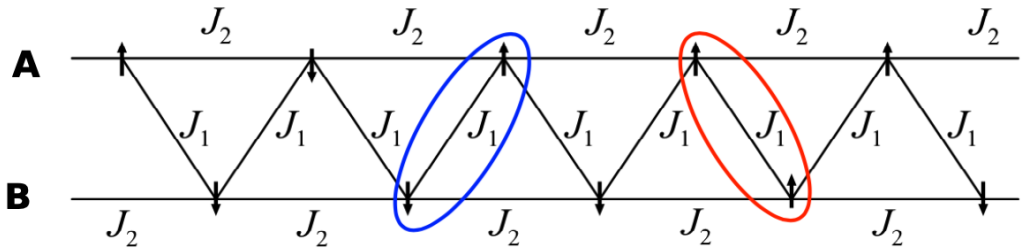

Figure 1.9: Spin-half chain composes of the nearest- and next-nearest-neighbor interactions illustrated as a zig-zag ladder [2].

1.4.4 Majumdar-Ghosh model in spin-half chain

Majumdar and Ghosh studied the AFM spin-half chain with isotropic interactions including nearest J_1 and next-nearest J_2 neighbors:

$$\hat{H}_{\text{chain}} = \sum_i (J_1 \mathbf{S}_i \cdot \mathbf{S}_{i+1} + J_2 \mathbf{S}_i \cdot \mathbf{S}_{i+2}). \tag{1.17}$$

The J_1 and J_2 parameters are positive. Instead of a single chain with two different interactions, it is better visualization to be illustrated as a zig-zag ladder (Fig. 1.9). Spins locate at even and odd sites (A or B legs) of the original chain form two AFM chains – the legs of the ladder. Each spin on one leg couples antiferromagnetically with two spins on the other leg by the magnitude J_1 (nearest-neighbor interaction). The coupling parameter J_2 is to align the internal spins on the same leg into AFM state.The competition between the strengths of J_1 and J_2 results in a frustrated effect. For example, if $J_1 > J_2$, the nearest-neigh coupling between two spins forms an AFM state (blue ellipse in Fig. 1.9); otherwise, it can be an FM state (red ellipse). Therefore, several configurations can be emerged in a chain because of that effect [2].

When $J_2 = J_1/2$, this model is known as the Majumdar-Ghosh point. The ground state includes two dimerized phase (show in Fig. 1.10). We can explain that model by rewriting its Hamiltonian [Eq. (1.17)] by the projection $P_{3/2}^{(i,i+1,i+2)}$ of three spin-half particles into a spin-3/2 subspace as:

$$\hat{H}_{\text{MG}} = \frac{1}{4}\sum_i \hat{H}_i, \quad \hat{H}_i = (\mathbf{S}_i + \mathbf{S}_{i+1} + \mathbf{S}_{i+2})^2 - \frac{3}{4} = P_{3/2}^{(i,i+1,i+2)}.$$

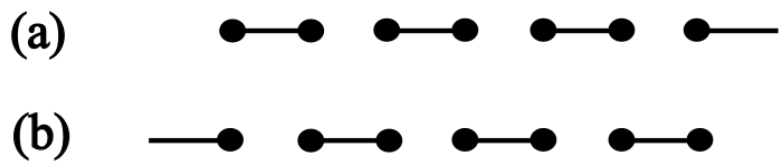

Figure 1.10: Nearest-neighbor valence-bond state of a spin-half chain. There are two degenerate states (a) and (b), which correspond to the dimerized states [13].

Clearly, any state in which the total spin of three neighboring spins is $S = 1/2$ will be destroyed by $\hat{H}_i$. (The total spin of three spin-halves can only be 1/2 or 3/2, as $\frac{1}{2} \otimes \frac{1}{2} \otimes \frac{1}{2} = \frac{1}{2} \oplus \frac{1}{2} \oplus \frac{3}{2}$.) In the system, this is always the case as two of the three neighboring spins form in one singlet bond, and $\mathbf{0} \otimes \frac{1}{2} = \frac{1}{2}$.

As $\hat{H}_i$ is positive definite, the ground-state energy of $\hat{H}_{\mathrm{MG}}$ is zero. They remarked that two Majumdar-Ghosh dimered states are not the universal generic wave function for 1D spin-half chain. This is because the states violate the translational symmetry with two lattice spacings, while the generic one should be invariant. Nonetheless, the dimerized chain shares an important property with the generic liquid and agrees with the *Lieb-Schultz-Mattis theorem* in some points. For example, the spinon excitation—domain walls between even and odd ground states—are *deconfined*. Furthermore, the ground state and the excitation continuum may be separated by a gap only if the ground state is degenerate and breaks the translational symmetry spontaneously like the Majumdar-Ghosh chain [43, 45].

The dimerized chain has further meaning as a piece of a general paradigm. The two degenerate dimer states can be combined into a spin-1 AKLT chain, which serves as a generic prototype for spin-1 chain, exhibits the Haldane gap (described below) and provides the intellectual background for several exact models [45].

1.4.5 AKLT model

Spin-1 chain AKLT model and Haldane phase: In contrast to the spin-half chain, the ground state and the excitation spectrum of the AFM Heisenberg models with spin $S > 1/2$ cannot

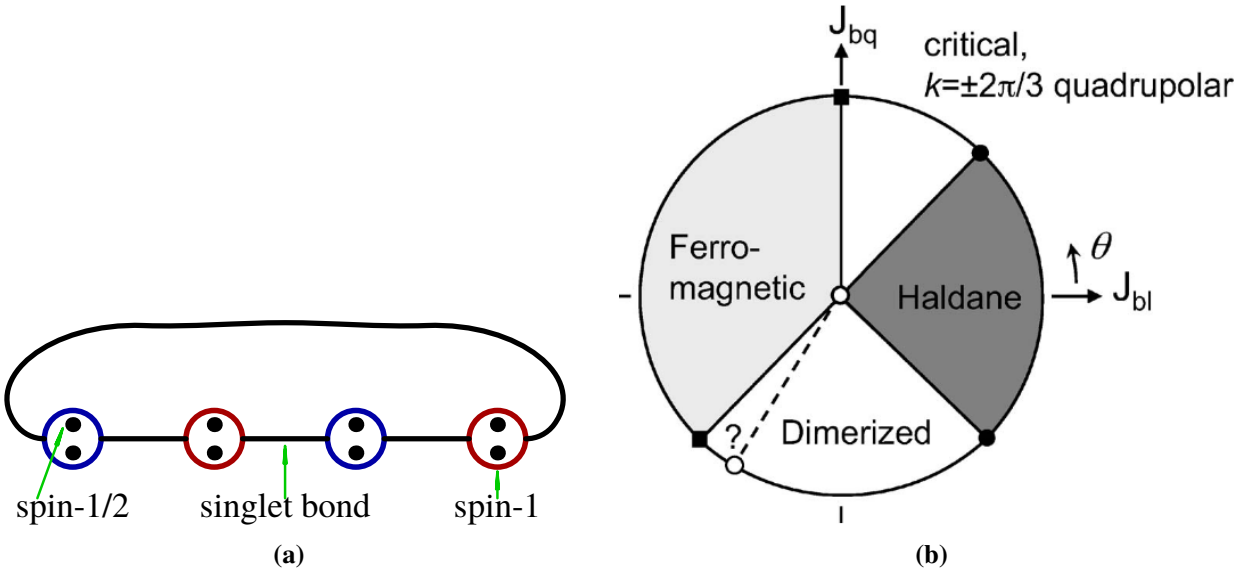

Figure 1.11: (a) VBS state in spin-1 chain. Each spin-1 on a site consists of two spin-halves and connects with its neighbors by singlet bonds. (b) Visualization of phase diagram in spin-1 chain by varying the parameter $\beta = J_{\rm bq}/J_{\rm bl} = \tan\theta$ in Eq. (1.18) [48, 49].

determined exactly. Furthermore, we cannot use the *Bethe ansatz* for spin $S > 1/2$ in 1D. In the spin-1 chain, the construction of a candidate for the ground state via valence bonds turns out to be quite interesting. Affleck, Kennedy, Lieb and Tasaki did construct a translation invariant state in terms of the valence-bond basis [46, 47]. Each spin-1 on a site consists of two virtual $S = 1/2$ spins [Fig. 1.11(a)]. Then, the ground state in which every neighboring pair of $S = 1/2$ particles does form a singlet bond is fully symmetrized [11]. This AKLT state is a kind of *valence-bond solid* (VBS) because it reflects the static configuration of valence bonds and preserves the translation symmetry of the lattices. Each spin-half particle belongs to one bond, so it is a QSL (or a disordered state).

The AKLT Hamiltonian includes a bilinear Heisenberg $\mathbf{S}_i \cdot \mathbf{S}_{i+1}$ and biquadratic term $(\mathbf{S}_i \cdot \mathbf{S}_{i+1})^2$:

$$\hat{\mathcal{H}}_{\rm AKLT} = J \sum_i \left[\mathbf{S}_i \cdot \mathbf{S}_{i+1} + \beta(\mathbf{S}_i \cdot \mathbf{S}_{i+1})^2\right]. \tag{1.18}$$

The VBS state is not the exact ground state of the standard spin-1 AFM Heisenberg chain (we also prove it in the next chapter). However, it is the exact ground state of the AKLT Hamiltonian with

the value $\beta = 1/3$ in Eq. (1.18). It is similar to the dimerized phase which is the exact ground state of Majumdar-Ghosh Hamiltonian but not a general spin-half chain. By a simple proof, we argue that the above VBS state is the exact ground-state of the AKLT Hamiltonian. The interaction at each bond in the AKLT model can be written as:

$$2P_2^{(i,i+1)} - \frac{2}{3} = \mathbf{S}_i \cdot \mathbf{S}_{i+1} + \frac{1}{3}(\mathbf{S}_i \cdot \mathbf{S}_{i+1})^2, \tag{1.19}$$

where $P_2^{(i,i+1)}$ is the projection operator onto the states in which $\mathbf{S}_i + \mathbf{S}_{i+1}$ has the total spin $S = 2$.

By the quantum mechanical addition of spins, the total spin for two sites can take on one of the values 0, 1, and 2. In the AKLT state, because two $S = 1/2$ spins form a singlet, adding up the two remaining $S = 1/2$ spins can not go up to spin $S = 2$. When the AKLT Hamiltonian acts on the ground state, the eigenenergy is zero. The spin-spin correlation function decays exponentially in contrast to the power decay in spin-half chain [46, 47].

Although the AKLT model is different from the standard Heisenberg chain by an amount of the biquadratic term, we observe that their properties are similar. Both of cases have the exponential decaying correlation functions and gap to an excited state, which are confirmed by theoretical, experimental and numerical studies. Furthermore, there is no quantum phase transition (QPT) between the standard Heisenberg and the AKLT point, in which the coefficient of the biquadratic term β varies from 0 to 1/3. They are considered as the same topological phase in Fig. 1.11(b).

Generally, we see that a similar translation-invariant AKLT state exists for any integer spin S, e.g. spin-2 AKLT chain with double valence-bond states connecting every two spin sites [50]. In contrast to the 1D spin half-integer, various states with different degree dimerization can be constructed in a similar manner, but not having the translation-invariant state. The excitation gap, characteristics of integer-spin AFM chains, is now called the "*Haldane gap*" (it belongs to the Haldane phase).

Spin $S > 1$ in the higher dimension: In contrast to the distinctive properties between half-odd and integer spin state on the chain, there is no restriction for spin in higher dimension ($d > 1$). Here, we discuss two AKLT cases: spin-3/2 on a hexagonal lattice and spin-2 on a square lattice, known as the simplest formation of VBS state in 2D. We have not seen many investigations of the two cases. Most of the numerical work is based on a kind of *tensor-network technique*, which only works well in $1D$ lattice [51]. For higher dimensions, it is hard to simulate problems using this approach. Some numerical results suggested that the AFM Heisenberg models on spin-2 square lattice and spin-3/2 hexagonal lattice are the Néel states at zero temperature [52–55]. Along with that point, we also observe the VBS state in spin-3/2 hexagonal and spin-2 square lattice by adding fixed coefficients of the cubic and quartic power of the Heisenberg term into the Hamiltonian [11, 46, 47]. Otherwise, there is an emergence of XY-like phase in those models by deforming the AKLT wave function. There would be some QPTs connecting these proposed phases together by varying the coupling parameters in the general Hamiltonian.

In the AKLT model, there is a parameter called *multiplicity (M)*, which is defined as $M = 2S/z$, where S and z are spin and coordination numbers (or the number of nearest-neighbors), respectively. In spin-3/2 hexagonal or spin-2 square lattices, $M = 1$. For example, in hexagonal lattice, $S = 3/2$ and $z = 3$, so $M = (2\times3/2)/3 = 1$. In the other way, we can explain that the number of virtual spin-half particles at each site is equal to the number of nearest-neighbor sites [11]. That parameter will restrict the AKLT Hamiltonian is the summation of highest spin projections on two spin sites (e.g. the projection of spin-3 on two spin-3/2 sites on a hexagonal lattice). The spin-3/2 hexagonal and spin-2 square AKLT state is so-called a weak SPT phase that cannot be protected by on-site symmetry alone. Rather, it is protected by the translational symmetry [11, 54]. One of the most important applications for the two cases is paradigm of measurement-based quantum computation [56, 57].

Edge state: For all spin properties above, we consider systems in terms of the *periodic boundary conditions*. Another peculiar characteristic of the Haldane phase is the appearance of free spin

degrees of freedom at open ends. Let us consider the $S = 1$ AKLT state on an open chain. In this state each $S = 1/2$ spin forms a valence bond with a spin on the neighboring site (on its left and right). However, at the edges of the chain, the remaining $S = 1/2$ spin does not have a partner to form a valence bond, and they remain free. Also, they can point upward or downward freely. So we have in total four-fold degenerate states which are similar to the two-spin states described in the Heitler-London picture.

The free spin-half at each end is called an *edge state*, which is analogous to the gapless mode at open boundaries in the quantum Hall effect [12, 58]. The trivial disordered states, e.g. the large-D state, do not have such edge states. We may conclude that the existence of the edge state can be regarded as a signature of the *topological order*, although not all topological ordered phases have the edge state (Chapter 4, "*Fractionalization and Topological Order*" by Masaki Oshikawa [13]).

1.5 Solve the Heisenberg Hamiltonian for quantum spin model by the Schwinger bosons

Generally, an electron is a fermionic particle. Except when we suppress its charge component in magnetic insulators, in that case, effective interactions between spins occur (the Heisenberg model). Then we do not exactly know which kind of quantum particles, fermions or bosons, to use to treat spins. Each kind of formalism has its own advantages and disadvantages to understand the properties of the spin system. We call the Schwinger bosonic and Bardeen-Cooper-Schrieffer (BCS) fermionic trial wave function. The most important difference between the fermionic and bosonic constructions is that they lead very different sign structures in the spin wave function. For the bosonic case, when two spins at different sites are interchanged, the wave function does not change its sign; whereas it does change sign when we exchange two spins in a fermionic representation. These different sign structures represent very different quantum entanglement structures in the corresponding RVB wave functions [16]. In this thesis, I only describe the bosonic wave function which is similar to my work.

We start with a technique called the large-N approximation, which is not very far from

$1/S$ expansion. First, the Heisenberg Hamiltonian and corresponding wave function of a spin system are written in terms of a bosonic field. Second, an appropriate partition function is constructed, and the interacting terms are decoupled by using the complex Hubbard-Stratonovich technique [16, 22, 41, 59]. There is a static mean field around some condensate phases, e.g. Néel state (a long-range antiferromagnetic order) in the bipartite AFM case. This approach is called the Schwinger Boson Mean Field Theory (SBMFT), which is set up as the large-N limit of the Heisenberg model. Here, in the SU(N) case, the spin operators are represented by N flavors of the Schwinger bosons. Both ordered and disordered phases are described by this theory at zero and finite temperatures, and they complement the semiclassical approaches. In most cases, the large-N approximation has been applied to treat the spin Hamiltonians, where the symmetry is SU(2), and $N = 2$ is not a truly large parameter (this is the main limitation of the technique). Nevertheless, the $1/N$ expansion provides an approximation method for obtaining simple mean field theories. In that way, the mean field equations are solved, and the ground state wave function, order parameter and excitation dispersion are calculated.

The large-N approach handles strong local interactions in terms of constraints. It is not a perturbation expansion in the size of the interactions but rather a saddle point expansion which usually preserves the spin symmetry of the Hamiltonian. At the mean field level, the constraints are enforced only on average. Their effects are systematically reintroduced by higher-order corrections in $1/N$ by using the Feyman diagrams. It turns out that different N generalizations are suitable for different Heisenberg models, depending on the sign of couplings, spin size, and lattice [21, 31, 60].

Bipartite antiferromagnet First, the spin components are represented by two Schwinger bosons $a^\dagger, a; b^\dagger, b$, which satisfy the commutation relations:

$$\begin{cases} [a, a^\dagger] = [b, b^\dagger] = 1, \\ [a, b^\dagger] = [b, a^\dagger] = 0, \\ [a, b] = [a^\dagger, b^\dagger] = 0. \end{cases} \tag{1.20}$$

$$\begin{cases} S_i^+ = a_i^\dagger b_i, \\ S_i^- = a_i b_i^\dagger, \\ S_i^z = \frac{1}{2}\left(a_i^\dagger a_i - b_i^\dagger b_i\right), \\ S = \frac{1}{2}\left(a_i^\dagger a_i + b_i^\dagger b_i\right). \end{cases} \tag{1.21}$$

This makes sense of the properties of a spin, e.g.

$$S_i^+ \left|\downarrow_i\right\rangle = a_i^\dagger b_i b_i^\dagger \left|0\right\rangle = a_i^\dagger \left|0\right\rangle = \left|\uparrow_i\right\rangle, \tag{1.22}$$

$$S_i^- \left|\uparrow_i\right\rangle = a_i b_i^\dagger a_i^\dagger \left|0\right\rangle = b_i^\dagger \left|0\right\rangle = \left|\downarrow_i\right\rangle. \tag{1.23}$$

We consider the case of a nearest neighbor SU(2) antiferromagnet, with interaction strength $J > 0$, on a bipartite lattice with sublattices A and B. A bond $\langle i, j\rangle$ is defined such that $i \in A$ and $j \in B$. the antiferromagnetic bond operator is defined as

$$\mathcal{A}_{ij} = a_i b_j - b_i a_j. \tag{1.24}$$

This is antisymmetric under interchange of the site indices i and j, and transforms as a singlet under a global SU(2) rotation. Consider a rotation by π about the y axis on sublattice B only, the antiferromagnetic bond operator takes the form:

$$\mathcal{A}_{ij} \rightarrow a_i b_j + b_i a_j. \tag{1.25}$$

The SU(2) Heisenberg model is written in the form

$$\begin{aligned} \hat{\mathcal{H}} &= J \sum_{\langle i,j\rangle} \mathbf{S}_i \cdot \mathbf{S}_j \\ &= \frac{J}{2} \sum_{\langle i,j\rangle} \left(2S^2 - \mathcal{A}_{ij}^\dagger \mathcal{A}_{ij}\right). \end{aligned} \tag{1.26}$$

The extension to SU(N) for $N = 2S + 1 > 2$ is straightforward. With the N species of bosons, Eq. (1.25) is

$$\mathcal{A}_{ij} = \sum_{\alpha=1}^{N} b_i^\alpha b_j^\alpha, \tag{1.27}$$

with α: boson flavors. The nearest-neighbor SU(N) antiferromagnetic Heisenberg model becomes:

$$\hat{\mathcal{H}} = \frac{J}{N} \sum_{\langle i,j \rangle} \left(NS^2 - \mathcal{A}_{ij}^\dagger \mathcal{A}_{ij} \right). \tag{1.28}$$

Then, the authors wrote a functional integral approach, and introduced a single real field $\lambda_i(\tau)$ (τ: imaginary time) on each site to enforce the occupancy constraint, and a complex Hubbard-Stratonovich field $Q_{ij}(\tau)$ on each link decouples the interaction in a many-body partition function [60]. The bosonic partition function for spin-S Heisenberg AFM is:

$$\begin{aligned} Z &= \int D[b^\dagger, b; Q^*, Q; \lambda] \exp\left[- L(b^\dagger, b; Q^*, Q; \lambda) \right], \qquad \text{with} \\ L &= \int_0^\beta d\tau \Bigg\{ \frac{1}{2} \sum_{i,\alpha} \left[b_{i,\alpha}^\dagger \left(\frac{\partial}{\partial \tau} b_{i,\alpha} \right) - \left(\frac{\partial}{\partial \tau} b_{i,\alpha}^\dagger \right) b_{i,\alpha} \right] + N \sum_{\langle i,j \rangle} Q_{ij}^* Q_{ij} + \sum_{\langle i,j \rangle, \alpha} \left(Q_{ij}^* b_{i\alpha} b_{j\alpha} + Q_{ij} b_{i\alpha}^\dagger b_{j\alpha}^\dagger \right) \\ &\qquad + \sum_{i\alpha} \lambda_i (b_{i\alpha}^\dagger b_{i\alpha} - S) \Bigg\}. \end{aligned} \tag{1.29}$$

These fields are assumed to be static. The mean field Hamiltonian is obtained

$$\begin{aligned} \hat{H}^{\mathrm{MF}} = \frac{pN}{J} \sum_{i<j} |Q_{ij}|^2 + \sum_{i<j} (Q_{ij} A_{ij}^\dagger + Q_{ij}^* A_{ij}) \\ + \sum_i (b_{i\alpha}^\dagger b_{i\alpha} - n_b) + (VN)^{-1/2} \sum_{i\alpha} (\phi_{i\alpha}^* b_{i\alpha} + \phi_{i\alpha} b_{i\alpha}^\dagger), \end{aligned} \tag{1.30}$$

where the volume V is the number of the (Bravais) lattice sites, and α runs from 1 to N for SU(N) ($p = 1$). $Q_{ij} = \langle A_{ij} \rangle$ is the expectation value of A_{ij} in a coherent state. The number of bosons is $n_b = \sum_{\alpha=1}^N b_\alpha^\dagger b_\alpha$. They further assumed that the mean field solution has the symmetry of the underlying lattice, and the interactions are only between the nearest-neighbor sites on Bravais

lattice. Then they used the Fourier transformation:

$$\begin{aligned}\hat{H}^{\mathrm{MF}} = VN\Big(\frac{pz}{2J}|Q|^2 - \frac{n_b}{N}\lambda\Big) \\ + \frac{z}{2}\sum_{\mathbf{k},\alpha,\alpha'}\Big[Q\xi_{\mathbf{k}}K_{\alpha\alpha'}b^{\dagger}_{\mathbf{k},\alpha}b^{\dagger}_{-\mathbf{k},\alpha'} + Q^*\xi^*_{\mathbf{k}}K_{\alpha\alpha'}b_{\mathbf{k},\alpha}b_{-\mathbf{k},\alpha'}\Big] \\ + \lambda\sum_{\mathbf{k},\alpha}b^{\dagger}_{\mathbf{k},\alpha}b_{\mathbf{k},\alpha} + (VN)^{-1/2}\sum_{\mathbf{k},\alpha}(\phi^*_{\mathbf{k},\alpha}b_{\mathbf{k},\alpha} + \phi_{\mathbf{k},\alpha}b^{\dagger}_{\mathbf{k},\alpha}),\end{aligned} \tag{1.31}$$

where z is the lattice coordination number, and $K_{\alpha,\alpha'} = \delta_{\alpha,\alpha'}$ for SU(N). The Hamiltonian $\hat{H}^{\mathrm{MF}}$ is brought to a diagonal form by the Bogoliubov transformation, and integrating out the Schwinger bosons.

The solutions are summarized:

$$\begin{cases}\beta_{\mathbf{k}\alpha}\Psi^{\mathrm{MF}} = 0 \quad \forall \quad \mathbf{k},\alpha, \\ \beta_{\mathbf{k}\alpha} = \cosh\theta_{\mathbf{k}}b_{\mathbf{k}\alpha} - \sinh\theta_{\mathbf{k}}b^{\dagger}_{-\mathbf{k}\alpha}, \\ \tanh 2\theta_{\mathbf{k}} = -\dfrac{zQ\gamma_{\mathbf{k}}}{\lambda}.\end{cases} \tag{1.32}$$

The ground state wave function Ψ^{MF} can be explicitly written in terms of the original Schwinger bosons (i.e. the bosonic coherent state) as:

$$\begin{cases}|\Psi\rangle^{\mathrm{MF}} = C\exp\Big[\dfrac{1}{2}\sum_{ij}u_{ij}\sum_{\alpha}b^{\dagger}_{i,\alpha}b^{\dagger}_{j,\alpha}\Big]|0\rangle, \qquad \text{with} \\ u_{ij} = \dfrac{1}{V}\sum_{\mathbf{k}}e^{i\mathbf{k}\cdot\mathbf{R}_{ij}}\tanh\theta_{\mathbf{k}}.\end{cases} \tag{1.33}$$

At the zone center and the zone corners, the mean field dispersion is that of free massive relativistic bosons,

$$\omega_{\mathbf{k}} \approx c\sqrt{(2\xi)^{-2} + |\mathbf{k} - \mathbf{k}_\gamma|^2}, \quad \mathbf{k}_\gamma = 0, \pi. \tag{1.34}$$

When the gap (or "mass" $c/2\xi$) vanishes, $\omega_{\mathbf{k}}$ reduces to the dispersions of antiferromagnic spin waves [Fig. 1.7(a)] or the classical limit [31, 41].

1.6 Motivations

With the background information which I have provided above, I will discuss some motivations.

(i) We would construct a universal language in hope of studying the quantum spin model as fundamentally as possible over a range from the quantum limit (i.e. small spin value in low dimensional cases) to the classical limit (i.e. magnetic orders for large spins or in higher dimensions). Our language is represented in terms of the valence-bond basis, which is non-orthogonal and overcomplete. Any spin$-S$ Hamiltonian and states can be written by that construction. We will provide some examples to prove how our valence-bond algebra is appropriate to treat interacting spin systems.

(ii) According to the content in Chapter 4 of "*Understanding quantum phase transition*" and the original results of the VBS state published by Affleck, Kennedy, Lieb and Tasaki [13, 46, 47], until now there has been no step-by-step derivation of the VBS state for the fixed point AKLT Hamiltonian. Theoretical works have predicted that the AKLT Hamiltonian is the sum of spin-2 projections on two spin-1 sites. Because of the existence of a singlet pair between two spins, we cannot reach the spin-2 state. Therefore, the VBS state is the ground state of the Hamiltonian. Other numerical studies have used the *matrix product state*, the *tensor product* of spin sites and deformed *density matrix renormalization group*, to calculate them. In our work, by representing the general AKLT model and the VBS state by using hard-core bosons combined with the singlet-projector operator, we will explicitly show the the VBS state is the exact ground state of the fixed-point AKLT model.

(iii) Based on our language, we create an update projector which is used to build the algorithm for the Monte Carlo simulation in quantum spin systems. Furthermore, the coherent state, which is similar to the construction of the state in terms of the fermions or bosons is derived. We will use that state to evaluate "*exactly*" the Heisenberg AFM for simple cases, and we prove that it is different from using mean-field theory at large-N limit. We also provide the trial wave functions to minimize the energy of the AFM system.

CHAPTER 2

VALENCE-BOND ALGEBRA AND ITS APPLICATION TO AKLT MODEL

2.1 General AFM model

The physical significance of investigations to the quantum spin model starts from the Heisenberg model (i.e. a bilinear interaction between two spins). For spin-half system, it restricts to the Heisenberg term. However, for the $S > 1/2$ cases, the systems may contain the higher order the bilinear terms which provide additional information. For example, the spin-1 AKLT model in a chain includes both bilinear and biquadratic terms with the fixed ratio between them. We are possible to solve exactly the ground state of energy and wave function for this model. Therefore, we can exapand the general form of a spin-rotation-invariant, short-range AFM Hamiltonian as a sum of powers up to $2S$ of the nearest-neighbor Heisenberg interaction:

$$\hat{H} = \sum_{n=1}^{2S} \sum_{\langle i,j \rangle} \alpha_n (\mathbf{S}_i \cdot \mathbf{S}_j)^n. \tag{2.1}$$

Here, n is an integer ranging from 1 to $2S$; it is assumed that there is a common value of $S = 1/2, 1, 3/2, 2, \ldots$ for the spin degrees of freedom at each lattice site. The α_n are positive coefficients that parametrize the strengths of the various interaction terms between two adjacent spins, labelled $\langle i, j \rangle$. For the $S = 1/2$ case, there is only the conventional Heisenberg model $H_{\text{Heis}} = \alpha_1 \sum_{\langle i,j \rangle} \mathbf{S}_i \cdot \mathbf{S}_j$ [as per Eq. (1.6)], with the interaction limited to the bilinear term. The $S = 1$ case also allows for a biquadratic term $(\mathbf{S}_i \cdot \mathbf{S}_j)^2$. In general, the complexity of the allowed interactions increases with $2S$, in the sense that there are $2S$ valence bonds emerging from each lattice site [2] and a correspondingly increasing number of ways to carry out their geometric rearrangement.

2.1.1 Hard-core bosons as a bookkeeping trick of the singlet bond construction

We construct a valence-bond algebra by first introducing fictitious hard-core bosons and then removing them at the end. We consider the spin-S at each lattice site to consist of $2S$ virtual $s = 1/2$ particles, appropriately symmetrized to remove unphysical states. We choose to manipulate those spin-half particles by the annihilation and creation of bosons: via a, $a^\dagger$, b and $b^\dagger$. Here, spin-up and spin-down do not necessarily conform to a global definition of the z-axis. The quantization axis can be chosen at each site as a matter of convention. It can be chosen to match some ordering, as in Fig. 1.5.

$$|\uparrow_i\rangle = a_i^\dagger |\text{vac}\rangle , \tag{2.2}$$

$$|\downarrow_i\rangle = b_i^\dagger |\text{vac}\rangle . \tag{2.3}$$

Here, $a_i^\dagger$ and a_i are the creation and annihilation operators of spin-up at a site i, whereas $b_i^\dagger$ and b_i are the creation and annihilation operators of spin-down at a site i. This is a case of spin-1/2 system because each site only has one virtual $s = 1/2$ particle. For $S > 1/2$ spin systems, we use more indices to represent the spin-1/2 on a site :

$$[a_i^\alpha, a_j^{\beta\dagger}] = \delta_{ij}\delta^{\alpha\beta}, \qquad [b_i^\alpha, b_j^{\beta\dagger}] = \delta_{ij}\delta^{\alpha\beta}, \qquad [a_i^\alpha, b_j^{\beta\dagger}] = 0. \tag{2.4}$$

The subscripts i and j are site indices for the spins. The superscripts α and β distinguish the virtual spins $s = 1/2$ on each site. For example, if we have the spin $S = 1$ system, the number of particles $s = 1/2$ on each site is $2S = 2$ (and hence α ranges over 1, 2).

$$a_i^{\alpha\dagger} a_i^\alpha + b_i^{\alpha\dagger} b_i^\alpha = 1, \tag{2.5}$$

$$(a_i^{\alpha\dagger})^2 |\text{vac}\rangle = (b_i^{\alpha\dagger})^2 |\text{vac}\rangle = 0. \tag{2.6}$$

Any spin particle can be represented by a bosonic operator which follows a single-occupancy constraint, a so-called **hard-core boson** [Eq. (2.5)]. It is meant that each virtual spin-half on a site is occupied by exactly one particle: spin-up or spin-down. So, we cannot put more than two particles on one position [Eq. (2.6)].

From the above definition of hard-core boson, we have constructed a singlet creation and annihilation $\chi_{ij}^{\dagger}$, χ_{ij}, transition T_{ij}, and number operators N_{ii}:

$$\chi_{ij}^{\dagger} = \frac{1}{2S\sqrt{2}} \sum_{\alpha,\beta=1}^{2S} \left(a_i^{\alpha\dagger} b_j^{\beta\dagger} - b_i^{\alpha\dagger} a_j^{\beta\dagger}\right), \tag{2.7}$$

$$\chi_{ij} = \frac{1}{2S\sqrt{2}} \sum_{\alpha,\beta=1}^{2S} \left(a_i^{\alpha} b_j^{\beta} - b_i^{\alpha} a_j^{\beta}\right), \tag{2.8}$$

$$T_{ij} = \frac{1}{2S} \sum_{\alpha,\beta=1}^{2S} \left(a_i^{\alpha\dagger} a_j^{\beta} + b_i^{\alpha\dagger} b_j^{\beta}\right), \tag{2.9}$$

$$N_{ii} = \frac{1}{2S} \sum_{\alpha,\beta=1}^{2S} \left(a_i^{\alpha\dagger} a_i^{\beta} + b_i^{\alpha\dagger} b_i^{\beta}\right). \tag{2.10}$$

Singlet creation $\chi_{ij}^{\dagger}$ and annihilation χ_{ij} operators represent creating and destroying a valence bond between two neighboring sites i and j. Each valence bond is an entangled object in superposition. This is also able to form a *qubit* in which a spin at a position i correlates with other on position j. We illustrate in Figure 2.1, each bond in a spin-1 chain represents the superposition of a singlet state which is formed by any two spin-half particles on site i and j. Here, $\alpha, \beta = 1$ or 2. The transition operator T_{ij} composes of creating and annihilating the same kind of bosons between two sites like a hopping operator [61]. The number operatorN_{ii} counts the number of bonds emerging from each spin site. These operators satisfy some commutator relations:

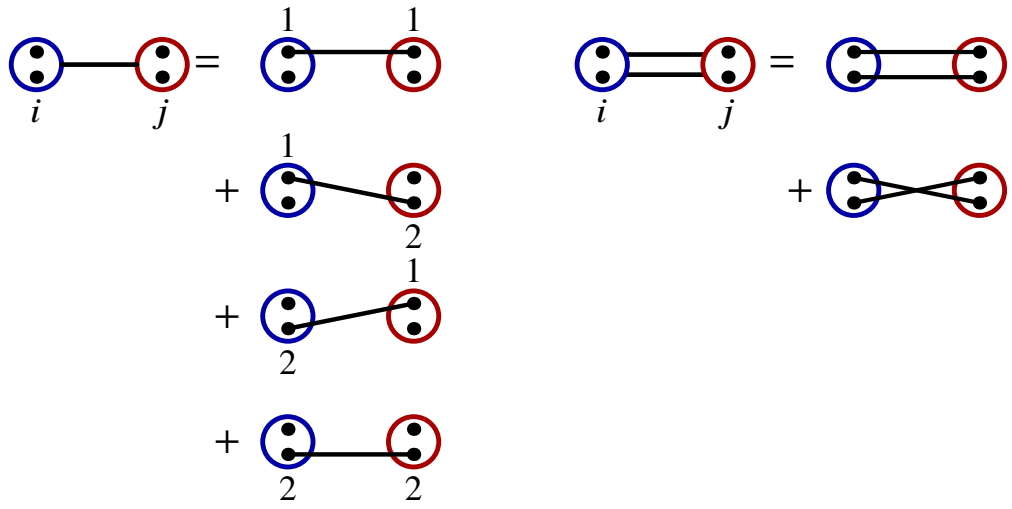

Figure 2.1: Representation of a valence-bond creation $\chi_{ij}^{\dagger}$ (left) and $(\chi_{ij}^{\dagger})^2$ (right) in terms of connecting spin pairs between sites i and j in a spin-1 chain.

$$[\chi_{ij}, \chi_{kl}^{\dagger}] = (\delta_{ik}\delta_{jl} - \delta_{il}\delta_{jk}) + \frac{1}{2}\big(\delta_{ik}T_{lj} + \delta_{jl}T_{ki} - \delta_{il}T_{kj} - \delta_{jk}T_{li}\big), \tag{2.11}$$

$$[T_{ij}, \chi_{kl}^{\dagger}] = \delta_{jk}\chi_{il}^{\dagger} - \delta_{jl}\chi_{ik}^{\dagger}, \tag{2.12}$$

$$[\chi_{ij}, \chi_{ij}^{\dagger}] = 1 + \frac{1}{2}N_{ij}, \quad \text{with :} \quad N_{ij} = N_{ii} + N_{jj}, \tag{2.13}$$

$$[N_{ii}, \chi_{kl}^{\dagger}] = \delta_{ik}\chi_{il}^{\dagger} - \delta_{il}\chi_{ik}^{\dagger}, \tag{2.14}$$

$$[N_{ii}, \chi_{kl}] = -\delta_{ik}\chi_{il} + \delta_{il}\chi_{ik}. \tag{2.15}$$

The meaning of Eqs. (2.11) – (2.13) is that the states which are created by singlet bonds are nonorthogonal and overcomplete (we will prove subsequently). Because a valence bond includes two site indices, it does not only act on the same bond [with two same indices as in Eq. (2.13)] but also other bonds which only share one common index. The other physical significance of the commutation relation is if two valence bonds do not share any common index, they are measured separately. Otherwise, they will influence each other in our measurement. This construction recasts spin configurations into the language of entangled pairs and quantum information [62]. Consequently, QSL states will be advantageous in the race to build a universal quantum computer. Some qubits can form in a cluster to store information if they are related. Others are independent if they do not have common indices.

For bipartite lattices, it turns out that we can eliminate all negative terms in the above commutation relations. It is convenient to work in a bipartite basis, in which it is understood that all entangled bond begin on a site in the A sublattice and end on a site in the B sublattice. The lack of negative contributions is a consequence of the Marshall sign theorem.

$$
\begin{aligned}
[\chi_{ij}, \chi^{\dagger}_{kl}] &= \delta_{ik}\delta_{jl} + \frac{1}{2}\big[\delta_{ik}T_{lj} + \delta_{jl}T_{ki}\big], && (2.16)\\
[T_{ij}, \chi^{\dagger}_{kl}] &= \delta_{jk}\chi^{\dagger}_{il}, && (2.17)\\
[\chi_{ij}, \chi^{\dagger}_{ij}] &= 1 + \frac{1}{2}N_{ij}, \quad \text{with :} \quad N_{ij} = N_{ii} + N_{jj}, && (2.18)\\
[N_{ii}, \chi^{\dagger}_{kl}] &= \delta_{ik}\chi^{\dagger}_{il}, && (2.19)
\end{aligned}
$$

Here, i and k are always in the A sublattice, whereas j and l are in B. Note that the bipartite basis, while reduced, is still overcomplete and spans the total-spin-zero sector of the Hilbert space.

2.1.2 General construction of the valence bond operator

The formalism must be extended to span all the other total spin sectors. To form a complete algebra for a many-body system consisting of an even number of spin-S degrees of freedom, the general valence bond algebra should be built for both singlet ($\mu = 0$) and triplet ($\mu = 1, 2, 3$) flavors. We find it convenient to denote $\sigma^{\mu} = (\sigma^0, \sigma^1, \sigma^2, \sigma^3) = (\mathbb{1}, \sigma)$, which groups the 2×2 identity together with the Pauli matrices, and $\tau^{\mu} = \sigma^{\mu} i\sigma^2 = (i\sigma^2, -\sigma^3, i\mathbb{1}, \sigma^1)$, which defines our convention for the spin states of bound spin-half pairs:

$$
\frac{1}{\sqrt{2}} \sum_{s,s'} \tau^{\mu}_{s,s'} \, |s\rangle \otimes |s'\rangle = \frac{1}{\sqrt{2}} \begin{cases} |\uparrow\downarrow\rangle - |\downarrow\uparrow\rangle & \text{if } \mu = 0 \\ -(|\uparrow\uparrow\rangle - |\downarrow\downarrow\rangle) & \text{if } \mu = 1 \\ i(|\uparrow\uparrow\rangle - |\downarrow\downarrow\rangle) & \text{if } \mu = 2 \\ |\uparrow\downarrow\rangle + |\downarrow\uparrow\rangle & \text{if } \mu = 3 \end{cases} \tag{2.20}
$$

We reintroduce operators $\chi^{\mu\dagger}_{ij}$ and χ^{μ}_{ij} that create and annihilate a μ-flavored bond between distinct sites i and j. Like operators can be reordered among themselves, viz., $[\chi^{\mu}_{ij}, \chi^{\nu}_{kl}] = [\chi^{\mu\dagger}_{ij}, \chi^{\nu\dagger}_{kl}] = 0$,

but the commutation relation between unlike operators is nontrivial:

$$[\chi^{\mu}_{ij}, \chi^{\nu\dagger}_{kl}] = (\delta_{ik}\delta_{jl} + s^{\mu}\delta_{il}\delta_{jk})\delta^{\mu\nu} + \frac{1}{2}M^{\mu\nu\lambda}\big(\delta_{jl}T^{\lambda}_{ki} + s^{\mu}s^{\nu}\delta_{ik}T^{\lambda}_{ki} + s^{\mu}\delta_{il}T_{kj} + s^{\nu}\delta_{jk}T^{\lambda}_{li}\big), \quad (2.21)$$

Here, a summation over $\lambda = 0, 1, 2, 3$ is implied; the vector $s^{\mu} = (1 - 2\delta^{\mu,0}) = (-1)^{\delta^{\mu,0}} = (-1, 1, 1, 1)$ is a signature; and

$$M^{\mu\nu\lambda} = \frac{1}{2}\mathrm{tr}\sigma^{\mu}\sigma^{\nu}\sigma^{\lambda} \quad (2.22)$$

$$= \delta^{\mu 0}\delta^{\nu\lambda} + \delta^{\nu 0}\delta^{\mu\lambda} + (1 - 2\delta^{\mu 0}\delta^{\nu 0})\delta^{\mu\nu} + i\epsilon^{0\mu\nu\lambda} \quad (2.23)$$

is a mixing matrix between singlet and triplet flavors. The operator T^{μ}_{ij} on the right of Eq. (2.21) moves the end-point of a valence bond from site j to i, rotating its flavor directions by μ. The rearrangements are encoded by

$$\big[T^{\mu}_{ij}, \chi^{\nu}_{kl}\big] = M^{\mu\nu\lambda}\big(\delta_{jk}\chi^{\lambda\dagger}_{il} + s^{\nu}\delta_{jl}\chi^{\lambda\dagger}_{ik}\big). \quad (2.24)$$

Another way, we can define a valence-bond operator explicitly:

$$\chi^{\mu\dagger}_{ij} = \frac{1}{2S\sqrt{2}}\sum_{ss'}\sum_{\alpha\beta}\tau^{\mu}_{ss'}b^{\alpha\dagger}_{is}b^{\beta\dagger}_{js'} \quad (2.25)$$

with $s, s' = \uparrow, \downarrow$ and the pseudo-Pauli spin matrices $\tau^{\mu} = \sigma^{\mu}i\sigma^{2}$, as mentioned previously. We have extended the notation so that the operators $b^{\dagger}_{i\uparrow} \equiv a^{\dagger}_{i}$ and $b^{\dagger}_{i\downarrow} \equiv b^{\dagger}_{i}$. The valence bond operator does not only represent the singlet but also triplet bonds for an arbitrary spin-S. Also, we can write

Eq. (2.21) in more detail:

$$\begin{cases} \chi_{ij}^{0\dagger} = \dfrac{1}{2S\sqrt{2}} \sum\limits_{\alpha,\beta} \left(a_i^{\alpha\dagger} b_j^{\beta\dagger} - b_i^{\alpha\dagger} a_j^{\beta\dagger}\right) & \text{if } \mu = 0, \\ \chi_{ij}^{1\dagger} = \dfrac{-1}{2S\sqrt{2}} \sum\limits_{\alpha,\beta} \left(a_i^{\alpha\dagger} a_j^{\beta\dagger} - b_i^{\alpha\dagger} b_j^{\beta\dagger}\right) & \text{if } \mu = 1, \\ \chi_{ij}^{2\dagger} = \dfrac{i}{2S\sqrt{2}} \sum\limits_{\alpha,\beta} \left(a_i^{\alpha\dagger} a_j^{\beta\dagger} + b_i^{\alpha\dagger} b_j^{\beta\dagger}\right) & \text{if } \mu = 2, \\ \chi_{ij}^{3\dagger} = \dfrac{1}{2S\sqrt{2}} \sum\limits_{\alpha,\beta} \left(a_i^{\alpha\dagger} b_j^{\beta\dagger} + b_i^{\alpha\dagger} a_j^{\beta\dagger}\right) & \text{if } \mu = 3. \end{cases} \tag{2.26}$$

The general transition operator is redefined as

$$T^{\mu} = \frac{1}{2S} \sum_{ss'} \sum_{\alpha\beta} \sigma_{ss'}^{\mu} b_{is}^{\alpha\dagger} b_{js'}^{\beta\dagger}, \tag{2.27}$$

This operator will serve for transiting both the singlet and triplet states. We can summarize these operators as follows:

$$\left[\chi_{ij}^{0}, \chi_{kl}^{0\dagger}\right] = (\delta_{ik}\delta_{jl} - \delta_{il}\delta_{jk}) + \frac{1}{2}\left[\delta_{ik}T_{lj}^{0} + \delta_{jl}T_{ki}^{0} - \delta_{il}T_{kj}^{0} - \delta_{jk}T_{li}^{0}\right], \tag{2.28}$$

$$\left[\chi_{ij}^{0}, \chi_{kl}^{\mu\dagger}\right] = \frac{i}{2}\left[\delta_{ik}T_{lj}^{\mu} + \delta_{jl}T_{ki}^{\mu} - \delta_{il}T_{kj}^{\mu} - \delta_{jk}T_{li}^{\mu}\right], \qquad \text{with} \quad \mu \neq 0, \tag{2.29}$$

$$\left[\chi_{ij}^{\mu}, \chi_{kl}^{\mu\dagger}\right] = (\delta_{ik}\delta_{jl} + \delta_{il}\delta_{jk}) + \frac{1}{2}\left[\delta_{ik}T_{lj}^{0} + \delta_{jl}T_{ki}^{0} + \delta_{il}T_{kj}^{0} + \delta_{jk}T_{li}^{0}\right] \quad \text{with} \quad \mu \neq 0, \tag{2.30}$$

$$\left[\chi_{ij}^{\mu}, \chi_{kl}^{\nu\dagger}\right] = \frac{i\epsilon^{\mu\nu\lambda}}{2}\left[\delta_{ik}T_{lj}^{\lambda} + \delta_{il}T_{kj}^{\lambda} + \delta_{jl}T_{ki}^{\lambda} + \delta_{jk}T_{li}^{\lambda}\right], \qquad \text{with} \quad \mu, \nu \neq 0. \tag{2.31}$$

FFor any spin-S, the general states forms a nonorthogonal basis.

$$[T_{ij}^{\mu}, \chi_{kl}^{0\dagger}] = -\delta_{jk}\chi_{il}^{\mu\dagger} + \delta_{jl}\chi_{ik}^{\mu\dagger}, \qquad \text{with} \quad \mu \neq 0, \tag{2.32}$$

$$[T_{ij}^{0}, \chi_{kl}^{\mu\dagger}] = \delta_{jk}\chi_{il}^{\mu\dagger} + \delta_{jl}\chi_{ik}^{\mu\dagger}, \tag{2.33}$$

$$[T_{ij}^{\mu}, \chi_{kl}^{\nu\dagger}] = i\epsilon^{\mu\nu\lambda}\left(\delta_{jk}\chi_{il}^{\lambda\dagger} + \delta_{jl}\chi_{ik}^{\lambda\dagger}\right), \tag{2.34}$$

With the relations constructed in this section, we can provide a complete algebra for the ground

state and all excited states of the spin-S quantum system. Spin-rotation-breaking terms, such as a magnetic field can even be included within the Hamiltonian. However, for all the remaining calculations in this dissertation, I focus on the total spin singlet sector, and I will suppress the flavor label. Only singlet operators are used.

2.1.3 Valence bond as a nonorthogonal basis

A quantum many-body state, constructed from fermion or boson particles is orthogonal to other such states in the Hilbert space. However, the general valence bond state is *nonorthogonal* and *overcomplete*. We denote fermionic and bosonic states by a single index i or j (usually a site index); they satisfy three important relations:

$$[a_i, a_j^\dagger]_\zeta = \delta_{ij}, \quad [a_i, a_j]_\zeta = 0, \quad [a_i^\dagger, a_j^\dagger]_\zeta = 0, \tag{2.35}$$

where $\zeta = \pm 1$ for bosons and fermions, respectively. The commutation relation of the annihilation and creation valence operators does not followed the simple delta function [Eqs. (2.11) and (2.13)]. The nonorthogonal property is proved by overlapping the valence bond states in spin-half, spin-1 and spin-3/2 chains below.

If we consider a case of four-site spin-half in a chain, there are two physical states: $|\psi_1\rangle$ and $|\psi_2\rangle$,

$$|\psi_1\rangle = \chi_{12}^\dagger \chi_{3,4}^\dagger |\text{vac}\rangle, \tag{2.36}$$

$$|\psi_2\rangle = \chi_{3,2}^\dagger \chi_{1,4}^\dagger |\text{vac}\rangle, \tag{2.37}$$

as illustrated by graphs:

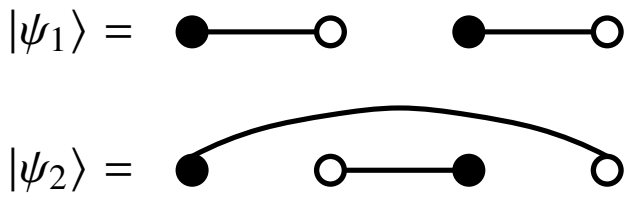

We take the overlap of the same state $\langle\psi_1|\psi_1\rangle = \langle \text{vac}| \chi_{12}\chi_{34}\chi^\dagger_{34}\chi^\dagger_{12} |\text{vac}\rangle = 1$, but two different states:

$\langle\psi_1|\psi_2\rangle = \langle \text{vac}| \chi_{12}\chi_{34}\chi^\dagger_{32}\chi^\dagger_{14} |\text{vac}\rangle = 1/2 \neq 0$. We can summarize them in terms of a real 2×2 matrix,

$$\begin{pmatrix} \langle\psi_1|\psi_1\rangle & \langle\psi_1|\psi_2\rangle \\ \langle\psi_2|\psi_1\rangle & \langle\psi_2|\psi_2\rangle \end{pmatrix} = \begin{pmatrix} 1 & 1/2 \\ 1/2 & 1 \end{pmatrix}. \tag{2.38}$$

In a four-site spin-1 chain, there are three physical states:

$$|\psi_{\text{VBS}}\rangle = \chi^\dagger_{12}\chi^\dagger_{32}\chi^\dagger_{3,4}\chi^\dagger_{1,4} |\text{vac}\rangle, \tag{2.39}$$

$$|\psi_{\text{dimer1}}\rangle = (\chi^\dagger_{1,2})^2(\chi^\dagger_{3,4})^2 |\text{vac}\rangle, \tag{2.40}$$

$$|\psi_{\text{dimer2}}\rangle = (\chi^\dagger_{3,2})^2(\chi^\dagger_{1,4})^2 |\text{vac}\rangle. \tag{2.41}$$

We can draw them as following:

$|\Psi_{\text{VBS}}\rangle =$ 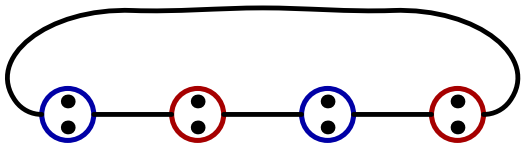

$|\Psi_{\text{dimer1}}\rangle =$ 

$|\Psi_{\text{dimer2}}\rangle =$ 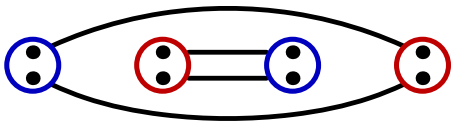

Similarly, we can summarize the overlapping of the three states in terms of a real 3×3

matrix:

$$\begin{pmatrix} \langle\psi_{\rm VBS}|\psi_{\rm VBS}\rangle & \langle\psi_{\rm VBS}|\psi_{\rm dimer1}\rangle & \langle\psi_{\rm VBS}|\psi_{\rm dimer2}\rangle \\ \langle\psi_{\rm dimer1}|\psi_{\rm VBS}\rangle & \langle\psi_{\rm dimer1}|\psi_{\rm dimer1}\rangle & \langle\psi_{\rm dimer1}|\psi_{\rm dimer2}\rangle \\ \langle\psi_{\rm dimer2}|\psi_{\rm VBS}\rangle & \langle\psi_{\rm dimer2}|\psi_{\rm dimer1}\rangle & \langle\psi_{\rm dimer2}|\psi_{\rm dimer2}\rangle \end{pmatrix} = \begin{pmatrix} 21/4 & 9/2 & 9/2 \\ 9/2 & 9 & 3 \\ 9/2 & 3 & 9 \end{pmatrix} = 9 \begin{pmatrix} 7/12 & 1/2 & 1/2 \\ 1/2 & 1 & 1/3 \\ 1/2 & 1/3 & 1 \end{pmatrix}. \tag{2.42}$$

In the spin-3/2 case, there are four physical states in a four-site chain:

$$|\psi_1\rangle = \chi^\dagger_{12}(\chi^\dagger_{32})^2\chi^\dagger_{3,4}(\chi^\dagger_{1,4})^2\,|{\rm vac}\rangle, \tag{2.43}$$

$$|\psi_2\rangle = (\chi^\dagger_{1,2})^2\chi^\dagger_{32}(\chi^\dagger_{3,4})^2\chi^\dagger_{1,4}\,|{\rm vac}\rangle, \tag{2.44}$$

$$|\psi_3\rangle = (\chi^\dagger_{1,2})^3(\chi^\dagger_{3,4})^3\,|{\rm vac}\rangle, \tag{2.45}$$

$$|\psi_4\rangle = (\chi^\dagger_{3,2})^3(\chi^\dagger_{1,4})^3\,|{\rm vac}\rangle, \tag{2.46}$$

The overlap of these four states is summarized in a 4×4 matrix:

$$\begin{aligned} \begin{pmatrix} \langle\psi_1|\psi_1\rangle & \langle\psi_1|\psi_2\rangle & \langle\psi_1|\psi_3\rangle & \langle\psi_1|\psi_4\rangle \\ \langle\psi_2|\psi_1\rangle & \langle\psi_2|\psi_2\rangle & \langle\psi_2|\psi_3\rangle & \langle\psi_2|\psi_4\rangle \\ \langle\psi_3|\psi_1\rangle & \langle\psi_3|\psi_2\rangle & \langle\psi_3|\psi_3\rangle & \langle\psi_3|\psi_4\rangle \\ \langle\psi_4|\psi_1\rangle & \langle\psi_4|\psi_2\rangle & \langle\psi_4|\psi_3\rangle & \langle\psi_4|\psi_4\rangle \end{pmatrix} &= \begin{pmatrix} 156 & 129 & 108 & 108 \\ 129 & 156 & 108 & 108 \\ 108 & 108 & 324 & 162 \\ 108 & 108 & 162 & 324 \end{pmatrix} \\ &= 324 \begin{pmatrix} 13/27 & 43/108 & 1/3 & 1/3 \\ 43/108 & 13/27 & 1/3 & 1/3 \\ 1/3 & 1/3 & 1 & 1/2 \\ 1/3 & 1/3 & 1/2 & 1 \end{pmatrix} \end{aligned} \tag{2.47}$$

A comparable demonstration can be made for the bond patterns allowed for each spin value S.

2.1.4 Representation of the interacting spin terms by valence-bond operators

Based on the above definitions, we develop a translation table from the language of conventional spin operators to the language of valence bond operators. We define spin-S in terms of the

creation and annihilation of singlet bonds:

$$\mathbf{S}_i \cdot \mathbf{S}_j = S^2 - \chi_{ij}^\dagger \chi_{ij}. \tag{2.48}$$

We construct the higher powers of the bilinear Heisenberg term by expanding and normal ordering:

$$\begin{aligned}(\mathbf{S}_i \cdot \mathbf{S}_j)^2 &= (S^2 - \chi_{ij}^\dagger \chi_{ij})(S^2 - \chi_{ij}^\dagger \chi_{ij}), \\ &= S^4 - 2S^2 \chi_{ij}^\dagger \chi_{ij} + \chi_{ij}^\dagger \chi_{ij} \chi_{ij}^\dagger \chi_{ij}.\end{aligned} \tag{2.49}$$

Here, $N_{ij} = N_{ii} + N_{jj}$. When N_{ij} acts on properly constructed physical state, it will give the number $4S$. Accordingly,

$$\chi_{ij}^\dagger \chi_{ij} \chi_{ij}^\dagger \chi_{ij} = \chi_{ij}^\dagger \chi_{ij} \frac{1}{2} N_{ij} + (\chi_{ij}^\dagger)^2 (\chi_{ij})^2, \tag{2.50}$$

$$\chi_{ij}^\dagger \chi_{ij} (\chi_{ij}^\dagger)^2 (\chi_{ij})^2 = (\chi_{ij}^\dagger)^2 (\chi_{ij})^2 \left(-1 + N_{ij}\right) + (\chi_{ij}^\dagger)^3 (\chi_{ij})^3, \tag{2.51}$$

$$\chi_{ij}^\dagger \chi_{ij} (\chi_{ij}^\dagger)^3 (\chi_{ij})^3 = (\chi_{ij}^\dagger)^3 (\chi_{ij})^3 \left(-3 + \frac{3}{2} N_{ij}\right) + (\chi_{ij}^\dagger)^4 (\chi_{ij})^4, \tag{2.52}$$

$$\chi_{ij}^\dagger \chi_{ij} (\chi_{ij}^\dagger)^4 (\chi_{ij})^4 = (\chi_{ij}^\dagger)^4 (\chi_{ij})^4 \left(-6 + 2N_{ij}\right) + (\chi_{ij}^\dagger)^5 (\chi_{ij})^5, \tag{2.53}$$

$$\chi_{ij}^\dagger \chi_{ij} (\chi_{ij}^\dagger)^5 (\chi_{ij})^5 = (\chi_{ij}^\dagger)^5 (\chi_{ij})^5 \left(-10 + \frac{5}{2} N_{ij}\right) + (\chi_{ij}^\dagger)^6 (\chi_{ij})^6 \tag{2.54}$$

$$\vdots \tag{2.55}$$

$$\chi_{ij}^\dagger \chi_{ij} (\chi_{ij}^\dagger)^n (\chi_{ij})^n = (\chi_{ij}^\dagger)^n (\chi_{ij})^n \left(-\frac{n(n-1)}{2} + \frac{n}{2} N_{ij}\right) + (\chi_{ij}^\dagger)^{n+1} (\chi_{ij})^{n+1} \tag{2.56}$$

Now, I can represent all terms of the Hamiltonian up to quartic power.

$$\mathbf{S}_i \cdot \mathbf{S}_j = S^2 - \chi_{ij}^\dagger \chi_{ij}, \tag{2.57}$$

$$(\mathbf{S}_i \cdot \mathbf{S}_j)^2 = S^4 - 2S^2 \chi_{ij}^\dagger \chi_{ij} + \frac{1}{2}\chi_{ij}^\dagger \chi_{ij} N_{ij} + (\chi_{ij}^\dagger)^2 (\chi_{ij})^2, \tag{2.58}$$

$$\begin{aligned}(\mathbf{S}_i \cdot \mathbf{S}_j)^3 = {} & S^6 - 3S^4 \chi_{ij}^\dagger \chi_{ij} + \frac{3S^2}{2}\chi_{ij}^\dagger \chi_{ij} N_{ij} - \frac{1}{4}\chi_{ij}^\dagger \chi_{ij} (N_{ij})^2 \\ & + (3S^2+1)(\chi_{ij}^\dagger)^2 (\chi_{ij})^2 - \frac{3}{2}(\chi_{ij}^\dagger)^2 (\chi_{ij})^2 N_{ij} - (\chi_{ij}^\dagger)^3 (\chi_{ij})^3.\end{aligned} \tag{2.59}$$

$$\begin{aligned}(\mathbf{S}_i \cdot \mathbf{S}_j)^4 = {} & S^8 - 3S^6 \chi_{ij}^\dagger \chi_{ij} + 3S^4 \chi_{ij}^\dagger \chi_{ij} N_{ij} - S^2 \chi_{ij}^\dagger \chi_{ij} (N_{ij})^2 + \frac{1}{8}\chi_{ij}^\dagger \chi_{ij} (N_{ij})^3 \\ & + (6s^4 + 4S^2 + 1)(\chi_{ij}^\dagger)^2 (\chi_{ij})^2 - (6S^2 + \frac{5}{2})(\chi_{ij}^\dagger)^2 (\chi_{ij})^2 N_{ij} + \frac{7}{4}(\chi_{ij}^\dagger)^2 (\chi_{ij})^2 (N_{ij})^2 \\ & - (4S^2+4)(\chi_{ij}^\dagger)^3 (\chi_{ij})^3 + 3(\chi_{ij}^\dagger)^3 (\chi_{ij})^3 N_{ij} + (\chi_{ij}^\dagger)^4 (\chi_{ij})^4.\end{aligned} \tag{2.60}$$

There is no impediment to carrying out this procedure for high powers still.

2.1.5 Update Projector

Our definition starts from a proof by Sandvik [63] that: "any singlet state can be expressed as a sum of valence bond states, and the ground state can be **projected** out of an arbitrary valence bond state by applying a high power of the Hamiltonian". It is the heart of *Projector Monte Carlo* method [63, 64]. For each time when the state is acted by the Hamiltonian, a new valence bond configuration may occur, at least the spin-half case. We called that the *reconfiguration* or *rearrangement* —**update**, which is the central properties of the valence bond basis. The spin Hamiltonian includes the different powers of normal ordering of the creation and annihilation operators (proved in the next section). Therefore, we define the operators as their products

$$\mathcal{P}_{i,j}^{(n)} = \frac{2^n}{n!(n+1)!}(\chi_{i,j}^\dagger)^n (\chi_{i,j})^n. \tag{2.61}$$

Such operators are free to act on all possible valence bond configurations, with n running up to the maximum of $2S$ bonds emerging per site. $\mathcal{P}_{i,j}^0$ is the identity operator; otherwise $\mathcal{P}_{i,j}^n$ projects onto

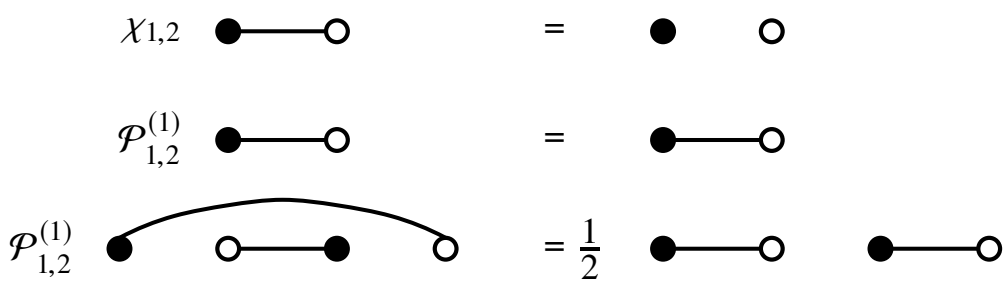

Figure 2.2: Singlet operator and update projector $\mathcal{P}^{(1)}_{1,2}$ in spin-half chain. The spin site is counted from left to right.

the state with n bonds connecting i and j.

$$\begin{cases} \mathcal{P}^{(0)}_{i,j} = \dfrac{2^0}{0!(0+1)!}(\chi^\dagger_{i,j})^0(\chi_{i,j})^0 = \mathbb{1}, \\ \mathcal{P}^{(1)}_{i,j} = \dfrac{2^1}{1!(1+1)!}(\chi^\dagger_{i,j})^1(\chi_{i,j})^1 = \chi^\dagger_{i,j}\chi_{i,j}, \\ \mathcal{P}^{(2)}_{i,j} = \dfrac{2^2}{2!(2+1)!}(\chi^\dagger_{i,j})^2(\chi_{i,j})^2 = \dfrac{1}{3}(\chi^\dagger_{i,j})^2(\chi_{i,j})^2, \\ \mathcal{P}^{(3)}_{i,j} = \dfrac{2^3}{3!(3+1)!}(\chi^\dagger_{i,j})^3(\chi_{i,j})^3 = \dfrac{1}{18}(\chi^\dagger_{i,j})^3(\chi_{i,j})^3, \\ \mathcal{P}^{(4)}_{i,j} = \dfrac{2^4}{4!(4+1)!}(\chi^\dagger_{i,j})^4(\chi_{i,j})^4 = \dfrac{1}{180}(\chi^\dagger_{i,j})^4(\chi_{i,j})^4, \end{cases} \tag{2.62}$$

The normalization factors (1, 1, 3, 18, 180, 2700, 56700, 1587600, . . . ; see https://oeis.org/A006472) are chosen such that

$$\mathcal{P}^{(n)}_{i,j}\big(\chi^\dagger_{i,j}\big)^n |\mathrm{vac}\rangle = 1\big(\chi^\dagger_{i,j}\big)^n |\mathrm{vac}\rangle\,, \tag{2.63}$$

is an eigenvector of $\mathcal{P}^{(n)}_{i,j}$ with eigenvalue 1. In terms of such projectors, the recurrence relation equivalent to Eq. (2.56) is

$$2\mathcal{P}^{(1)}_{i,j}\mathcal{P}^{(n)}_{i,j} = \big[(4S+1)n - n^2\big]\mathcal{P}^{(n)}_{i,j} + (n+1)(n+2)\mathcal{P}^{(n+1)}_{i,j}. \tag{2.64}$$

It is then straightforward to express the powers of $\mathbf{S}_i \cdot \mathbf{S}_j$ as linear combinations of the $\mathcal{P}_{i,j}^{(n)}$ operators:

$$
\begin{aligned}
\mathbf{S}_i \cdot \mathbf{S}_j &= S^2 - \mathcal{P}_{i,j}^{(1)} \\
\left(\mathbf{S}_i \cdot \mathbf{S}_j\right)^2 &= S^4 + 2S\left(1 - S\right)\mathcal{P}_{i,j}^{(1)} + 3\mathcal{P}_{i,j}^{(2)} \\
\left(\mathbf{S}_i \cdot \mathbf{S}_j\right)^3 &= S^6 - S^2(4 - 6S + 3S^2)\mathcal{P}_{i,j}^{(1)} + 3(1 - 6S + 3S^2)\mathcal{P}_{i,j}^{(2)} - 18\mathcal{P}_{i,j}^{(3)} \\
\left(\mathbf{S}_i \cdot \mathbf{S}_j\right)^4 &= S^8 + 4(1 - S)S^3(2 - 2S + S^2)\mathcal{P}_{i,j}^{(1)} + 3(1 - 10S + 32S^2 - 24S^3 + 6S^4)\mathcal{P}_{i,j}^{(2)} \\
&\qquad - 72(1 - 3S + S^2)\mathcal{P}_{i,j}^{(3)} + 180\mathcal{P}_{i,j}^{(4)} \\
\left(\mathbf{S}_i \cdot \mathbf{S}_j\right)^5 &= S^{10} - S^4(16 - 40S + 40S^2 - 20S^3 + 5S^4)\mathcal{P}_{i,j}^{(1)} + \\
&\qquad 3(1 - 14S + 73S^2 - 170S^3 + 150S^4 - 60S^5 + 10S^6)\mathcal{P}_{i,j}^{(2)} \\
&\qquad - 18(13 - 70S + 120S^2 - 60S^3 + 10S^4)\mathcal{P}_{i,j}^{(3)} \\
&\qquad + 900(2 - 4S + S^2)\mathcal{P}_{i,j}^{(4)} - 2700\mathcal{P}_{i,j}^{(5)} \\
&\vdots \\
\left(\mathbf{S}_i \cdot \mathbf{S}_j\right)^n &= S^{2n}\Bigg[1 + \left(-\frac{n}{S^2} + \frac{n(n-1)}{S^3} - \frac{2n(n+1)(n-1)}{3S^4} + \cdots\right)\mathcal{P}_{i,j}^{(1)} \\
&\qquad + \left(\frac{3n(n-1)}{2S^4} + \cdots\right)\mathcal{P}_{i,j}^{(2)} + \cdots\Bigg]
\end{aligned}
\tag{2.65}
$$

We demonstrate application of these operators for some simple cases of spin-S in a chain.

The first example is cases of two- and four-site spin-half on a chain (Fig. 2.2). The annihilation operator $\chi_{1,2}$ destroys the singlet bond connecting between site 1 and 2. The first-order update projector $\mathcal{P}_{i,j}^{(1)}$ acting on the singlet bond connecting site i and j gives us the eigenvalue 1. However, if the operator acts on a state which does not include bond $(i = 1, j = 2)$ like

$$
\begin{aligned}
\mathcal{P}_{1,2}^{(1)}\chi_{3,2}^{\dagger}\chi_{1,4}^{\dagger}\left|\mathrm{vac}\right\rangle &= \chi_{1,2}^{\dagger}\chi_{1,2}\left|\mathrm{vac}\right\rangle \chi_{3,2}^{\dagger}\chi_{1,4}^{\dagger}\left|\mathrm{vac}\right\rangle \\
&= \chi_{1,2}^{\dagger}\left(\frac{1}{2}T_{3,1}\right)\chi_{1,4}^{\dagger}\left|\mathrm{vac}\right\rangle = \frac{1}{2}\chi_{1,2}^{\dagger}\chi_{3,4}^{\dagger}\left|\mathrm{vac}\right\rangle .
\end{aligned}
\tag{2.66}
$$

This process is called the *reconfiguration* (lowest plot in Fig. 2.2). Now if we want to act the second-order projector $\mathcal{P}_{1,2}^{(1)}$ on the spin-half chain, that physical states will be vanished. So, the

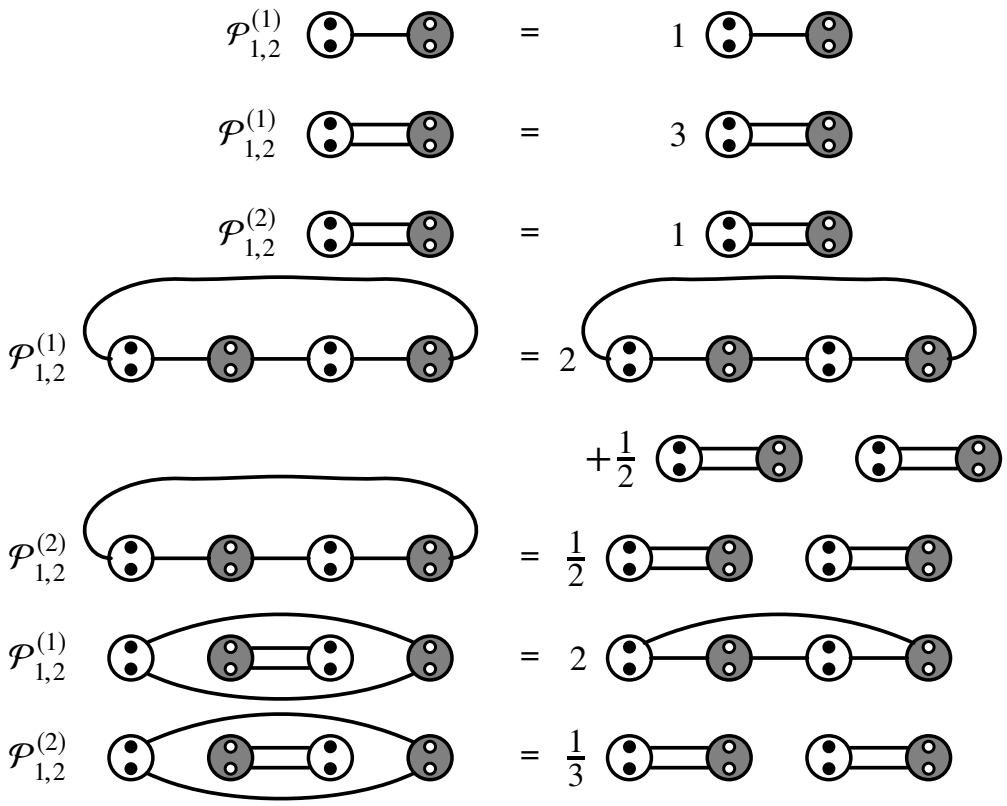

Figure 2.3: Update projectors $\mathcal{P}^{(n)}_{1,2}$ acting on physical states of spin-1 chain.

higher power term in Eq. (2.1) for the spin-half contains no useful information. For example,

$$\begin{aligned}\mathcal{P}^{(2)}_{1,2}\chi^{\dagger}_{3,2}\chi^{\dagger}_{1,4}\,|\mathrm{vac}\rangle &= (\chi^{\dagger}_{1,2})^2(\chi_{1,2})^2\,|\mathrm{vac}\rangle\,\chi^{\dagger}_{3,2}\chi^{\dagger}_{1,4}\,|\mathrm{vac}\rangle \\ &= (\chi^{\dagger}_{1,2})^2\chi_{1,2}\Big(\frac{1}{2}T_{3,1}\Big)\chi^{\dagger}_{1,4}\,|\mathrm{vac}\rangle = \frac{1}{2}(\chi^{\dagger}_{1,2})^2\chi_{1,2}\chi^{\dagger}_{3,4}\,|\mathrm{vac}\rangle = 0\,|\mathrm{vac}\rangle\,.\end{aligned} \tag{2.67}$$

Therefore, the general Hamiltonian for the spin-half cases restricts to the Heisenberg term.

For the spin-1 case, there are two update projectors $\mathcal{P}^{(1)}_{i,j}$ and $\mathcal{P}^{(2)}_{i,j}$ which are included in the Hamiltonian [Eq. (2.1)]. Furthermore, the biquadratic term consists of the two projectors [Eq. (2.65)] while the bilinear term only contains the first-order projector. The two update projectors are able to act on the physical states in the spin-1 cases. That is the physical significance to explain why we extend to the higher power sums in the general Hamiltonian [Eq. (2.1)]. For the two-site spin-1 chain, this is a trivial case on which we take the update projectors act (Fig. 2.3). We will start with the case of four sites.

If we take the first-order update projector $\mathcal{P}^{(1)}_{i=1,j=2}$ act on the VBS state (filling by all single bonds) in a chain, we will receive back the original state and a dimerized state (only double bonds connecting two nearest-neighbor sites). However, by acting the second-order $\mathcal{P}^{(1)}_{i=1,j=2}$on the VBS state, the result is only the dimerized state (Fig. 2.3), and so on. This is because there are only three physical states in the four-site spin-1 chain (previous section).

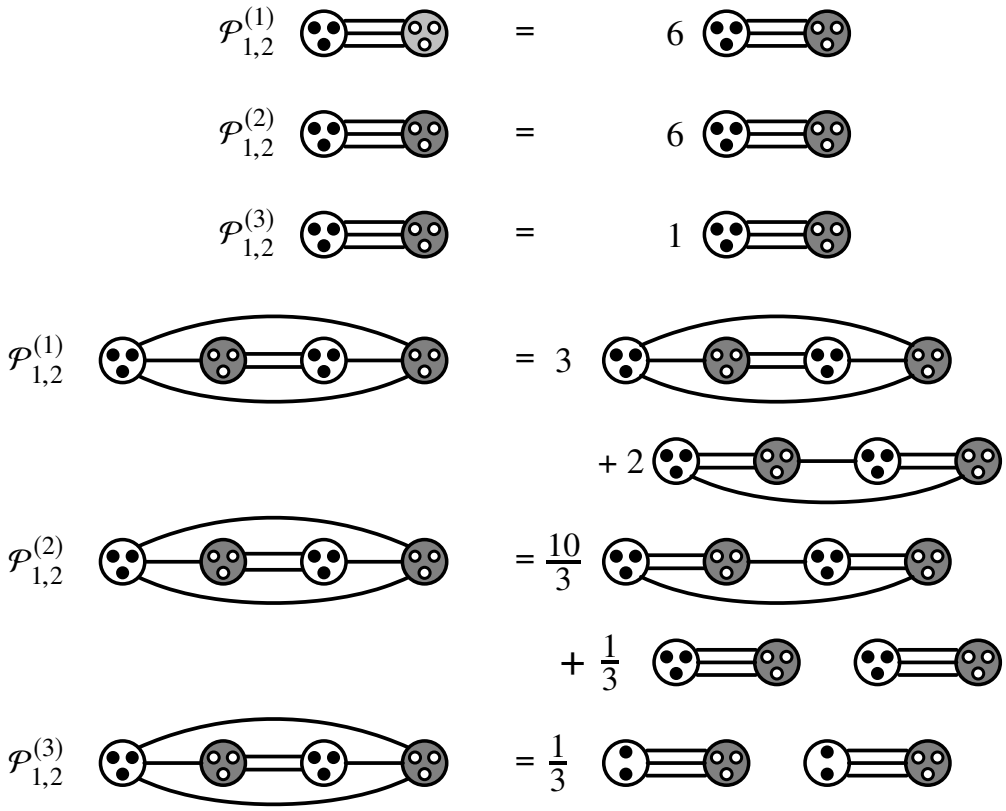

Figure 2.4: Update projectors $\mathcal{P}^{(n)}_{1,2}$ acting on physical states of a spin-3/2 chain.

For the spin-3/2 chain, the situation become more complicated because there are mixing of single, double and triple bond(s) emerging from each site. When acting the update projectors on the four physical states, several other states are created (illustrated in Fig. 2.4).

2.2 Verify the AKLT model in spin-1 chain, spin-3/2 hexagonal, and spin-2 system in a chain and square lattice

Using identities in Sect. 2.1, we prove how our language works for quantum spin systems by providing four different examples of the fixed-point AKLT model. Those coefficients [Eq. (2.1)]

agree with the non-deformed AKLT models which are stated in Table. 1 of Ref. [11].

First, we break the global Hamiltonian into the sum of local terms: $\hat{H} = \sum_{\langle ij \rangle} H_{ij}$. Then, we take the local H_{ij} terms acting on a presumptive valence-bond-solid state, which only contains the static short bonds uniformly tiling the entire lattice. It is believed to be the ground state of the AKLT model.

Because both situations are on bipartite lattices and an even number of spin sites, we can set $i \in A$ sublattice, and $j \in B$ sublattice. Each valence-bond symbol always starts from site i and ends at site j. We hold the periodic boundary conditions for our calculations.

2.2.1 Spin-1 chain AKLT model

First, we transform the local Hamiltonian $H_{i,j}$ represented by the valence-bond operators. In the spin-1 chain, the next-nearest-neighbor is on the left or on the right.

$$\begin{aligned} \hat{H}_{i,j} &= \alpha_1(\mathbf{S}_i \cdot \mathbf{S}_j) + \alpha_2(\mathbf{S}_i \cdot \mathbf{S}_j)^2 \qquad \text{(Spin language)} \\ &= (\alpha_1 S^2 + \alpha_2 S^4) - \left(\alpha_1 + 2\alpha_2 S^2\right)\chi^\dagger_{i,j}\chi_{i,j} + \frac{\alpha_2}{2}\chi^\dagger_{i,j}\chi_{i,j}\hat{N}_{i,j} \\ &\quad + \alpha_2(\chi^\dagger_{i,j})^2(\chi_{i,j})^2. \qquad \text{(Valence-bond language)} \end{aligned} \tag{2.68}$$

Alternatively, we can write the Hamiltonian in terms of the update projectors $\mathcal{P}^{(n)}_{i,j}$ from the previous section:

$$\hat{H}_{i,j} = (\alpha_1 S^2 + \alpha_2 S^4)\mathcal{P}^{(0)}_{i,j} - \left[\alpha_1 + 2\alpha_2 S(S-1)\right]\mathcal{P}^{(1)}_{i,j} + 3\alpha_2\mathcal{P}^{(2)}_{i,j} \qquad \text{(Update projector language).} \tag{2.69}$$

As the above introduction, Affleck *et al*. proposed the ground state of the fixed-point AKLT Hamiltonian is a valence-bond-solid state $|\Psi_{\text{VBS}}\rangle$ [46]. In a spin-1 chain, each site is composed of two spin-halves: $\frac{1}{2} \otimes \frac{1}{2} = 0 \oplus 1$. We remove the singlet state on the same site, so two spin-halves form a pure spin-1. The VBS state has each spin-1 on the site i connecting through one bond with the site $i-1$ on the left and another with the site $i+1$ on the right. There are only two states when

we take the local Hamiltonian acting on the VBS state:

$$|\Psi_{\text{VBS}}\rangle = \prod_{\langle i\in \text{A}, j\in \text{B}\rangle} \chi^{\dagger}_{i,j} |\text{vac}\rangle, \tag{2.70}$$

$$|\Psi_{\text{Perturb}}\rangle = \chi^{\dagger}_{12}\chi^{\dagger}_{23}\cdots\chi^{\dagger}_{i-1,i+2}(\chi^{\dagger}_{i,i+1})^2\cdots\chi^{\dagger}_{N,1}|\text{vac}\rangle. \tag{2.71}$$

They are described graphically:

$|\Psi_{\text{VBS}}\rangle =$

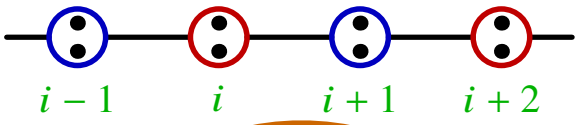

$|\Psi_{\text{Perturb}}\rangle =$

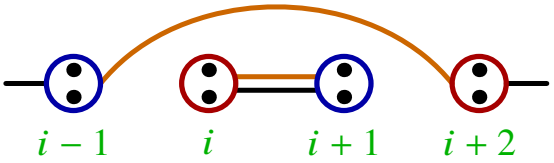

However, when the first-order projector operator $\mathcal{P}^{(1)}_{i,j}$ acts on the VBS state, it gives back the original state and creates an additional perturbation state $|\Psi_{\text{Perturb}}\rangle$. For the perturbed state, a double valence-bond connecting two sites i and $i+1$, and a "bridge", long valence-bond, matching site $i-1$ with $i+2$ are created.

$$\mathcal{P}^{(1)}_{i,j}|\Psi_{\text{VBS}}\rangle = 2|\Psi_{\text{VBS}}\rangle + \frac{1}{2}|\Psi_{\text{Perturb}}\rangle, \tag{2.72}$$

$$\mathcal{P}^{(2)}_{i,j}|\Psi_{\text{VBS}}\rangle = \frac{1}{2}|\Psi_{\text{Perturb}}\rangle. \tag{2.73}$$

We take the Hamiltonian in Eq. (2.68) act on the valence-bond-state:

$$\begin{aligned}\hat{H}_{ij}|\Psi_{\text{VBS}}\rangle = {} & (\alpha_1 S^2 + \alpha_2 S^4) + [-2\alpha_1 + (4 - 4S^2)\alpha_2]|\Psi_{\text{VBS}}\rangle \\ & + \left[\frac{\alpha_1}{2} - \frac{3\alpha_2}{2} + (S^2 - 1)\right]|\Psi_{\text{Perturb}}\rangle,\end{aligned} \tag{2.74}$$

With the value $\alpha_2 = 1/3\alpha_1$ and $S = 1$, the perturbation term vanishes in Eq. (2.74). The result that I have derived is exactly similar to the calculations in Refs. [11, 46, 47].

2.2.2 Spin-3/2 hexagonal lattice

Now, the general spin-3/2 Hamiltonian is represented in our new language:

$$\hat{H}_{i,j} = \alpha_1(\mathbf{S}_i \cdot \mathbf{S}_j) + \alpha_2(\mathbf{S}_i \cdot \mathbf{S}_j)^2 + \alpha_3(\mathbf{S}_i \cdot \mathbf{S}_j)^3, \qquad \text{(spin language)} \tag{2.75}$$

$$\begin{aligned}\hat{H}_{i,j} = (\alpha_1 S^2 + \alpha_2 S^4 + \alpha_3 S^6) - \left(\alpha_1 + 2\alpha_2 S^2 + 3\alpha_3 S^4\right)\chi^\dagger_{i,j}\chi_{i,j} + \left(\frac{\alpha_2}{2} + \frac{3\alpha_3 S^2}{2}\right)\chi^\dagger_{i,j}\chi_{i,j}N_{i,j} \\ - \frac{\alpha_3}{4}\chi^\dagger_{i,j}\chi_{i,j}(N_{i,j})^2 + \left[\alpha_2 + (3S^2+1)\alpha_3\right](\chi^\dagger_{i,j})^2(\chi_{i,j})^2 - \frac{3\alpha_3}{2}(\chi^\dagger_{i,j})^2(\chi_{i,j})^2 N_{i,j} \\ - \alpha_3(\chi^\dagger_{i,j})^3(\chi_{i,j})^3, \qquad \text{(bond language).}\end{aligned} \tag{2.76}$$

When we substitute $S = 3/2$ and $N_{i,j} = 6$ (because there are three valence bonds emerging from each spin site), the local Hamiltonian is reduced to:

$$\hat{H}_{i,j} = \frac{9}{4}\left(\alpha_1 + \frac{9}{4}\alpha_2 + \frac{81}{16}\alpha_3\right) - \left(\alpha_1 + \frac{3}{2}\alpha_2 + \frac{63}{16}\alpha_3\right)\chi^\dagger_{i,j}\chi_{i,j} + \left(\alpha_2 - \frac{5}{4}\alpha_3\right)(\chi^\dagger_{i,j})^2(\chi_{i,j})^2 - \alpha_3(\chi^\dagger_{i,j})^3(\chi_{i,j})^3, \tag{2.77}$$

or in terms of the update projector language:

$$\hat{H}_{i,j} = \frac{9}{4}\left(\alpha_1 + \frac{9}{4}\alpha_2 + \frac{81}{16}\alpha_3\right)\mathcal{P}^{(0)}_{i,j} - \left(\alpha_1 + \frac{3}{2}\alpha_2 + \frac{63}{16}\alpha_3\right)\mathcal{P}^{(1)}_{i,j} + 3\left(\alpha_2 - \frac{5}{4}\alpha_3\right)\mathcal{P}^{(2)}_{i,j} - 18\alpha_3\mathcal{P}^{(3)}_{i,j}. \tag{2.78}$$

As shown in Fig. 2.5, we separate the hexagonal lattice into A (red circle) and B (blue circle) sublattices. We choose a bond $\langle ij \rangle$ around which we label five bonds. The local Hamiltonian only acts on those five bonds. The global spin-3/2 VBS on the hexagonal lattice is denoted as $|\Psi_{\text{VBS, Hex}}\rangle$, which covers the lattice by all short bonds. We define the first perturbation state $|\Psi_{\text{Pert1},1\to4}\rangle$, which includes four different configurations, each of which contains one long bond as illustrated in Fig. 2.6(b). The second perturbation state $|\Psi_{\text{Pert2},1\to2}\rangle$ includes two different configurations, with two long bonds as shown in Fig. 2.6(c).

Reconfiguration of the valence bonds when we act with each term of the Hamiltonian $\hat{H}_{i,j}$

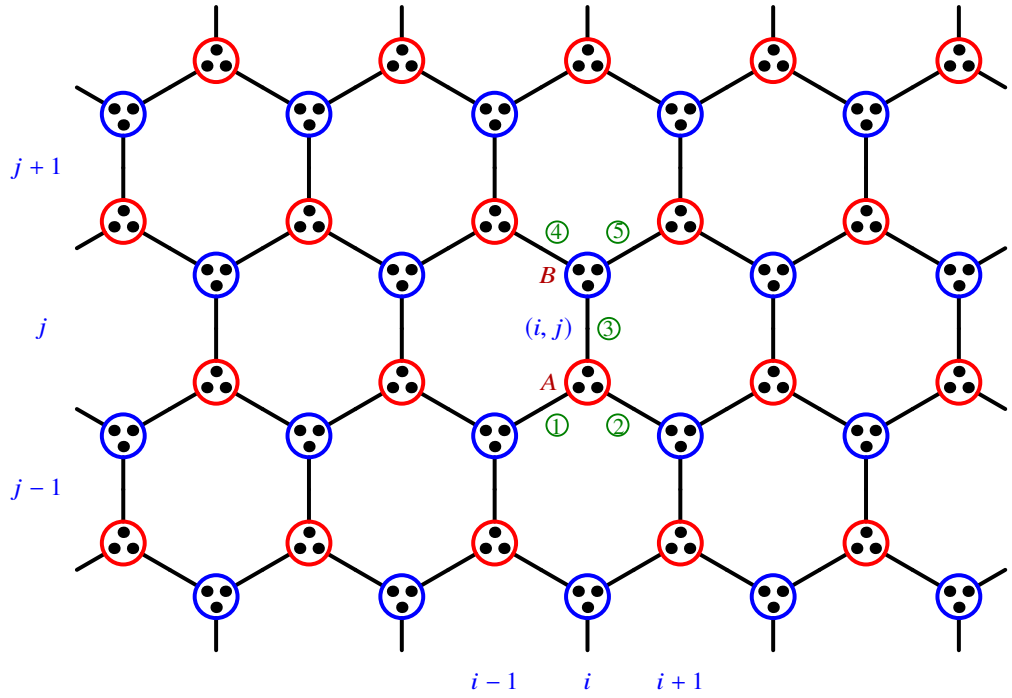

Figure 2.5: Representation of the spin-3/2 VBS state on a hexagonal lattice. Each spin-3/2 site (a red or blue circle) contains three virtual spin-half particles (black dots). It is like an atom consisting of three localized valence spin-half electrons. Each spin site connects with its neighbors by singlet bonds.

[Eq. (2.78)] on the valence-bond basis $|\Psi_{\text{VBS, Hex}}\rangle$ appeared as:

$$\mathcal{P}^{(1)}_{i,j,\text{A};i,j,\text{B}}\,|\Psi_{\text{VBS, Hex}}\rangle = 3\,|\Psi_{\text{VBS, Hex}}\rangle + \frac{1}{2}\,|\Psi_{\text{Pert1,1}\to 4}\rangle\,, \tag{2.79}$$

$$\mathcal{P}^{(2)}_{i,j,\text{A};i,j,\text{B}}\,|\Psi_{\text{VBS, Hex}}\rangle = \frac{5}{6}\,|\Psi_{\text{Pert1,1}\to 4}\rangle + \frac{1}{6}\,|\Psi_{\text{Pert2,1}\to 2}\rangle\,, \tag{2.80}$$

$$\mathcal{P}^{(3)}_{i,j,\text{A};i,j,\text{B}}\,|\Psi_{\text{VBS, Hex}}\rangle = \frac{1}{6}\,|\Psi_{\text{Pert2,1}\to 2}\rangle\,. \tag{2.81}$$

Now we obtain

$$\hat{H}_{i,j}\,|\Psi_{\text{VBS, Hex}}\rangle = \Big(-\frac{3}{4}\alpha_1 + \frac{9}{16}\alpha_2 - \frac{3}{8}\alpha_3\Big)\,|\Psi_{\text{VBS, Hex}}\rangle + \Big(-\frac{1}{2}\alpha_1 + \frac{7}{4}\alpha_2 - \frac{163}{32}\alpha_3\Big)\,|\Psi_{\text{Pert1,1}\to 4}\rangle + \Big(\frac{1}{2}\alpha_2 - \frac{29}{8}\alpha_3\Big)\,|\Psi_{\text{Pert2,1}\to 2}\rangle\,. \tag{2.82}$$

Comparison with the known result of the VBS state on the hexagonal lattice from Ref. [11] confirms

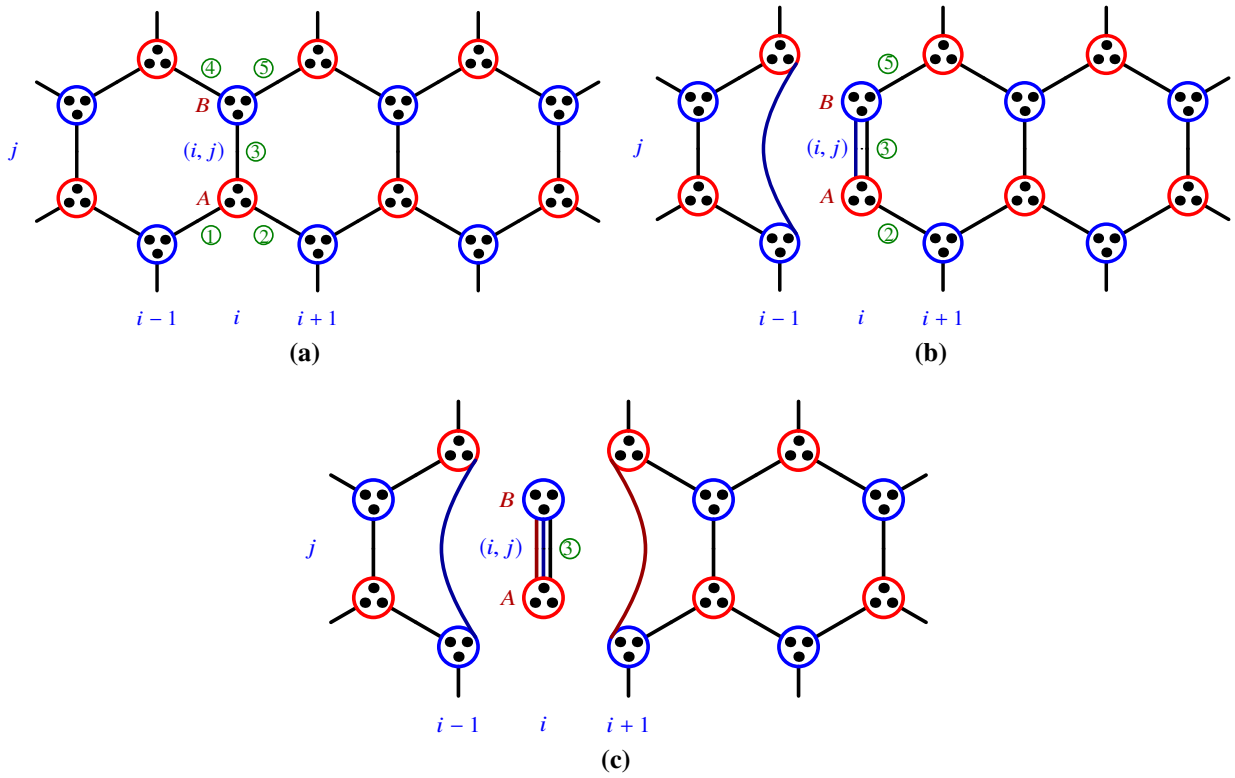

Figure 2.6: (a) Detail of a bond $\langle i, j\rangle$ and its neighboring bonds for the VBS state in hexagonal lattice. Illustrating (b) one graph of four configurations of the $|\Psi_{\text{Pert1},1\to4}\rangle$ state, and (c) one of two configurations of the $|\Psi_{\text{Pert2},1\to2}\rangle$ state.

that $\alpha_1 = 27/160$, $\alpha_2 = 29/360$ and $\alpha_3 = 1/90$. The second and the third term of Eq. (2.82) are zero in value. The VBS state is exactly the ground state of the Hamiltonian $\hat{H}_{i,j}$.

2.2.3 Spin-2 on a chain

The AKLT model can be defined on the linear chain with high multiplicity so that $2S$ bonds connect each neighboring pair of sites. For the spin-2 case, each site connects with its nearest neighbors by two bonds compared with one bond in spin-1 case (for this case $M = 2$).

$$|\Psi_{\text{VBS},S=2}\rangle = \prod_{\langle i,j\rangle} (\chi^{\dagger}_{i,j})^2 \, |\text{vac}\rangle \, . \tag{2.83}$$

Here, site j is the nearest neighbor of i. A graphical representation of the VBS state in spin-2 chain is

$|\Psi_{\mathrm{VBS},S=2}\rangle =$ 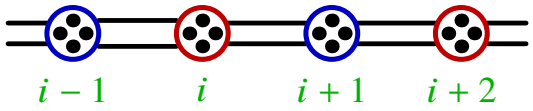

The general Hamiltonian of a spin-2 chain is

$$\hat{H}_{ij} = \alpha_1(\mathbf{S}_i \cdot \mathbf{S}_j) + \alpha_2(\mathbf{S}_i \cdot \mathbf{S}_j)^2 + \alpha_3(\mathbf{S}_j \cdot \mathbf{S}_j)^3 + \alpha_4(\mathbf{S}_i \cdot \mathbf{S}_j)^4. \tag{2.84}$$

$$\begin{aligned}
\hat{H}_{i,j} \;=\; & \big(\alpha_1 S^2 + \alpha_2 S^4 + \alpha_3 S^6 + \alpha_4 S^8\big) - (\alpha_1 + 2\alpha_2 S^2 + 3\alpha_3 S^4 + 4\alpha_4 S^6)\chi^\dagger_{i,j}\chi_{i,j} \\
& + \Big[\frac{\alpha_2}{2} + \frac{3\alpha_3 S^2}{2} + 3\alpha_4 S^4\Big]\chi^\dagger_{i,j}\chi_{i,j}\hat{N}_{i,j} \\
& - \Big[\frac{\alpha_3}{4} + \alpha_4 S^2\Big]\chi^\dagger_{i,j}\chi_{i,j}(\hat{N}_{i,j})^2 + \frac{\alpha_4}{8}\chi^\dagger_{i,j}\chi_{i,j}(\hat{N}_{i,j})^3 \\
& + \big[\alpha_2 + (3S^2+1)\alpha_3 + (6S^4 + 4S^2 + 1)\alpha_4\big](\chi^\dagger_{i,j})^2(\chi_{i,j})^2 \\
& - \Big[\frac{3\alpha_3}{2} + (6S^2 + \frac{5}{2})\alpha_4\Big](\chi^\dagger_{i,j})^2(\chi_{i,j})^2\hat{N}_{i,jj} \\
& + \frac{7\alpha_4}{4}(\chi^\dagger_{i,j})^2(\chi_{i,j})^2(\hat{N}_{i,j})^2 - \big[\alpha_3 + (4S^2+4)\alpha_4\big](\chi^\dagger_{i,j})^3(\chi_{i,j})^3 \\
& + 3\alpha_4(\chi^\dagger_{i,j})^3(\chi_{i,j})^3\hat{N}_{i,j} + \alpha_4(\chi^\dagger_{i,j})^4(\chi_{i,j})^4.
\end{aligned} \tag{2.85}$$

With $S = 2$ and $N_{i,j} = 8$ when it acts on the physical state. The Hamiltonian is simplified to:

$$\begin{aligned}
\hat{H}_{i,j} \;=\; & \big(4\alpha_1 + 16\alpha_2 + 64\alpha_3 + 256\alpha_4\big) - \big(\alpha_1 + 4\alpha_2 + 16\alpha_3 + 64\alpha_4\big)\chi^\dagger_{i,j}\chi_{i,j} \\
& + \big(\alpha_2 + \alpha_3 + 13\alpha_4\big)(\chi^\dagger_{i,j})^2(\chi_{i,j})^2 + (-\alpha_3 + 4\alpha_4)(\chi^\dagger_{i,j})^3(\chi_{i,j})^3 \\
& + \alpha_4(\chi^\dagger_{i,j})^4(\chi_{i,j})^4,
\end{aligned} \tag{2.86}$$

or in terms of the update projectors:

$$\begin{aligned}
\hat{H}_{i,j} \;=\; & \big(4\alpha_1 + 16\alpha_2 + 64\alpha_3 + 256\alpha_4\big)\mathcal{P}^{(0)}_{i,j} - \big(\alpha_1 + 4\alpha_2 + 16\alpha_3 + 64\alpha_4\big)\mathcal{P}^{(1)}_{i,j} \\
& + 3\big(\alpha_2 + \alpha_3 + 13\alpha_4\big)\mathcal{P}^{(2)}_{i,j} + 18(-\alpha_3 + 4\alpha_4)\mathcal{P}^{(3)}_{i,j} + 180\alpha_4\mathcal{P}^{(4)}_{i,j}.
\end{aligned} \tag{2.87}$$

By taking each update projector in Eq. (2.87) and acting on $|\Psi_{\mathrm{VBS},S=2}\rangle$, we have:

$$\mathcal{P}^{(1)}_{i,j}\,|\Psi_{\mathrm{VBS},S=2}\rangle = 7\,|\Psi_{\mathrm{VBS},S=2}\rangle + 2\,|\Psi_{\mathrm{Pert1},S=2}\rangle\,, \tag{2.88}$$

$$\mathcal{P}^{(2)}_{i,j}\,|\Psi_{\mathrm{VBS},S=2}\rangle = 7\,|\Psi_{\mathrm{VBS},S=2}\rangle + 8\,|\Psi_{\mathrm{Pert1},S=2}\rangle + \frac{1}{3}\,|\Psi_{\mathrm{Pert2},S=2}\rangle\,, \tag{2.89}$$

$$\mathcal{P}^{(3)}_{i,j}\,|\Psi_{\mathrm{VBS},S=2}\rangle = 5\,|\Psi_{\mathrm{pert1},S=2}\rangle + \frac{5}{6}\,|\Psi_{\mathrm{Pert2},S=2}\rangle\,, \tag{2.90}$$

$$\mathcal{P}^{(4)}_{i,j}\,|\Psi_{\mathrm{VBS},S=2}\rangle = \frac{1}{3}\,|\Psi_{\mathrm{Pert2},S=2}\rangle\,. \tag{2.91}$$

The two perturbed states are drawn graphically, which is similar to the spin-1 chain:

$|\Psi_{\mathrm{Pert1},S=2}\rangle =$

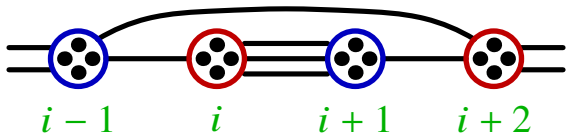

$|\Psi_{\mathrm{Pert2},S=2}\rangle =$

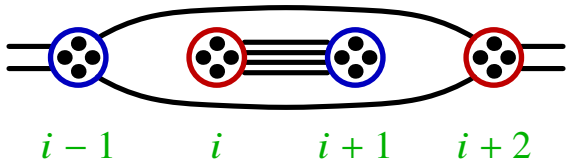

So, the local Hamiltonian acts on the VBS state:

$$\begin{aligned}\hat{H}_{i,j}\,|\Psi_{\mathrm{VBS},S=2}\rangle = {} & \left(-3\alpha_1 + 9\alpha_2 - 27\alpha_3 + 81\alpha_4\right)|\Psi_{\mathrm{VBS},S=2}\rangle \\ & - \left(2\alpha_1 - 16\alpha_2 + 98\alpha_3 - 544\alpha_4\right)|\Psi_{\mathrm{Pert1},S=2}\rangle \\ & + \left(\alpha_2 - 14\alpha_3 + 133\alpha_4\right)|\Psi_{\mathrm{pert2},S=2}\rangle\,.\end{aligned} \tag{2.92}$$

In order for the VBS state to be a stationary state of the Hamiltonian, the coefficients for the perturbed states in Eq. (2.92) must both be zero.

$$\begin{cases} 2\alpha_1 - 16\alpha_2 + 98\alpha_3 - 544\alpha_4 = 0 \\ \alpha_2 - 14\alpha_3 + 133\alpha_4 = 0 \end{cases} \tag{2.93}$$

However, the four variables are not uniquely fixed by these two equations. In practice, there is

a continuous family of Hamiltonians having the AKLT configuration as an eigenstate. Whether it is always the ground state is a separate question. The coefficients from Ref. [11, 65–67] with $\alpha_1 = 17/35$, $\alpha_2 = 1/180$, $\alpha_3 = -1/45$ and $\alpha_4 = -1/420$ satisfy Eqs. (2.93).

We have reproduced the AKLT points in both the spin-1 and spin-2 chains. By varying the values of the coupling parameters, we may obtain the phase transition between different phases in a chain. We hope to explore this point in the future.

2.2.4 Spin-2 square lattice

Similar to the above cases, the Hamiltonian for spin-2 in a square lattice is analogous to that in a chain [Eq. 2.86)]. We just expand it in one more dimension, compared with the 1D spin chain. We now use a notation where a pair of indices represents the Cartesian coordinates of a site.

$$\hat{H}_{i,j;i+1,j} = \alpha_1(\mathbf{S}_{i,j}\cdot\mathbf{S}_{i+1,j}) + \alpha_2(\mathbf{S}_{i,j}\cdot\mathbf{S}_{i+1,j})^2 + \alpha_3(\mathbf{S}_{i,j}\cdot\mathbf{S}_{i+1,j})^3 + \alpha_4(\mathbf{S}_{i,j}\cdot\mathbf{S}_{i+1,j})^4. \tag{2.94}$$

$$\begin{aligned}
\hat{H}_{i,j;i+1,j} \;=\; & \big(\alpha_1 S^2 + \alpha_2 S^4 + \alpha_3 S^6 \\
& + \alpha_4 S^8\big) - (\alpha_1 + 2\alpha_2 S^2 + 3\alpha_3 S^4 + 4\alpha_4 S^6)\chi^{\dagger}_{i,j;i+1,j}\chi_{i,j;i+1,j} \\
& + \left[\frac{\alpha_2}{2} + \frac{3\alpha_3 S^2}{2} + 3\alpha_4 S^4\right]\chi^{\dagger}_{i,j;i+1,j}\chi_{i,j;i+1,j}\hat{N}_{i,j;i+1,j} \\
& - \left[\frac{\alpha_3}{4} + \alpha_4 S^2\right]\chi^{\dagger}_{i,j;i+1,j}\chi_{i,j;i+1,j}(\hat{N}_{i,j;i+1,j})^2 \\
& + \frac{\alpha_4}{8}\chi^{\dagger}_{i,j;i+1,j}\chi_{i,j;i+1,j}(\hat{N}_{i,j;i+1,j})^3 \\
& + \big[\alpha_2 + (3S^2+1)\alpha_3 + (6S^4+4S^2+1)\alpha_4\big](\chi^{\dagger}_{i,j;i+1,j})^2(\chi_{i,j;i+1,j})^2 \\
& \quad - \left[\frac{3\alpha_3}{2} + (6S^2+\frac{5}{2})\alpha_4\right](\chi^{\dagger}_{i,j;i+1,j})^2(\chi_{i,j;i+1,j})^2\hat{N}_{i,j;i+1,j} \\
& \quad + \frac{7\alpha_4}{4}(\chi^{\dagger}_{i,j;i+1,j})^2(\chi_{i,j;i+1,j})^2(\hat{N}_{i,j;i+1,j})^2 \\
& \quad - \big[\alpha_3 + (4S^2+4)\alpha_4\big](\chi^{\dagger}_{i,j;i+1,j})^3(\chi_{i,j;i+1,j})^3 \\
& \quad + 3\alpha_4(\chi^{\dagger}_{i,j;i+1,j})^3(\chi_{i,j;i+1,j})^3\hat{N}_{i,j;i+1,j} \\
& \quad + \alpha_4(\chi^{\dagger}_{i,j;i+1,j})^4(\chi_{i,j;i+1,j})^4.
\end{aligned} \tag{2.95}$$

Identities are expanded in one more dimension:

$$\begin{aligned}\left[\chi_{i,j;k,l}, \chi^{\dagger}_{m,n;p,q}\right] &= (\delta_{im}\delta_{jn}\delta_{kp}\delta_{lq} - \delta_{ip}\delta_{jp}\delta_{km}\delta_{ln}) + \frac{1}{2}\big(\delta_{im}\delta_{jn}T_{p,q;k,l} + \delta_{kp}\delta_{lq}T_{m,n;i,j} \\ &\quad - \delta_{ip}\delta_{jq}T_{m,n;k,l} - \delta_{km}\delta_{ln}T_{p,q;i,j}\big), \qquad (2.96)\\ \left[T_{i,j;k,l}, \chi^{\dagger}_{m,n;p,q}\right] &= \delta_{km}\delta_{ln}\chi^{\dagger}_{i,j;p,q} - \delta_{kp}\delta_{lq}\chi^{\dagger}_{i,j;m,n}, \qquad (2.97)\\ \left[N_{i,j;i,j}, \chi^{\dagger}_{m,n;p,q}\right] &= \delta_{im}\delta_{jn}\chi^{\dagger}_{i,j;p,q} - \delta_{ip}\delta_{jq}\chi^{\dagger}_{i,j;m,n}. \qquad (2.98)\end{aligned}$$

The VBS state is a product of all valence bonds covering the square lattice. Each bond begins from site (i, j) in the A sublattice and end at site (k, l) in the B sublattice (Fig. 2.7).

$$|\Psi_{\text{VBS, square}}\rangle = \prod_{(i,j)\in \text{A};(k,l)\in \text{B}} \chi^{\dagger}_{(i,j;k,l)} |\text{vac}\rangle \, . \qquad (2.99)$$

i, k and j, l indices are along x- and y-directions, respectively. With $S = 2$ and $N_{i,j;i+1,j} |\Psi_{\text{AKLT, square}}\rangle =$

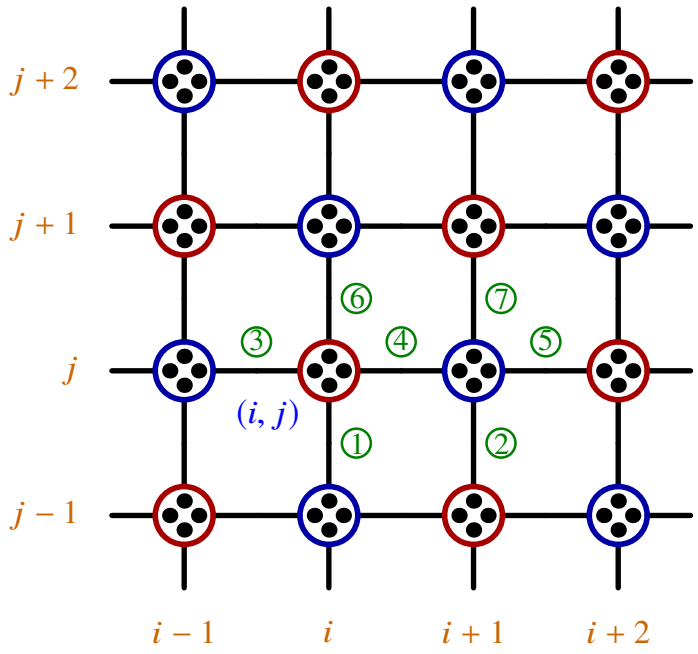

Figure 2.7: Representation of the spin-2 VBS state on a square lattice. Each spin-2 site composes of four virtual spin-half particles like an atom consisting of four localized electrons. Solid lines represent singlet bonds connections between two spins on adjacent sites.

$8\,|\Psi_{\text{AKLT, square}}\rangle$, the Hamiltonian of the system is simplified in terms of update projectors:

$$\begin{aligned}\hat{H}_{i,j;i+1,j} &= \big(4\alpha_1 + 16\alpha_2 + 64\alpha_3 + 256\alpha_4\big)\mathcal{P}^{(0)}_{i,j;i+1,j} - \big(\alpha_1 + 4\alpha_2 + 16\alpha_3 + 64\alpha_4\big)\mathcal{P}^{(1)}_{i,j;i+1,j} \\ &\quad + 3\big(\alpha_2 + \alpha_3 + 13\alpha_4\big)\mathcal{P}^{(2)}_{i,j;i+1,j} + 18(-\alpha_3 + 4\alpha_4)\mathcal{P}^{(3)}_{i,j;i+1,j} + 180\alpha_4\mathcal{P}^{(4)}_{i,j;i+1,j} \qquad (2.100)\end{aligned}$$

Here, we define the Hamiltonian acting on the bond $(i, j; i+1, j)$ which lies along the x-direction. Because of the isotropic symmetry in a square lattice, the bond $(i, j; i, j+1)$ behaves similarly. The rules are the following:

$$\mathcal{P}^{(1)}_{i,j;i+1,j}|\Psi_{\text{AKLT, square}}\rangle = 4|\Psi_{\text{AKLT, square}}\rangle + \frac{1}{2}\Big(|\Psi_{\text{pert1};1\to9}\rangle\Big), \qquad (2.101)$$

$$\mathcal{P}^{(2)}_{i,j;i+1,j}|\Psi_{\text{AKLT, square}}\rangle = \frac{7}{6}\Big(|\Psi_{\text{pert1};1\to9}\rangle\Big) + \frac{1}{6}\Big(|\Psi_{\text{pert2};1\to18}\rangle\Big), \qquad (2.102)$$

$$\mathcal{P}^{(3)}_{i,j;i+1,j}|\Psi_{\text{AKLT, square}}\rangle = \frac{1}{4}\Big(|\Psi_{\text{pert2};1\to18}\rangle\Big) + \frac{1}{12}\Big(|\Psi_{\text{pert3};1\to6}\rangle\Big), \qquad (2.103)$$

$$\mathcal{P}^{(4)}_{i,j;i+1,j}|\Psi_{\text{AKLT, square}}\rangle = \frac{1}{12}\Big(|\Psi_{\text{pert3};1\to6}\rangle\Big). \qquad (2.104)$$

The $|\Psi_{\text{AKLT, square}}\rangle$, $|\Psi_{\text{pert1};1\to9}\rangle$, $|\Psi_{\text{pert2};1\to18}\rangle$ and $|\Psi_{\text{pert3};1\to6}\rangle$ are illustrated graphically in Figs. 2.8, 2.8 and 2.9. The corresponding perturbed states contain one, two or three long bond(s), respectively.

Thus, we achieve

$$\begin{aligned}\hat{H}_{i,j;i+1,j}|\Psi_{\text{VBS, square}}\rangle &= 0\,|\Psi_{\text{VBS, square}}\rangle + \frac{1}{2}(-\alpha_1 + 3\alpha_2 - 9\alpha_3 + 27\alpha_4)\,|\Psi_{\text{pert1,1}\to9}\rangle \\ &\quad + \frac{1}{2}(\alpha_2 - 8\alpha_3 + 49\alpha_4)\,|\Psi_{\text{pert2};1\to18}\rangle \\ &\quad - \frac{3}{2}(-\alpha_3 + 14\alpha_4)\,|\Psi_{\text{pert3};1\to6}\rangle\,. \qquad (2.105)\end{aligned}$$

By setting the coefficients of $|\Psi_{\text{pert1,1}\to9}\rangle$, $|\Psi_{\text{pert2};1\to18}\rangle$ and $|\Psi_{\text{pert3};1\to6}\rangle$, we have a system of linear equations:

$$\begin{cases} -\alpha_1 + 3\alpha_2 - 9\alpha_3 + 27\alpha_4 = 0 \\ \alpha_2 - 8\alpha_3 + 49\alpha_4 = 0 \\ -\alpha_3 + 14\alpha_4 = 0 \end{cases} \tag{2.106}$$

By solving the above system of equations, we get: $\alpha_1 = 90\alpha_4$, $\alpha_2 = 63\alpha_4$, and $\alpha_3 = 14\alpha_4$. Comparing with the results in Ref. [11], the spin-2 ALKT model on the square lattice is solved analytically, and the ground state energy is zero.

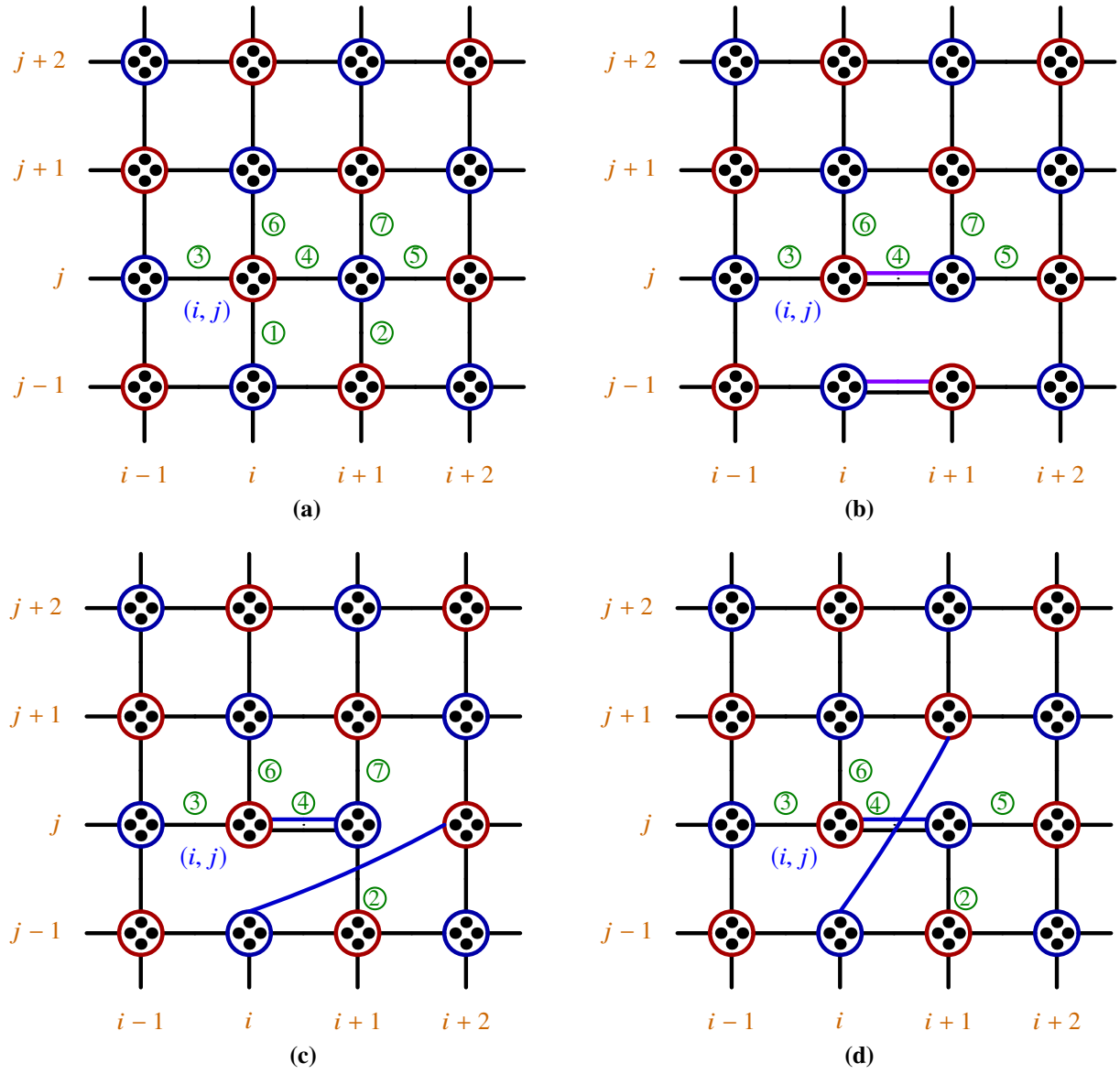

Figure 2.8: (a) VBS state on the square lattice labeling 7 related bonds around which the local Hamiltonian acts on the VBS state. (b), (c) and (d) Illustrated the first perturbed states with one long bond when the bilinear term acts on the VBS state.

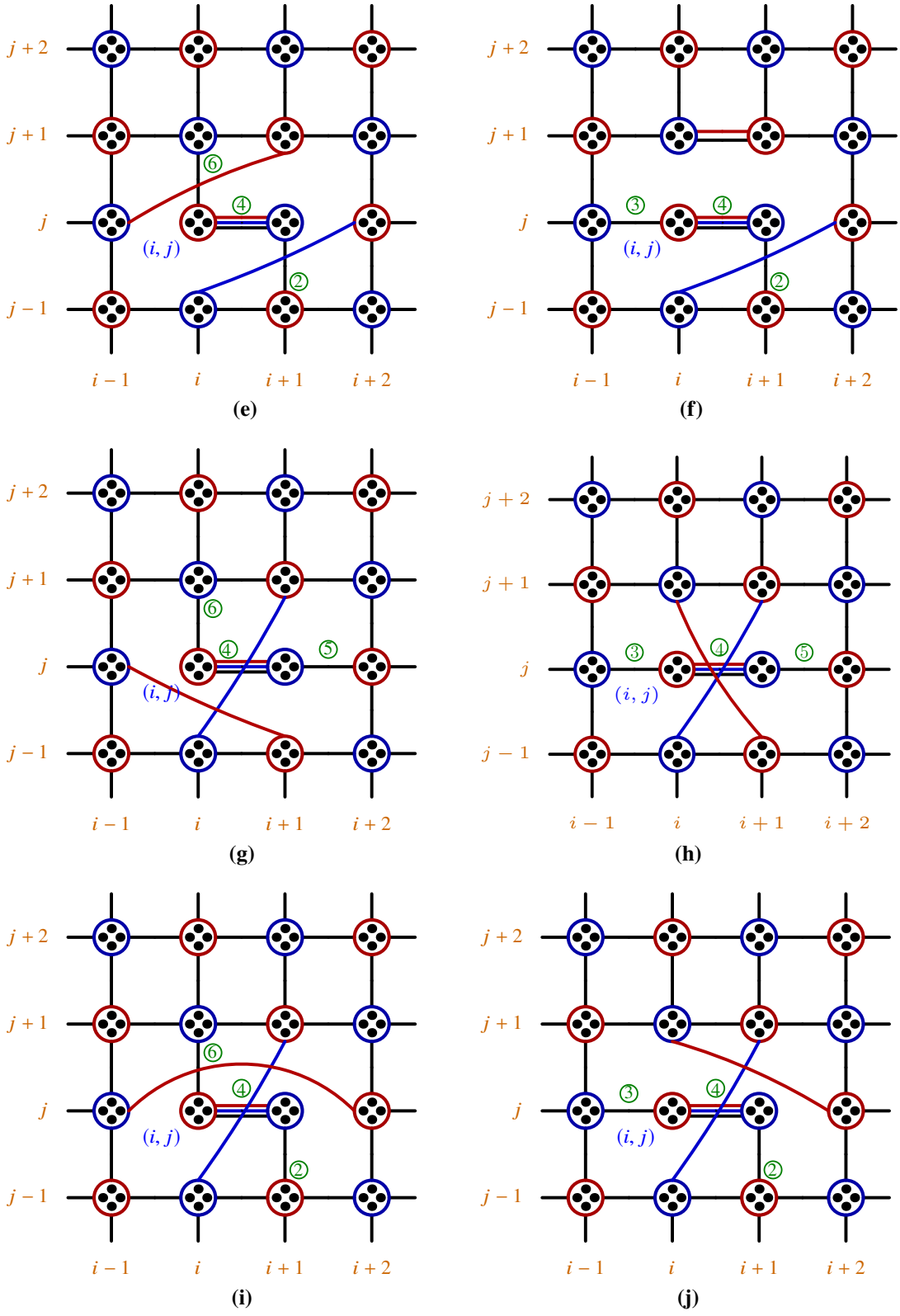

Figure 2.8: Six of eighteen configurations of the $|\Psi_{\text{pert2};1\to 18}\rangle$ state with two long bonds.

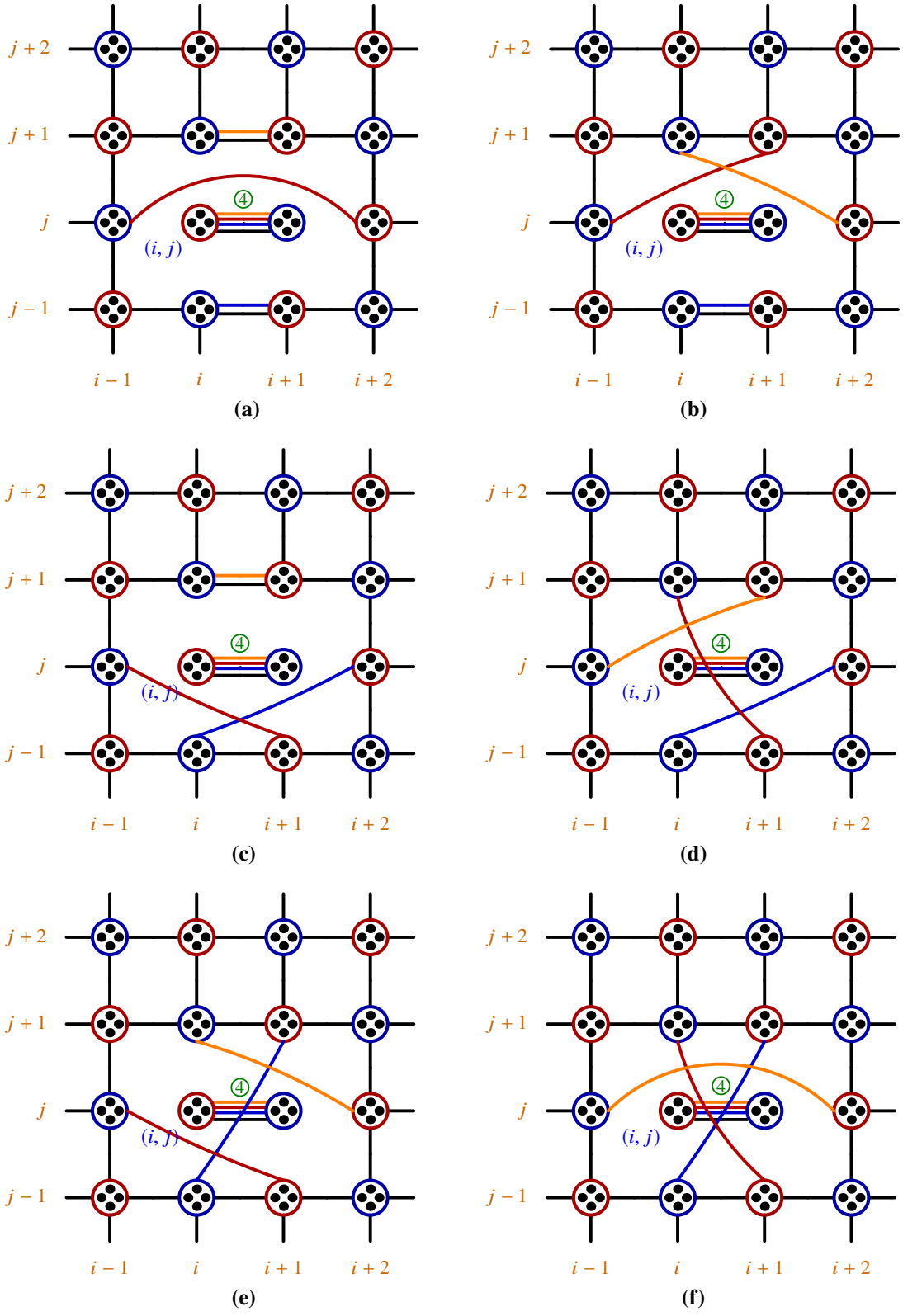

Figure 2.9: Six configurations of the $|\Psi_{\text{pert3};1\to6}\rangle$ state with three long bonds.

CHAPTER 3

COHERENT STATE APPROACH TO QUANTUM HEISENBERG MODEL

3.1 Brief introduction on quantum systems and coherent states

In classical physics, we can keep track of an *individual particle* by measuring its velocity, position, momentum, etc. In quantum mechanics (QM), we formulate a single particle in terms of the position operator $\hat{\mathbf{x}}$ and the momentum operator $\hat{\mathbf{p}}$. Other physical operators such as angular momentum and Hamiltonian may be expressed in terms of these operators, and the coordinate representation is a natural description for quantum mechanics, which is defined by an eigenfunction of the position operator. We describe the state of a particle by a general ket state $|\psi\rangle$, which belongs to the single particle Hilbert space $\mathscr{H}$. The wave function is constructed by overlapping the bra state $\langle\psi|$ with the position or momentum vectors as we expect to solve QM problems in real-space or momentum representations. It represents the probability amplitude to find a quantum particle at position $\mathbf{r}$ or momentum $\mathbf{p}$ [68]. The two kinds of representations are connected to each other by the Fourier transforms. Furthermore, the ket state and wave function satisfy the Schrödinger equations:

$$\begin{cases} i\hbar\partial_t |\psi\rangle = \hat{H}|\psi\rangle, & \text{(time-dependent) or} \\ \hat{H}|\psi_\alpha\rangle = \epsilon_\alpha |\psi_\alpha\rangle & \text{(time-independent).} \end{cases} \tag{3.1}$$

By solving the above eigenequations, we can obtain the wave function and the energy of the system. However, the Schrödinger equations are generally difficult to solve in analytic form, except for some simple cases such as a free particle in an infinite well and simple harmonic motion. One prominent method of solving the time-dependent Schrödinger equation is the Feynman path integral. The idea is that we construct the time evolution operator, then discretize the continuous time into small slices, and evaluate it in infinitesimal time intervals. Finally, we integrate all

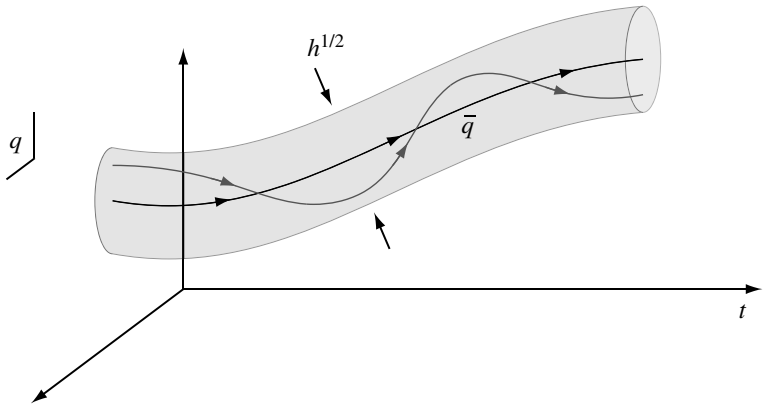

Figure 3.1: Quantum fluctuations around a classical path in coordinate space. (Here, we assume a set of two-dimensional coordinates). The correct paths q fluctuating around a classical solutions $q_{\rm cl}$ typically extend a distance $O(h^{1/2})$ [41].

possible paths through the classical phase of the system which the same beginning and end points for all configurations. However, in most quantum problems, this method is still difficult to apply. Alternatively, the *semiclassical* or varational approach finds the classical path by extremizing the classical action. Then, the quantum fluctuation is added around the classical path (Fig. 3.1). That is the central idea of the *mean-field theory*. This theory is applied to many cases, especially the interacting spin systems. As we described in the last part of chapter one, that approach is used to find a mean-field solution for the quantum Heisenberg AFM [16, 21, 22].

However, QM systems usually contain many particles, e.g. 1 mole of matter contains 6.02×10^{23} particles. The identical particles in a QM system (e.g. a number of electrons in an atom) are truly *indistinguishable*. When we exchange two similar quantum particles, no observable change is made. For these systems, it is useful to define operators which create or annihilate a particle in specified states. We express other operators of a physical interest via these creation and annihilation operators, this is the "**second quantization**" process. This procedure is like a *discrete limit* which can be counted. The operators generate the entire Hilbert space by their action on a single reference state and provide a basis for the algebra of operators in the Hilbert space. The creation operators increase the particle number by one, while the annihilation operator lowers it by one. For our cases, the valence-bond creation will create a bond connecting two sites. Its

annihilation will destroy not only exact bonds between two sites, but also two bonds simultaneously if they have common indices. The valence bond solid which I described above is not the eigenstate of the general Heisenberg AFM Hamiltonian but of the extended fixed-point AKLT Hamiltonian.

Physicists want to find the eigenstates of the annihilation operators which are defined as *coherent states*. This state will span the whole Fock space (the sum of all Hilbert space for the n number of particles) of quantum particles such as bosons and fermions. A natural representation of many-particle systems, the holomorphic representation, is defined in terms of these coherent states [68, 69]. The coherent state in general is nonorthogonal and overcomplete. It is like a *continuous limit* for a quantum system (or maybe a semiclassical approach). In our case, we also construct a coherent state for the valence bond basis with which we hope to find a better result for solving the general AFM case. Before starting to derive the coherent state for our case, we will summarize the properties of the Fourier transforms which is heavily used for this work.

3.2 Fourier transform (FT) for lattice system

We note that the conversion of wavevector sums to integrals involves

$$\sum_{\mathbf{k}} \to \frac{\Omega}{(2\pi)^D} \int d^D k = (N/V_c^*) \int d^D k, \tag{3.2}$$

where the direct volume Ω contains N primitive cells, D is the dimension of the system, and $V_c^* = (2\pi)^D/V_c$, V_c is the volume of the Bravais cell in real space [29].

In general, the Fourier transform in solid state physics is defined by two theorems:

Theorem 4. *A function $f(\mathbf{x})$ which is periodic with the period of the lattice may be expanded in a Fourier series in the reciprocal lattice vectors $\mathbf{G}$:*

$$f(\mathbf{x}) = \sum_{\mathbf{G}} a_{\mathbf{G}} e^{i\mathbf{G}\cdot\mathbf{x}}. \tag{3.3}$$

Theorem 5. *If $f(\mathbf{x})$ has the periodicity of the lattice: $\int d^3x f(\mathbf{x}) e^{i\mathbf{K}\cdot\mathbf{x}} = 0$, unless $\mathbf{K}$ is a vector in the reciprocal lattice.*

Fourier lattice series: Consider the series:

$$q_r = \frac{1}{\sqrt{N}} \sum_k Q_k e^{ikr}. \tag{3.4}$$

We determine the allowed values of k by the periodic boundary condition $q_{r+N} = q_r$, when $e^{ikN} = 1$; this condition is satisfied by $k = 2\pi n/N$, where n is an integer. Only N values of n give independent values of the N coordinates q_r. It is convenient to take N as a even number and to choose the values of n as 0, ± 1, ... , $\pm(N/2-1)$, $N/2$. The value $n = 0$ or $k = 0$ is associated with what is called the *uniform mode* in which all q_r are equal, independent of r.

The inverse Fourier transform is

$$Q_k = \frac{1}{\sqrt{N}} \sum_s q_s e^{-iks}. \tag{3.5}$$

The Fourier transform of a convolution of f_1 and f_2, which are as functions of the variables is

$$F(x) = \frac{1}{\sqrt{2\pi}} \int_{-\infty}^{\infty} f_1(t) f_2(x-t) dt, \tag{3.6}$$

$$F(x) = \frac{1}{\sqrt{2\pi}} \int_{-\infty}^{\infty} g_1(k) g_2(k) e^{ikx} dk, \tag{3.7}$$

where $g_1 = \tilde{f_1}$ and $g_2 = \tilde{f_2}$.

3.3 Fourier transform of the singlet projector operator

We can tune the two-index singlet projector operator in real space into a one-index operator in momentum space. This can be applied to any lattice which can be separated into A and B sublattices. For the bipartite lattices, we have only valence bonds connecting between two different sublattice; otherwise it is the existence of a valence bond on same sublattice in frustrated lattices. We call N the number of the basis (each basis includes two sites which correspond the A and B sublattices). A basis consists of one boson $a^\dagger$ and one boson $b^\dagger$. The total number of spin sites in

the lattice is $2N$. So, we define the Fourier transform for hard-core bosons:

$$\begin{cases} a_i = \dfrac{1}{\sqrt{N}} \sum\limits_{\mathbf{k}} e^{-i\mathbf{k}\cdot\mathbf{r}_i} a_{\mathbf{k}} \quad \&\& \quad a_i^\dagger = \dfrac{1}{\sqrt{N}} \sum\limits_{\mathbf{k}} e^{i\mathbf{k}\cdot\mathbf{r}_i} a_{\mathbf{k}}^\dagger \\ b_i = \dfrac{1}{\sqrt{N}} \sum\limits_{\mathbf{k}} e^{-i\mathbf{k}\cdot\mathbf{r}_i} b_{\mathbf{k}} \quad \&\& \quad b_i^\dagger = \dfrac{1}{\sqrt{N}} \sum\limits_{\mathbf{k}} e^{i\mathbf{k}\cdot\mathbf{r}_i} b_{\mathbf{k}}^\dagger \end{cases} \tag{3.8}$$

Now, the Brillouin zone shrinks to half of that normal case (compared with the Schwinger bosons formalism in Chapter 1). This is explained by the the real space lattice vector $\mathbf{r}$ and corresponding momentum vectors $\mathbf{k}$ relating by a relation: $\mathbf{r}\cdot\mathbf{k} = (2\pi)^D$. When we double the lattice vector, the momentum one is shrunk by half [29]. For a chain, it is $(\pi/2...\pi/2)$, and for a square lattice: $(\pi/2...\pi/2)\times(\pi/2...\pi/2)$. The pair of Fourier transforms for the creation operator of a valence bond is defined as

$$\chi_{ij}^\dagger = \frac{1}{N}\sum_{\mathbf{q}\in \mathrm{BZ}} e^{i\mathbf{q}\cdot\mathbf{r}_{ij}} \chi_{\mathbf{q}}^\dagger \qquad \text{and} \qquad \chi_{\mathbf{q}}^\dagger = \frac{1}{N}\sum_{i\in \mathrm{A}}\sum_{j\in \mathrm{B}} e^{-i\mathbf{q}\cdot\mathbf{r}_{ij}} \chi_{ij}^\dagger, \tag{3.9}$$

where, $\mathbf{r}_{ij}$ is a real-space vector connecting site i with j.

We write the real-space valence bond operator explicitly:

$$\chi_{ij}^\dagger = \frac{1}{2S\sqrt{2}} \sum_{\alpha,\beta}^{2S} \left(a_i^{\alpha\dagger} b_j^{\beta\dagger} - b_i^{\alpha\dagger} a_j^{\beta\dagger}\right). \tag{3.10}$$

Then, using the FT of each hard-core boson [Eq. (3.8)], we convert it into momentum space:

$$\begin{aligned} \chi_{\mathbf{q}}^\dagger &= \frac{1}{N}\sum_{i\in \mathrm{A}}\sum_{j\in \mathrm{B}} e^{-i\mathbf{q}\cdot(\mathbf{r}_j-\mathbf{r}_i)} \frac{1}{2S\sqrt{2}} \sum_{\alpha,\beta}^{2S} \left[\frac{1}{N}\sum_{\mathbf{k}}\sum_{\mathbf{k}'} e^{i\mathbf{k}\cdot\mathbf{r}_i} e^{i\mathbf{k}\cdot\mathbf{r}_j} \left(a_{\mathbf{k}}^{\alpha\dagger} b_{\mathbf{k}'}^{\beta\dagger} - b_{\mathbf{k}}^{\alpha\dagger} a_{\mathbf{k}'}^{\beta\dagger}\right)\right] \\ &= \sum_{\mathbf{k}}\sum_{\mathbf{k}'} \frac{1}{N}\sum_{i\in \mathrm{A}} e^{i(\mathbf{k}+\mathbf{q})\cdot\mathbf{r}_i} \frac{1}{N}\sum_{j\in \mathrm{B}} e^{i(\mathbf{k}'-\mathbf{q})\cdot\mathbf{r}_j} \frac{1}{2S\sqrt{2}} \sum_{\alpha,\beta} \left(a_{\mathbf{k}}^{\alpha\dagger} b_{\mathbf{k}'}^{\beta\dagger} - b_{\mathbf{k}}^{\alpha\dagger} a_{\mathbf{k}'}^{\beta\dagger}\right) \\ &= \sum_{\mathbf{k}}\sum_{\mathbf{k}'} \frac{1}{2S\sqrt{2}} \sum_{\alpha,\beta} \left(a_{\mathbf{k}}^{\alpha\dagger} b_{\mathbf{k}'}^{\beta\dagger} - b_{\mathbf{k}}^{\alpha\dagger} a_{\mathbf{k}'}^{\beta\dagger}\right) \delta(\mathbf{k}+\mathbf{q})\delta(\mathbf{k}'-\mathbf{q}), \end{aligned} \tag{3.11}$$

yieding the two identities,

$$\begin{cases} \dfrac{1}{N}\sum_{i\in \mathrm{A}} e^{i(\mathbf{k}+\mathbf{q})\cdot\mathbf{r}_i} = \delta(\mathbf{k}+\mathbf{q}), \\ \int d^D k F(\mathbf{k},\mathbf{k}')\delta(\mathbf{k}+\mathbf{q}) = F(-\mathbf{q},\mathbf{k}'). \end{cases} \tag{3.12}$$

Final results for the creation and annihilation operators in momentum space are:

$$\chi^{\dagger}_{\mathbf{q}} = \frac{1}{2S\sqrt{2}}\sum_{\alpha,\beta}\left(a^{\alpha\dagger}_{\mathbf{q}} b^{\beta\dagger}_{-\mathbf{q}} - b^{\alpha\dagger}_{\mathbf{q}} a^{\beta\dagger}_{-\mathbf{q}}\right), \tag{3.13}$$

$$\chi_{\mathbf{q}} = \frac{1}{2S\sqrt{2}}\sum_{\alpha,\beta}\left(a^{\alpha}_{\mathbf{q}} b^{\beta}_{-\mathbf{q}} - b^{\alpha}_{\mathbf{q}} a^{\beta}_{-\mathbf{q}}\right). \tag{3.14}$$

They are similar to the definitions in real space [Eq. (2.7)]. We reproduce the commutation between the annihilation and creation of valence bond operator:

$$\begin{aligned} \left[\chi_{\mathbf{q}}, \chi^{\dagger}_{\mathbf{q}'}\right] &= \frac{1}{8S^2}\sum_{\mu,\nu}\sum_{\alpha,\beta}\left[\left(a^{\alpha}_{\mathbf{q}} b^{\beta}_{-\mathbf{q}} - b^{\alpha}_{\mathbf{q}} a^{\beta}_{-\mathbf{q}}\right), \left(a^{\mu\dagger}_{\mathbf{q}'} b^{\nu\dagger}_{-\mathbf{q}'} - b^{\mu\dagger}_{\mathbf{q}'} a^{\nu\dagger}_{-\mathbf{q}'}\right)\right] \\ &= \frac{1}{8S^2}\sum_{\mu,\nu}\sum_{\alpha,\beta}\Big\{\left[a^{\alpha}_{\mathbf{q}} b^{\beta}_{-\mathbf{q}}, a^{\mu\dagger}_{\mathbf{q}'} b^{\nu\dagger}_{-\mathbf{q}'}\right] + \left[b^{\alpha}_{\mathbf{q}} a^{\beta}_{-\mathbf{q}}, b^{\mu\dagger}_{\mathbf{q}'} a^{\nu\dagger}_{-\mathbf{q}'}\right] - \left[a^{\alpha}_{\mathbf{q}} b^{\beta}_{-\mathbf{q}}, b^{\mu\dagger}_{\mathbf{q}'} a^{\nu\dagger}_{-\mathbf{q}'}\right] \\ &\quad - \left[b^{\alpha}_{\mathbf{q}} a^{\beta}_{-\mathbf{q}}, a^{\mu\dagger}_{\mathbf{q}'} b^{\nu\dagger}_{-\mathbf{q}'}\right]\Big\}. \end{aligned} \tag{3.15}$$

Each term in Eq. (3.15) is derived in Appendix B. Finally, we obtain

$$\left[\chi_{\mathbf{q}}, \chi^{\dagger}_{\mathbf{q}'}\right] = (\delta_{\mathbf{q},\mathbf{q}'} - \delta_{\mathbf{q},-\mathbf{q}'}) + \frac{1}{2}\Big[\delta_{\mathbf{q},\mathbf{q}'}(T_{\mathbf{q}',\mathbf{q}} + T_{-\mathbf{q}',-\mathbf{q}}) - \delta_{\mathbf{q},-\mathbf{q}'}(T_{\mathbf{q}',-\mathbf{q}} + T_{-\mathbf{q}',\mathbf{q}})\Big]. \tag{3.16}$$

This relation is exactly same to its commutation in the real space [Eq. (2.11)]. With the transition operator:

$$T_{\mathbf{q}',\mathbf{q}} = \frac{1}{2S}\sum_{\alpha,\beta}\left(a^{\alpha\dagger}_{\mathbf{q}'} a^{\beta}_{\mathbf{q}} + b^{\alpha\dagger}_{\mathbf{q}'} b^{\beta}_{\mathbf{q}}\right)$$

For bipartite lattices, we also set $T_{\mathbf{q}} = T_{\mathbf{q},\mathbf{q}'} + T_{-\mathbf{q},-\mathbf{q}'}$, and Eq. (3.16) reduces to:

$$\left[\chi_{\mathbf{q}}, \chi^{\dagger}_{\mathbf{q}'}\right] = \delta_{\mathbf{q},\mathbf{q}'}\Big(1 + \frac{1}{2}T_{\mathbf{q}}\Big). \tag{3.17}$$

in which all terms have positive sign. We also have relation:

$$\begin{aligned}\left[T_{\mathbf{q}_1,\mathbf{k}}, \chi^{\dagger}_{\mathbf{q}_2}\right] &= \frac{1}{4S^2\sqrt{2}}\sum_{\alpha,\beta}\sum_{\mu,\nu}\Big[\big(a^{\alpha\dagger}_{\mathbf{q}_1}a^{\beta}_{\mathbf{k}} + b^{\alpha\dagger}_{\mathbf{q}_1}b^{\beta}_{\mathbf{k}}\big), \big(a^{\mu\dagger}_{\mathbf{q}_2}b^{\nu\dagger}_{-\mathbf{q}_2} - b^{\mu\dagger}_{\mathbf{q}_2}a^{\nu\dagger}_{-\mathbf{q}_2}\big)\Big] \\ &= \frac{1}{2S\sqrt{2}}\Big[\delta_{\mathbf{k},\mathbf{q}_2}\sum_{\alpha\nu}\big(a^{\alpha\dagger}_{\mathbf{q}_1}b^{\nu\dagger}_{-\mathbf{q}_2} - b^{\alpha\dagger}_{\mathbf{q}_1}a^{\nu\dagger}_{-\mathbf{q}_2}\big) - \delta_{\mathbf{k},-\mathbf{q}_2}\sum_{\alpha\mu}\big(a^{\alpha\dagger}_{\mathbf{q}_1}b^{\nu\dagger}_{\mathbf{q}_2} - b^{\alpha\dagger}_{\mathbf{q}_1}a^{\nu\dagger}_{\mathbf{q}_2}\big)\Big].\end{aligned} \tag{3.18}$$

3.4 Fourier transform of the nearest-neighbor interacting in the Heisenberg AFM

Translation invariant of the singlet operator in momentum space: In the Hamiltonian, the summation $\langle i, j\rangle$ is not long-range, and we just consider the nearest neighbor sum. The total number of the local Hamiltonian is $2N$ terms. We define the basic vectors: $\tau_{\mathrm{A}} = (0, 0)$ and $\tau_{\mathrm{B}} = (1, 0) = \hat{i}$, and the lattice vector $\mathbf{r}_i = 2i\hat{i}$. Here, $\hat{i}$ is the unit vector of a spin chain. We separate two different singlet projector operators:

$$\bar{\chi}^{\dagger}_{i,1} = \frac{1}{2S\sqrt{2}}\sum_{\alpha\beta}\Big(a^{\alpha\dagger}_{\mathbf{r}_i+\tau_{\mathrm{A}}}b^{\beta\dagger}_{\mathbf{r}_i+\tau_{\mathrm{B}}} - b^{\alpha\dagger}_{\mathbf{r}_i+\tau_{\mathrm{A}}}a^{\beta\dagger}_{\mathbf{r}_i+\tau_{\mathrm{B}}}\Big), \tag{3.19}$$

$$\bar{\chi}^{\dagger}_{i,2} = \frac{1}{2S\sqrt{2}}\sum_{\alpha\beta}\Big(a^{\alpha\dagger}_{\mathbf{r}_{i+1}+\tau_{\mathrm{A}}}b^{\beta\dagger}_{\mathbf{r}_i+\tau_{\mathrm{B}}} - b^{\alpha\dagger}_{\mathbf{r}_{i+1}+\tau_{\mathrm{A}}}a^{\beta\dagger}_{\mathbf{r}_i+\tau_{\mathrm{B}}}\Big). \tag{3.20}$$

Here, the bar symbol represents the bond connection between two nearest sites. Now we use the similar Fourier transform approach for the above hard-core bosons to convert all real-space singlet

operators into momentum space:

$$\begin{aligned}
\bar{\chi}^{\dagger}_{\mathbf{q},1} &= \frac{1}{N}\sum_{i\in\mathrm{A}}\sum_{j\in\mathrm{B}} e^{-i\mathbf{q}\cdot(\mathbf{r}_j-\mathbf{r}_i)}\bar{\chi}^{\dagger}_{ij,1} \\
&= \frac{1}{N}\sum_{i} e^{-i\mathbf{q}\cdot(\mathbf{r}_i+\tau_\mathrm{B}-\mathbf{r}_i-\tau_\mathrm{A})}\frac{1}{N}\sum_{\mathbf{k},\mathbf{k}'} e^{-i\mathbf{k}\cdot(\mathbf{r}_i+\tau_\mathrm{A})}e^{-i\mathbf{k}'\cdot(\mathbf{r}_i+\tau_\mathrm{B})}\frac{1}{2S\sqrt{2}}\sum_{\alpha,\beta}\left(a^{\alpha\dagger}_{\mathbf{k}}b^{\beta\dagger}_{\mathbf{k}'}-b^{\alpha\dagger}_{\mathbf{k}}a^{\beta\dagger}_{\mathbf{k}'}\right) \\
&= \frac{1}{N}\sum_{\mathbf{k},\mathbf{k}'}\frac{1}{N}\sum_{i} e^{-i\mathbf{r}_i\cdot(\mathbf{k}+\mathbf{k}')}e^{-i(\mathbf{q}-\mathbf{k}')\cdot\tau_\mathrm{B}}\frac{1}{2S\sqrt{2}}\sum_{\alpha,\beta}\left(a^{\alpha\dagger}_{\mathbf{k}}b^{\beta\dagger}_{\mathbf{k}'}-b^{\alpha\dagger}_{\mathbf{k}}a^{\beta\dagger}_{\mathbf{k}'}\right) \\
&= \frac{1}{N}\sum_{\mathbf{k},\mathbf{k}'} e^{-i(\mathbf{q}-\mathbf{k}')\cdot\tau_\mathrm{B}}\frac{1}{2S\sqrt{2}}\sum_{\alpha,\beta}\left(a^{\alpha\dagger}_{\mathbf{k}}b^{\beta}\dot{\dagger}_{\mathbf{k}'}-b^{\alpha\dagger}_{\mathbf{k}}a^{\alpha\dagger}_{\mathbf{k}'}\right)\delta_{\mathbf{k}+\mathbf{k}'}.
\end{aligned} \tag{3.21}$$

Finally, we get

$$\bar{\chi}^{\dagger}_{\mathbf{q},1} = \frac{1}{N}\sum_{\mathbf{k}} e^{-i(\mathbf{k}+\mathbf{q})\cdot\tau_\mathrm{B}}\frac{1}{2S\sqrt{2}}\sum_{\mu,\nu}\left(a^{\dagger}_{\mathbf{k}}b^{\dagger}_{-\mathbf{k}}-b^{\dagger}_{\mathbf{k}}a^{\dagger}_{-\mathbf{k}}\right) = \frac{1}{N}\sum_{\mathbf{k}} e^{-i(\mathbf{k}+\mathbf{q})\cdot\tau_\mathrm{B}}\chi^{\dagger}_{\mathbf{k}}, \tag{3.22}$$

$$\bar{\chi}^{\dagger}_{\mathbf{q},2} = \frac{1}{N}\sum_{\mathbf{k}} e^{-i(\mathbf{q}-\mathbf{k})\cdot\tau_\mathrm{B}}\frac{1}{2S\sqrt{2}}\sum_{\mu,\nu}\left(a^{\dagger}_{\mathbf{k}}b^{\dagger}_{-\mathbf{k}}-b^{\dagger}_{\mathbf{k}}a^{\dagger}_{-\mathbf{k}}\right) = \frac{1}{N}\sum_{\mathbf{k}} e^{-i(\mathbf{q}-\mathbf{k})\cdot\tau_\mathrm{B}}\chi^{\dagger}_{\mathbf{k}}, \tag{3.23}$$

The Heisenberg Hamiltonian: Here, the Hamiltonian is translation invariant.

$$\hat{H}_{\mathrm{Heis}} = J\sum_{ij}\mathbf{S}_i\cdot\mathbf{S}_j \tag{3.24}$$

$$= JS^2 - J\sum_{ij}\bar{\chi}^{\dagger}_{ij}\bar{\chi}_{ij} \tag{3.25}$$

Using the identities in Eq. (3.22) and (3.23) above, we have the momentum representation of the Heisenberg term:

$$\begin{aligned}
\hat{H}_{\mathrm{Heis}} &= -J\sum_{\mathbf{q}}\left(\bar{\chi}^{\dagger}_{\mathbf{q},1}\bar{\chi}_{\mathbf{q},1}+\bar{\chi}^{\dagger}_{\mathbf{q},2}\bar{\chi}_{\mathbf{q},2}\right) \\
&= -J\Big[\frac{1}{N^2}\sum_{\mathbf{k}_1,\mathbf{k}'_1} e^{-i(\mathbf{k}_1-\mathbf{k}'_1)\cdot\tau_\mathrm{B}}\chi^{\dagger}_{\mathbf{k}_1}\chi_{\mathbf{k}'_1}+\frac{1}{N^2}\sum_{\mathbf{k}_2,\mathbf{k}'_2} e^{i(\mathbf{k}_2-\mathbf{k}'_2)\cdot\tau_\mathrm{B}}\chi^{\dagger}_{\mathbf{k}_2}\chi_{\mathbf{k}'_2}\Big] \\
&= \frac{-J}{N^2}\sum_{\mathbf{k},\mathbf{Q}}\left(e^{-i\mathbf{Q}\cdot\tau_\mathrm{B}}+e^{i\mathbf{Q}\cdot\tau_\mathrm{B}}\right)\chi^{\dagger}_{\mathbf{k}}\chi_{\mathbf{k}+\mathbf{Q}}.
\end{aligned} \tag{3.26}$$

The sums of $\mathbf{k}_1$ and $\mathbf{k}_2$ are similar because they are dummy indices. Setting $\mathbf{Q} = \mathbf{k}'_1 - \mathbf{k}_1$, we obtain

$$\hat{H}_{\text{Heis}} = \frac{-2J}{N^2} \sum_{\mathbf{k},\mathbf{Q}} \cos(\mathbf{Q} \cdot \tau_{\text{B}}) \chi^{\dagger}_{\mathbf{k}} \chi_{\mathbf{k}+\mathbf{Q}}. \tag{3.27}$$

3.5 Momentum representation of the coherent state

We propose the physical state of the valence bond basis:

$$|\Psi_{\text{phys}}\rangle = \hat{G} \exp\Big(\sum_{i\in\text{A}} \sum_{j\in\text{B}} h_{ij} \chi^{\dagger}_{ij} \Big) |\text{vac}\rangle \,. \tag{3.28}$$

The Gutzwiller projection operator $\hat{G} = \prod \delta(\hat{N}_i - 2S)$ [16] filters out all configurations that do not have exactly $2S$ bonds emerging from each lattice site. h_{ij} is called a *probability amplitude* which similar to the wave function definition for a single quantum particle. The physical meaning of that function is to find a weight for a bond connecting sites i and j. Finding the exact physical state for large system sites is a very difficult task. We define the mean field or coherent state: $|\Psi_{\text{c}}\rangle = \exp\Big(\sum_{i\in\text{A}} \sum_{j\in\text{B}} h_{ij} \chi^{\dagger}_{ij} \Big) |\text{vac}\rangle$. It is much easier to evaluate the Hamiltonian in terms of the coherent state rather than the physical state. It is better to work in momentum space because it will give us a more compact form. We use that pair of Fourier transforms:

$$\begin{cases} \chi^{\dagger}_{\mathbf{q}} = \dfrac{1}{N} \displaystyle\sum_{i\in\text{A}} \sum_{j\in\text{B}} e^{-i\mathbf{q}\cdot\mathbf{r}_{ij}} \chi^{\dagger}_{ij}, \\ h_{\mathbf{q}} = \dfrac{1}{N} \displaystyle\sum_{i\in\text{A}} \sum_{j\in\text{B}} e^{i\mathbf{q}\cdot\mathbf{r}_{ij}} h_{ij}. \end{cases} \tag{3.29}$$

The coherent state in momentum space is:

$$\begin{aligned} |\Psi_{\text{c}}\rangle &= \exp\Big(\sum_{\mathbf{q}} h_{\mathbf{q}} \chi^{\dagger}_{\mathbf{q}} \Big) |\text{vac}\rangle \,, \\ &= \Big(1 + \sum_{\mathbf{q}} h_{\mathbf{q}} \chi^{\dagger}_{\mathbf{q}} + \frac{1}{2!} \sum_{\mathbf{q}_1} \sum_{\mathbf{q}_2} h_{\mathbf{q}_1} h_{\mathbf{q}_2} \chi^{\dagger}_{\mathbf{q}_1} \chi^{\dagger}_{\mathbf{q}_2} + \ldots \Big) |\text{vac}\rangle \,. \end{aligned} \tag{3.30}$$

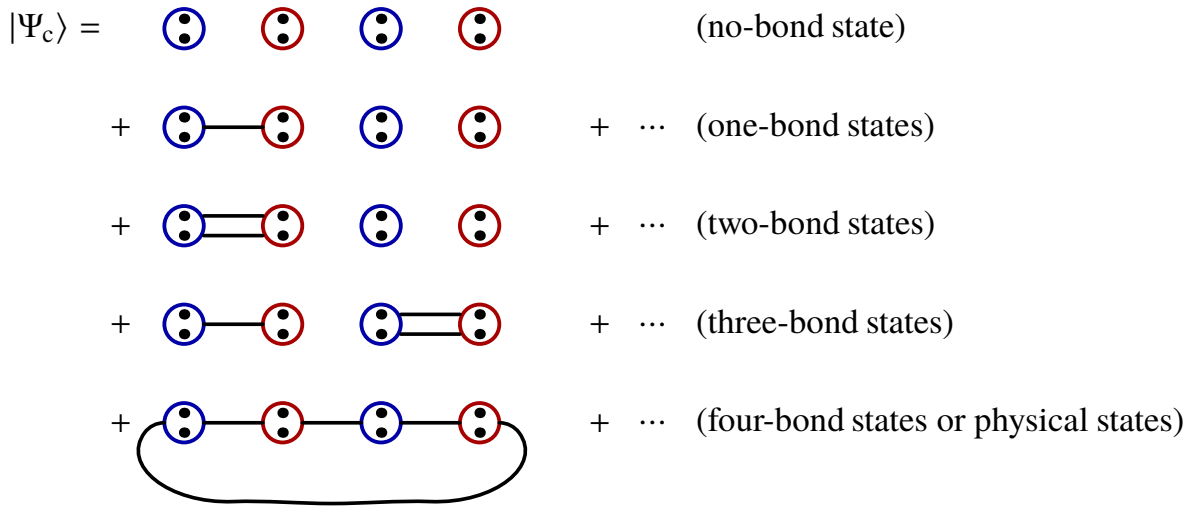

Figure 3.2: The coherent states of the valence bond basis for the four-site spin-1 chain which includes nonphysical and physical states. (For this case, we have only three physical states listed in section 2.1.3)

Using the identities proven in Eq. (3.16), we find the eigenvalue for the annihilation operator:

$$\chi_{\mathbf{k}} |\Psi_c\rangle = \chi_{\mathbf{k}} \Big(1 + \sum_{\mathbf{q}} h_{\mathbf{q}} \chi^{\dagger}_{\mathbf{q}} + \frac{1}{2!} \sum_{\mathbf{q}_1} \sum_{\mathbf{q}_2} h_{\mathbf{q}_1} h_{\mathbf{q}_2} \chi^{\dagger}_{\mathbf{q}_1} \chi^{\dagger}_{\mathbf{q}_2} + \ldots \Big) |\text{vac}\rangle \,. \tag{3.31}$$

We take $\chi_{\mathbf{k}}$ acting on each term of the coherent state. The first term is zero when the annihilation operator acts on the vacuum state. The next ones are:

$$\begin{aligned}
\text{(Second term)} \qquad \chi_{\mathbf{k}} \sum_{\mathbf{q}} h_{\mathbf{q}} \chi^{\dagger}_{\mathbf{q}} &= \sum_{\mathbf{q}} \left[\delta_{\mathbf{q},\mathbf{k}} h_{\mathbf{q}} + \frac{1}{2} h_{\mathbf{q}} \delta_{\mathbf{q},\mathbf{k}} (T_{\mathbf{q},\mathbf{k}} + T_{-\mathbf{q},-\mathbf{k}}) \right] \\
&= h_{\mathbf{k}} + \frac{1}{2} h_{\mathbf{k}} (T_{\mathbf{k},\mathbf{k}} + T_{-\mathbf{k},-\mathbf{k}}), \qquad (3.32) \\
\text{(Third term)} \quad \chi_{\mathbf{k}} \sum_{\mathbf{q}_1,\mathbf{q}_2} h_{\mathbf{q}_1} h_{\mathbf{q}_2} \chi^{\dagger}_{\mathbf{q}_1} \chi^{\dagger}_{\mathbf{q}_2} &= 2 h_{\mathbf{k}} \sum_{\mathbf{q}} h_{\mathbf{q}} \chi^{\dagger}_{\mathbf{q}} \\
&\quad + \frac{1}{2} \sum_{\mathbf{q}_1,\mathbf{q}_2} h_{\mathbf{q}_1} h_{\mathbf{q}_2} \delta_{\mathbf{k},\mathbf{q}_1} \left(T_{\mathbf{q}_1,\mathbf{k}} + T_{-\mathbf{q}_1,-\mathbf{k}} \right) \chi^{\dagger}_{\mathbf{q}_2}, \\
&= 2 h_{\mathbf{k}} \sum_{\mathbf{q}} h_{\mathbf{q}} \chi^{\dagger}_{\mathbf{q}} + h^2_{\mathbf{k}} \chi^{\dagger}_{\mathbf{k}}. \qquad (3.33)
\end{aligned}$$

Here, I use some identities in Eq. (3.33) when the transition operator $T_{\mathbf{q}_1,\mathbf{k}}$ and $T_{-\mathbf{q}_1,-\mathbf{k}}$ act on the singlet creation operator. For the bipartite lattice, we remove all negative terms which are generated

by our action.

$$\begin{aligned}\sum_{\mathbf{q}_1,\mathbf{q}_2} h_{\mathbf{q}_1} h_{\mathbf{q}_2} \delta_{\mathbf{k},\mathbf{q}_1} T_{\mathbf{q}_1,\mathbf{k}} \chi^\dagger_{\mathbf{q}_2} &= \sum_{\mathbf{q}_1,\mathbf{q}_2} h_{\mathbf{q}_1} h_{\mathbf{q}_2} \delta_{\mathbf{k},\mathbf{q}_1} \frac{1}{2S\sqrt{2}} \Big[\delta_{\mathbf{k},\mathbf{q}_2} (a^\dagger_{\mathbf{q}_1} b^\dagger_{-\mathbf{q}_2} - b^\dagger_{\mathbf{q}_1} a^\dagger_{-\mathbf{q}_2}) \\ &\qquad - \delta_{\mathbf{k},-\mathbf{q}_2} (a^\dagger_{\mathbf{q}_1} b^\dagger_{\mathbf{q}_2} - b^\dagger_{\mathbf{q}_1} a^\dagger_{-\mathbf{q}_2}) \Big] \\ &= h^2_{\mathbf{k}} \chi^\dagger_{\mathbf{k}} - h_{\mathbf{k}} h_{-\mathbf{k}} \chi^\dagger_{\mathbf{k}}.\end{aligned} \tag{3.34}$$

$$\begin{aligned}\sum_{\mathbf{q}_1,\mathbf{q}_2} h_{\mathbf{q}_1} h_{\mathbf{q}_2} \delta_{\mathbf{q}_1,\mathbf{k}} T_{-\mathbf{q}_1,-\mathbf{k}} \chi^\dagger_{\mathbf{q}_2} &= \sum_{\mathbf{q}_1,\mathbf{q}_2} h_{\mathbf{q}_1} h_{\mathbf{q}_2} \delta_{\mathbf{q}_1,\mathbf{k}} \frac{1}{2S\sqrt{2}} \Big[\delta_{-\mathbf{k},\mathbf{q}_2} (a^\dagger_{-\mathbf{q}_1} b^\dagger_{-\mathbf{q}_2} - b^\dagger_{-\mathbf{q}_1} a^\dagger_{-\mathbf{q}_2}) \\ &\qquad - \delta_{-\mathbf{k},-\mathbf{q}_2} (a^\dagger_{-\mathbf{q}_1} b^\dagger_{\mathbf{q}_2} - b^\dagger_{-\mathbf{q}_1} a^\dagger_{-\mathbf{q}_2}) \Big] \\ &= - h_{\mathbf{k}} h_{-\mathbf{k}} \chi^\dagger_{\mathbf{k}} + h^2_{\mathbf{k}} \chi^\dagger_{\mathbf{k}}.\end{aligned} \tag{3.35}$$

Similarly,

$$\begin{aligned}\chi_{\mathbf{k}} \sum_{\mathbf{q}_1,\mathbf{q}_2,\mathbf{q}_3} h_{\mathbf{q}_1} h_{\mathbf{q}_2} h_{\mathbf{q}_3} \chi^\dagger_{\mathbf{q}_1} \chi^\dagger_{\mathbf{q}_2} \chi^\dagger_{\mathbf{q}_3} &= 3 h_{\mathbf{k}} \sum_{\mathbf{q}_1,\mathbf{q}_2} h_{\mathbf{q}_1} h_{\mathbf{q}_2} \chi^\dagger_{\mathbf{q}_1} \chi^\dagger_{\mathbf{q}_2} \\ &\qquad + 3 h^2_{\mathbf{k}} \chi^\dagger_{\mathbf{k}} \sum_{\mathbf{q}} h_{\mathbf{q}} \chi^\dagger_{\mathbf{q}}.\end{aligned} \tag{3.36}$$

Finally, we obtain

$$\begin{aligned}\chi_{\mathbf{k}} |\Psi_c\rangle = h_{\mathbf{k}} \Big(1 + \sum_{\mathbf{q}} h_{\mathbf{q}} \chi^\dagger_{\mathbf{q}} + \frac{1}{2!} \sum_{\mathbf{q}_1} \sum_{\mathbf{q}_2} h_{\mathbf{q}_1} h_{\mathbf{q}_2} \chi^\dagger_{\mathbf{q}_1} \chi^\dagger_{\mathbf{q}_2} + \ldots \Big) |\text{vac}\rangle \\ + \frac{1}{2} h^2_{\mathbf{k}} \chi^\dagger_{\mathbf{k}} \big(1 + \sum_{\mathbf{q}} h_{\mathbf{q}} \chi^\dagger_{\mathbf{q}} + \frac{1}{2!} \sum_{\mathbf{q}_1} \sum_{\mathbf{q}_2} h_{\mathbf{q}_1} h_{\mathbf{q}_2} \chi^\dagger_{\mathbf{q}_1} \chi^\dagger_{\mathbf{q}_2} + \ldots \big) |\text{vac}\rangle\end{aligned} \tag{3.37}$$

If the sum of $\mathbf{q}$ in the mean field state goes to *infinity* or the thermodynamic limit, the eigenvalue-like of the $\chi_{\mathbf{k}}$ acts on $|\Psi_c\rangle$ is $h_{\mathbf{k}}(1 + \frac{1}{2}h_{\mathbf{k}}\chi^{\dagger}_{\mathbf{k}})$. We can summarize the properties of the coherent state as:

$$\chi_{\mathbf{k}} |\Psi_c\rangle = h_{\mathbf{k}}\left(1 + \frac{1}{2}h_{\mathbf{k}}\chi^{\dagger}_{\mathbf{k}}\right)|\Psi_c\rangle, \tag{3.38}$$

$$\langle\Psi_c| \chi^{\dagger}_{\mathbf{k}} = \langle\Psi_c| h^{*}_{\mathbf{k}}\left(1 + \frac{1}{2}h^{*}_{\mathbf{k}}\chi_{\mathbf{k}}\right), \tag{3.39}$$

$$T_{\mathbf{k},\mathbf{k}} |\Psi_c\rangle = h_{\mathbf{k}}\chi^{\dagger}_{\mathbf{k}} |\Psi_c\rangle, \tag{3.40}$$

$$\langle\Psi_c| T^{\dagger}_{\mathbf{k},\mathbf{k}} = \langle\Psi_c| h^{*}_{\mathbf{k}}\chi_{\mathbf{k}}. \tag{3.41}$$

These formulas are similar to finding the eigenvalue of the bosonic or fermionic annihilation operator on the coherent state ($a_\alpha |\phi_c\rangle = \phi_\alpha |\phi_c\rangle$ in Chapter 2 of *Quantum Many-Particle Systems* [68]). However, there are still operators in the eigenequations. The strategy is then applied to evaluate an operator by nonorthogonal states:

$$\frac{\langle\alpha_1 ... \alpha_N|\hat{U}|\beta_1 ... \beta_N\rangle}{\langle\alpha_1 ... \alpha_N|\beta_1 ... \beta_N\rangle} = \sum_{i=1}^{N} \frac{\langle\alpha_i| \hat{U} |\beta_i\rangle}{\langle\alpha_i|\beta_i\rangle}. \tag{3.42}$$

The one-body operator $\hat{U}$ is entirely determined by its matrix elements $\langle\alpha| \hat{U} |\beta\rangle$ in the single-particle Hilbert space $\mathscr{H}$.

Now we are able to evaluate the creation and annihilation operators for the valence bond and the transition operator. This is because the coherent state is also nonorthogonal.

$$\langle\Psi_c| \chi_{\mathbf{k}} |\Psi_c\rangle = \frac{h_{\mathbf{k}}}{1 - \frac{1}{2}|h_{\mathbf{k}}|^2} \langle\Psi_c|\Psi_c\rangle, \tag{3.43}$$

$$\langle\Psi_c| \chi^{\dagger}_{\mathbf{k}} |\Psi_c\rangle = \frac{h^{*}_{\mathbf{k}}}{1 - \frac{1}{2}|h_{\mathbf{k}}|^2} \langle\Psi_c|\Psi_c\rangle, \tag{3.44}$$

$$\langle\Psi_c| N_{\mathbf{k},\mathbf{k}} |\Psi_c\rangle = \frac{|h_{\mathbf{k}}|^2}{1 - \frac{1}{2}|h_{\mathbf{k}}|^2} \langle\Psi_c|\Psi_c\rangle. \tag{3.45}$$

These are the central results which we have found. We go further and use a similar approach to find

the exact eigenvalues of the operators by sandwiching them with the ket and bra of a coherent state. We calculate the product of the creation and annihilation operators [Eq. (3.27)] by acting them on bra and ket states.

$$\begin{aligned}\langle\Psi_c|\,\chi_{\mathbf{k}}^{\dagger}\chi_{\mathbf{k+Q}}\,|\Psi_c\rangle &= \langle\Psi_c|\,h_{\mathbf{k}}^{*}h_{\mathbf{k+Q}}\big(1+\frac{1}{2}h_{\mathbf{k}}^{*}\chi_{\mathbf{k}}\big)\big(1+\frac{1}{2}h_{\mathbf{k+Q}}\chi_{\mathbf{k+Q}}\big)\,|\Psi_c\rangle \\ &= h_{\mathbf{k}}^{*}h_{\mathbf{k+Q}}\,\langle\Psi_c|\left(1+\frac{1}{2}h_{\mathbf{k}}^{*}\chi_{\mathbf{k}}+\frac{1}{2}h_{\mathbf{k+Q}}\chi_{\mathbf{k+Q}}^{\dagger}\right)|\Psi_c\rangle \\ &\quad+\frac{1}{4}(h_{\mathbf{k}}^{*})^2h_{\mathbf{k+Q}}^{2}\,\langle\Psi_c|\,\chi_{\mathbf{k}}\chi_{\mathbf{k+Q}}^{\dagger}\,|\Psi_c\rangle\,.\end{aligned} \tag{3.46}$$

We pull all the amplitude probability and its conjugate functions out of the sandwiching process, and define the probability function $A_{\mathbf{k}} = |h_{\mathbf{k}}|^2$.

$$\begin{aligned}\langle\Psi_c|\,\chi_{\mathbf{k}}^{\dagger}\chi_{\mathbf{k+Q}}\,|\Psi_c\rangle = h_{\mathbf{k}}^{*}h_{\mathbf{k+Q}}&\frac{1-\frac{1}{4}A_{\mathbf{k}}A_{\mathbf{k+Q}}}{\big(1-\frac{1}{2}A_{\mathbf{k}}\big)\big(1-\frac{1}{2}A_{\mathbf{k+Q}}\big)}\,\langle\Psi_c|\Psi_c\rangle \\ &+\frac{1}{4}h_{\mathbf{k}}^{*}h_{\mathbf{k+Q}}A_{\mathbf{k}}A_{\mathbf{k+Q}}\frac{1-\frac{1}{4}A_{\mathbf{k}}A_{\mathbf{k+Q}}}{\big(1-\frac{1}{2}\omega_{\mathbf{k}}\big)\big(1-\frac{1}{2}A_{\mathbf{k+Q}}\big)}\,\langle\Psi_c|\Psi_c\rangle \\ &+\frac{1}{4}\delta_{\mathbf{Q},\mathbf{0}}(h_{\mathbf{k}}^{*})^2h_{\mathbf{k+Q}}^{2}\Big(\,\langle\Psi_c|\Psi_c\rangle+\langle\Psi_c|\,T_{\mathbf{k+Q},\mathbf{k}}\,|\Psi_c\rangle\,\Big) \\ &+\frac{1}{16}\delta_{\mathbf{Q},\mathbf{0}}A_{\mathbf{k}}^{2}A_{\mathbf{k+Q}}^{2}\Big(\,\langle\Psi_c|\Psi_c\rangle+\langle\Psi_c|\,T_{\mathbf{k+Q},\mathbf{k}}\,|\Psi_c\rangle\,\Big) \\ &+\frac{1}{16}A_{\mathbf{k}}^{2}A_{\mathbf{k+Q}}^{2}\,\langle\Psi_c|\,\chi_{\mathbf{k}}^{\dagger}\chi_{\mathbf{k+Q}}\,|\Psi_c\rangle\,.\end{aligned} \tag{3.47}$$

Finally, the operator term in the Heisenberg Hamiltonian is

$$\begin{aligned}\frac{\langle\Psi_c|\hat{H}_{\mathrm{Heis}}|\Psi_c\rangle}{\langle\Psi_c|\Psi_c\rangle} &= \frac{\sum_{\mathbf{k},\mathbf{Q}}\cos(\mathbf{Q}\cdot\tau_B)\,\langle\Psi_c|\,\chi_{\mathbf{k}}^{\dagger}\chi_{\mathbf{k+Q}}\,|\Psi_c\rangle}{\langle\Psi_c|\Psi_c\rangle} \\ &= \sum_{\mathbf{k},\mathbf{Q}}\frac{h_{\mathbf{k}}^{*}h_{\mathbf{k+Q}}\cos(\mathbf{Q}\cdot\tau_B)}{\big(1-\frac{1}{2}A_{\mathbf{k}}\big)\big(1-\frac{1}{2}A_{\mathbf{k+Q}}\big)}+\sum_{\mathbf{k}}\frac{1}{4}\frac{A_{\mathbf{k}}^{2}}{\big(1-\frac{1}{2}A_{\mathbf{k}}\big)^2}.\end{aligned} \tag{3.48}$$

3.6 Finding the solution for the Heisenberg Hamiltonian

The Heisenberg Hamiltonian is in the real space for a spin-S and AFM coupling J between two nearest-neighbor spins on sites i and j:

$$\hat{H}_{\text{Heis}} = JS^2 - J\sum_{\langle ij\rangle} \chi_{ij}^{\dagger}\chi_{ij}, \tag{3.49}$$

Because $2S$ valence bonds emerge at each site in a lattice, there is the total number of them: $2NS$. Here, N is the number of the basis. this gives

$$\sum_{i\in A} N_i = 2SN, \tag{3.50}$$

and in the momentum space with $J = 1$:

$$\langle \hat{H}_{\text{Heis}}\rangle = S^2 - \frac{1}{N}\sum_{\mathbf{k}}\left[\left(\frac{1}{N}\sum_{\mathbf{Q}}\frac{h_{\mathbf{k}+\mathbf{Q}}\cos Q}{1-\frac{1}{2}A_{\mathbf{k}+\mathbf{Q}}}\right)\frac{h_{\mathbf{k}}^{*}}{1-\frac{1}{2}A_{\mathbf{k}}} + \frac{1}{4}\frac{A_{\mathbf{k}}^2}{\left(1-\frac{1}{2}A_{\mathbf{k}}\right)^2}\right]. \tag{3.51}$$

From Eq. (3.45), we set:

$$\langle N_{\mathbf{k}}\rangle = \frac{1}{\pi}\int_{-\pi/2}^{\pi/2}\frac{A_{\mathbf{k}}}{1-\frac{1}{2}A_{\mathbf{k}}} = 2S. \tag{3.52}$$

Now our task is finding the form of function $h(\mathbf{k})$ such that it satisfies Eq. (3.52) and minimizes the expectation of the Hamiltonian [Eq. (3.51)]. In general, the function $h(\mathbf{k})$ is an arbitrary complex function. Its domain is the Brillouin zone, and its range is the complex plane. However, for bipartite lattices, it is a *real, positive and even function*. We will propose some simple trial function for $h(\mathbf{k}) = a \times f(\xi\mathbf{k})$ with a normalization a and a coherent length ξ, which defines how far two spins interact with each other in real space [18].

For the 1D spin chain or square lattice, the BZs are $(-\pi/2, \pi/2)$ and $(-\pi/2, \pi/2) \times (-\pi/2, \pi/2)$, respectively. First, we will work with the 1D case. The probability amplitude contains an ordinary function such as cos, cosh or a Gaussian. In those functions, the integral in Eq. (3.52) is defined, and we adjust the set of parameters (a and ξ) such that its value is $2S$.

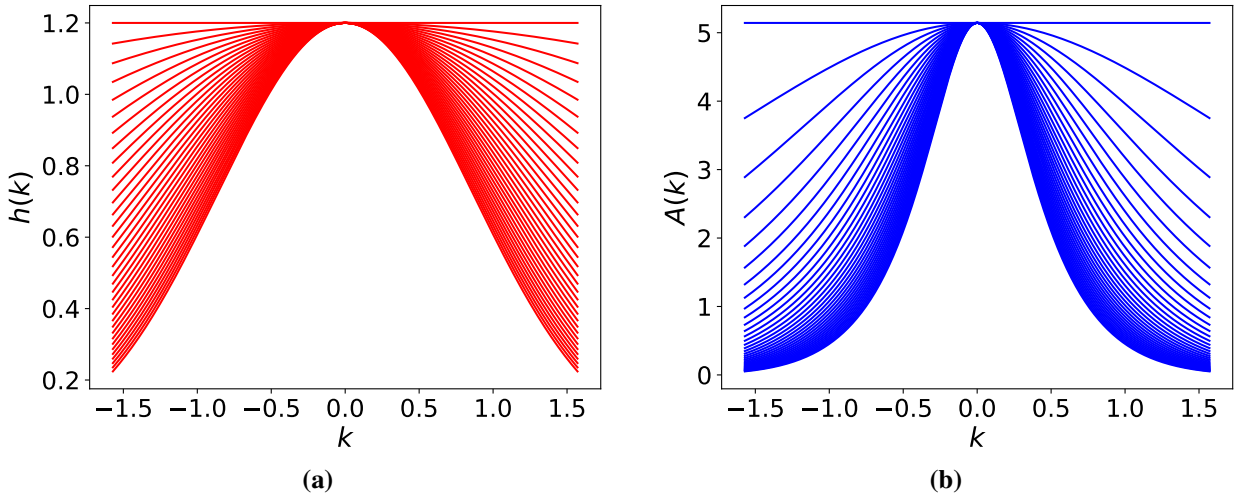

Figure 3.3: Changing parameter ξ for the (a) trial wave function $h(k) = 1.2 \times \exp\{(-\xi k^2)\}$ and corresponding (b) modulus amplitude $A(k)$. When we increase the value of $\xi = 0 \rightarrow 2$, the $h(k)$ and $A(k)$ converge.

For trial $\cos(\xi k)$ and Gaussian $e^{-\xi k^2}$ functions, our calculations behave similarly. The probability amplitude and its modulus with the Gaussian function are illustrated in Fig. 3.3. These functions have a peak at the value $k = 0$. Our results are reliable when we change the number of points N in BZ and the correlation length ξ. This is because there is no singularity in the functions as well as the function under the integral in Eq. (3.52). From the list of our results in Table 3.1, these functions work well for small values of the spin-S. The Gaussian function is a good trial for the spin-half case while the cos function is suitable for the spin-1 chain. For spin-half chain, we calculate the energy, $E_{\text{total}} = -0.4054J$, which is very close to the Bethe ansatz result ($E = -0.443J$) [2, 42] withabout 8.5% discrepancy.

For the spin-1 chain, the short-range bonds dominate. It seems that the VBS state is the ground state of the Heisenberg model, i.e. the Haldane phase. Affleck estimated the ground-state energy for the spin-1 AKLT model in a chain by the VBS state following the ground state energy $E_{\text{VBS}} = -\frac{4}{3} - 2\beta$ with $\beta = \alpha_2/\alpha_1$ in our model (Section 2.2 in Chapter 2) [70]. Our calculation for the ground-state energy is $E_{\text{total}} = -0.4276$, which is far from that estimation. Therefore, other proposed wave functions are needed for further investigation.

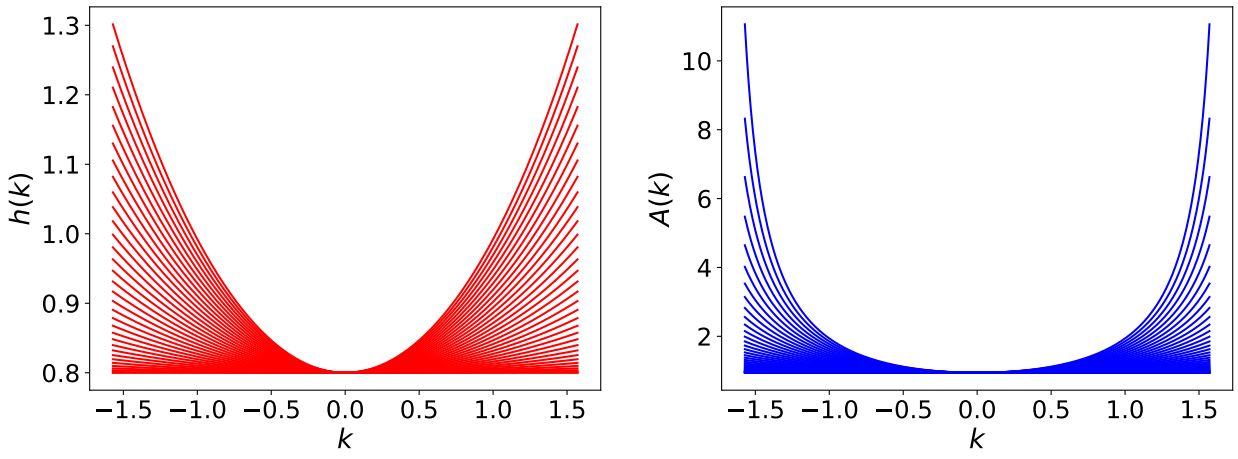

Figure 3.4: Changing parameter ξ for the (a) trial wave function $h(k) = 0.8 \times \cosh(\xi k^2)$ and corresponding (b) modulus amplitude $A(k)$. When we increase the value of $\xi = 0 \rightarrow 0.75$, the $h(k)$ and $A(k)$ converge.

Table 3.1: Summarizing a set of parameters a and ξ, and results for the calculated spin-S and the corresponding total energy in the 1D chain.

Trial function	a	ξ	S (calculated)	spin-S	E_{total}
$h(k) = a \times e^{-\xi k^2}$	1.2	0.0048	2.5019	5/2	10.3349
	1.2	0.0554	2.0026	2	5.0089
	1.2	0.1626	1.5001	3/2	2.0954
	1.2	0. 4442	1.0006	1	-0.3274
	1.2	1.836	0.5002	1/2	-0.4054
$h(k) = a \times \cos(\xi k)$	1.2	0.098	2.5017	5/2	10.325
	1.2	0.329	2.0025	2	4.8942
	1.2	0.553	1.5017	3/2	1.8383
	1.2	0.888	1.0011	1	-0.4276
$h(k) = a \times \cosh(\xi k)$	0.8	0.7415	2.4935	5/2	-40.3666
	0.8	0.7349	2.0028	2	-16.3713
	0.8	0.7155	1.5061	3/2	-5.79986
	0.8	0.65	1.0068	1	-2.51015
	0.8	0.225	0.5005	1/2	2.6454

From the momentum amplitude function, we can find the probability amplitude in real space by:

$$h(\mathbf{r}_{ij}) = \frac{1}{\pi}\int_{-\pi/2}^{\pi/2} dk e^{-i\mathbf{k}\cdot\mathbf{r}_{ij}} h(\mathbf{k}). \tag{3.53}$$

For the Gaussian function:

$$h_{\text{Gauss}}(r) = \frac{1}{\pi}\int_{-\pi/2}^{\pi/2} e^{-ikr} a e^{-\xi k^2} = \frac{a e^{-\frac{r^2}{4\xi}}}{\pi}\int_{-\pi/2}^{\pi/2} dk e^{-\left(\sqrt{\xi}k + \frac{ir}{2\sqrt{\xi}}\right)^2}. \tag{3.54}$$

for the cos function:

$$h_{\cos}(r) = \frac{a}{\pi}\int_{-\pi/2}^{\pi/2} e^{-ikr}\cos(\xi k). \tag{3.55}$$

Using an integral formula:

$$\int e^{bx}\cos(ax)dx = \frac{1}{b^2+a^2}e^{bx}[a\sin(ax) + b\cos(ax)].$$

We set an integral:

$$\begin{aligned} I &= \int_{-\pi/2}^{\pi/2} e^{-ikr}\cos(\xi k) \\ &= \frac{1}{\xi^2 + (-ir)^2} e^{-irk}\left[\xi\sin(\xi k) - ir\cos(\xi k)\right]\Big|_{-\pi/2}^{\pi/2} \\ &= \frac{2}{\xi^2 - r^2}\left[\xi\sin\left(\frac{\xi\pi}{2}\right)\cos\left(\frac{\pi r}{2}\right) - r\cos\left(\frac{\xi\pi}{2}\right)\sin\left(\frac{\pi r}{2}\right)\right]. \end{aligned} \tag{3.56}$$

The amplitude h_r for the spin-1 chain in real space is

$$h_{\cos}(r) = \frac{2a}{\pi(\xi^2 - r^2)}\left[\xi\sin\left(\frac{\xi\pi}{2}\right)\cos\left(\frac{\pi r}{2}\right) - r\cos\left(\frac{\xi\pi}{2}\right)\sin\left(\frac{\pi r}{2}\right)\right]. \tag{3.57}$$

We plot both functions in real space with the odd site number ($r = 1, 3, 5$) because we define A and B sublattices. The full spin-spin correlation function can be computed in a similar way by considering the same site interaction.

Both the trial probability amplitudes are decaying fast with respect to the distance between

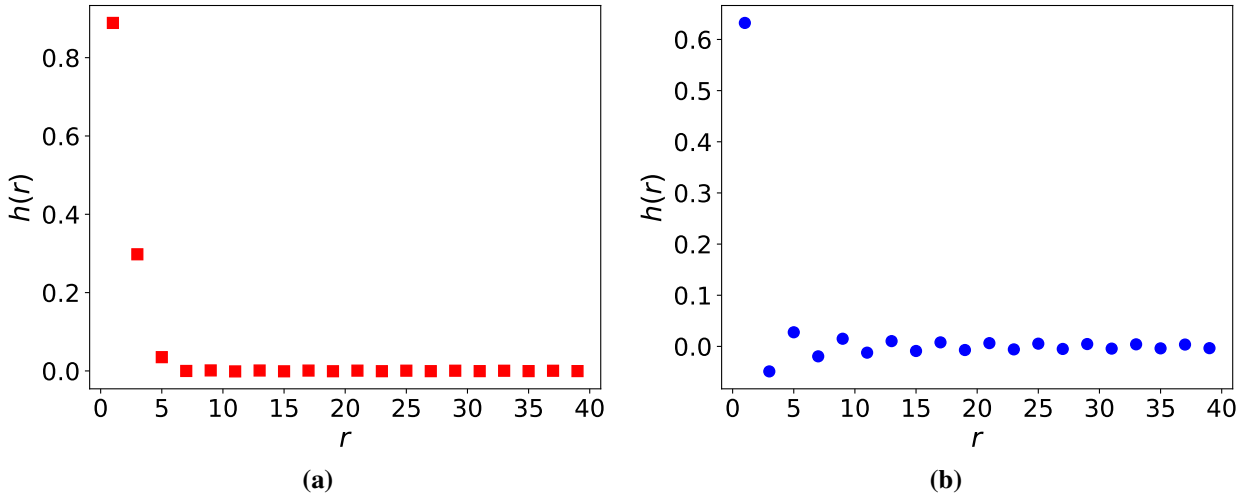

Figure 3.5: Plots of the amplitude function $h(r)$ in real space for (a) $S = 1/2$ and (b) $S = 1$ chain.

two spin sites. For the spin-half chain, the probability amplitude is like a Gaussian function with a very slow decay rate [Fig. 3.5(a)]. We compare that result with the prediction in $1D$, the amplitude of a bond connection between two sites in real space decaying with a power of $1/r^2$ by the Jastrow wave function approach and the "master's equation" [71, 72].

For the spin-1 case, the spin-spin correlation was predicted as an exponential decay [12, 46, 47]. However, our result seems to be different with the main decay rate of $1/r^2$. We need better trial wave function or different methods to rescue this issue.

CHAPTER 4

CONCLUSIONS AND SOME POSSIBLE FUTURE PLANS

4.1 Conclusions

To rsummarize, we use hard-core bosons as a bookkeeping trick to develop a mathematical language which can be used to represent a quantum spin Hamiltonian in terms of valence-bond creation and annihilation operators. We have successfully developed a formalism to express general models of spin-S objects. We have paid particular attention to models with spin-rotation-invariant, nearest-neighbor interactions that are powers of the usual bilinear Heisenberg interactions. This includes the famous AKLT model. First, we emphasize that our operator algebra is nonorthogonal and overcomplete by taking inner products of various physical states of a few-site spin-S chain. Then, we construct the family of operators that return eigenvalue 1 when they act on exactly n number of valence bonds connecting two sites. We tabulate their bond rearrangement properties and corresponding weights, which can serve as the input for quantum Monte Carlo simulations in the valence bond basis.

For the fixed-point AKLT Hamiltonian, we reaffirm by explicit calculation that the VBS state is an eigenstate. The VBS state is written as a product of short-range singlet creation operators uniformly covering the lattice. For each operation of the local Hamiltonian on a VBS state, we get back the target VBS state plus other perturbations that contain undesirable bond reconfigurations. The perturbed states may contain one or more long "bridge" valence bonds. We prove that the VBS construction is correct for single-short-bond cases—such as the spin-1 model on the linear chain, spin-3/2 on the hexagonal lattice, and spin-2 on the square lattice—but also for higher multiplicity, $2S/z > 1$. As a demonstration of the correctness and utility of our formalism, we reproduce the coefficients $\alpha_1 = 27/160$, $\alpha_2 = 29/360$ and $\alpha_3 = 1/90$ for the spin-3/2 hexagonal AKTL model

and $\alpha_1 = 1/28$, $\alpha_2 = 1/40$, $\alpha_3 = 1/180$ and $\alpha_4 = 1/2520$ for the spin-2 square-lattice model.

A coherent-state analysis is a significant tool to investigate properties of quantum systems that admit a ladder or raising/lowering operator formalism. It is typically applied to bosonic and fermionic systems, but it can also be harnessed for use with our valence-bond operators. In the bosonic case, the coherent state is widely used in quantum optics and even quantum computing, and it can be helpful in bridging the gulf between strongly quantum and semi-classical behavior. It is particularly useful in establishing the mean-field properties of a many-particle system. It can be viewed as a wavefunction Ansatz for strongly correlating systems, such as Mott insulators, superconductors, and superfluids. By representing the coherent state in term of the valence bond basis, we have evaluated the exact coherent-state expectation value of the energy for the spin-S Heisenberg model in simple bipartite lattices such as the 1D chain or square lattice. The original work for the valence bond coherent state is only built for dimension $d \geq 2$ for bipartite lattices because of the need to connect with the classical path [32]. However, we prove that this state also works in the 1D case (at least for gapped systems).

4.2 Some possible future plans

In order to promote our valence-bond language as a useful complement to the standard spin operators and to the fermionic or bosonic representations, there is still some work to do. Some possible directions:

(i) Write a program to expand the spin-S in a chain with a larger number of sites. The analytic limit is up to six sites by drawing graphs. With a larger site system, the number of configurations quickly increases.

(ii) Anotherimportant property of valence bond is the "energy gap" separating the ground state and excited states, which can be detected in real experiments by neutron diffraction or nuclear magnetic resonance. We constructed the bond relations between singlet (ground state) and triplet (excited) states. We will develop a way to simulate those properties by Monte Carlo calculations or strange correlator [11].

(iii) Detecting the properties of the "edge state" is one of the important criteria to establish the existence of topological order. The effective interaction on the edge can be different from the properties of the VBS in the bulk. For example, in the spin-1 chain, the bulk state is gapped, whereas the edge-state is degenerate and gapless [13]. In a hexagonal lattice, we can cut the VBS system along "zig-zag" or "arm-chair" paths. We predict different effective interactions which correspond to various physical properties will occur in this situation.

(iv) Based on the representation of the general AKLT Hamiltonian in terms of singlet creation and annihilation operators, we continue to approach other physical ideas about the AKLT model. For example, we intend to construct the general phase diagram of spin-3/2 hexagonal and spin-2 square lattices by a *mean-field theory* and, if possible, we will use a *projector quantum Monte Carlo* to verify the results. The latter amounts to a sampling over all the bond reconfigurations are induced by the Hamiltonian.

(v) To prove our formalism can work for any quantum spin system, we will apply our language to different frustrated cases: the spin-S in a chain or square lattice considering the next-nearest coupling [31], and the spin-half in a triangular or kagome lattice. We anticipate that the sign needs to be calculated very carefully because of the existence of bonds connecting two different sites, bonds connecting same type of sites also occur.

LIST OF REFERENCES

[1] N. W. Ashcroft and N. D. Mermin, *Solid State Physics*, 3rd ed. (Thomson Learning, 1975).

[2] J. Sólyom, *Fundamentals of the Physics of Solids*, Vol. 1 (Springer, 2007).

[3] P. Coleman, *Introduction to Many-Body Physics* (Cambridge University Press, 2015).

[4] H. L. Stormer, Nobel Lecture: The fractional quantum Hall effect, Rev. Mod. Phys. **71**, 875 (1999).

[5] H. D. Young and R. A. Freedman, *University physics with modern physics*, 13th ed. (Pearson, 2010).

[6] B. D. Cullity and C. D. Graham, *Introduction to Magnetic Materials*, 2nd ed. (John Willey and Sons, 2008).

[7] S. T. Bramwell and M. J. P. Gingras, Spin ice state in frustrated magnetic pyrochlore materials, Science **294**, 1495–1501 (2001).

[8] P. Malavi, S. Pal, D. V. S. Muthu, S. Sahoo, S. Karmakar, and A. K. Sood, Pressure-induced tuning of quantum spin liquid state in $ZnCu_3(OH)_6Cl_2$, Phys. Rev. B **101**, 214402 (2020).

[9] P. Anderson, Resonating valence bonds: A new kind of insulator?, Science **235**, 1196–1198 (1987).

[10] P. A. Lee, An End to the Drought of Quantum Spin Liquid, Science **321**, 1306 (2008).

[11] K. Wierschem and K. S. D. Beach, Detection of symmetry-protected topological order in AKLT states by exact evaluation of the strange correlator, Phys. Rev. B **93**, 245141 (2016).

[12] F. D. M. Haldane, Nobel lecture: Topological quantum matter, Rev. Mod. Phys. **89**, 045502 (2017).

[13] L. D. Carr, *Understanding quantum phase transition*, 1st ed. (Taylor and Francis Group, 2010).

[14] X.-G. Wen, Colloquium: Zoo of quantum-topological phases of matter, Rev. Mod. Phys. **89**, 041004 (2017).

[15] P. Anderson, The Resonating Valence Bond State in La_2CuO_4 and Superconductivity, Materials Research Bulletin **8**, 153–160 (1973).

[16] Y. Zhou, K. Kanoda, and T.-K. Ng, Quantum spin liquid states, Rev. Mod. Phys. **89**, 025003 (2017).

[17] M. Havilio and A. Auerbach, Superconductivity and Quantum Spin Disorder in Cuprates, Phys. Rev. Lett. **83**, 4848–4851 (1999).

[18] M. Havilio and A. Auerbach, Correlations in doped antiferromagnets, Phys. Rev. B **62**, 324–336 (2000).

[19] A. Banerjee and *at el.*, Proximate kitaev quantum spin liquid behaviour in a honeycomb magnet, Nature Materials **15**, 733–740 (2016).

[20] J. S. Helton, K. Matan, M. P. Shores, E. A. Nytko, B. M. Bartlett, Y. Yoshida, Y. Takano, A. Suslov, Y. Qiu, J.-H. Chung, D. G. Nocera, and Y. S. Lee, Spin Dynamics of the Spin-1/2 Kagome Lattice Antiferromagnet $ZnCu_3(OH)_6Cl_2$, Phys. Rev. Lett. **98**, 107204 (2007).

[21] A. Auerbach, *Interacting Electrons and Quantum Magnetism*, 1st ed. (Springer, 1994).

[22] D. P. Arovas and A. Auerbach, Functional integral theories of low-dimensional quantum Heisenberg models, Phys. Rev. B **38**, 316–332 (1988).

[23] M. Raykin and A. Auerbach, 1/N expansion and spin correlations in constrained wave functions, Phys. Rev. B **47**, 5118–5132 (1993).

[24] X. Chen, Z.-C. Gu, Z.-X. Liu, and X.-G. Wen, Symmetry protected topological orders and the group cohomogy of their symmtry group, Phys. Rev. B **87**, 155114 (2013).

[25] P. Li, H. Su, and S.-Q. Shen, Kagome antiferromagnet: A Schwinger-boson mean-field theory study, Phys. Rev. B **76**, 174406 (2007).

[26] S.-S. Zhang, E. A. Ghioldi, Y. Kamiya, L. O. Manuel, A. E. Trumper, and C. D. Batista, Large-S limit of the large-N theory for the triangular antiferromagnet, Phys. Rev. B **100**, 104431 (2019).

[27] Y. Yu and S. A. Kivelson, Phases of frustrated quantum antiferromagnets on the square and triangular lattices, Phys. Rev. B **101**, 214404 (2020).

[28] Y.-C. He, M. P. Zaletel, M. Oshikawa, and F. Pollmann, Signatures of Dirac cones in a DMRG Study of the Kagome Heisenberg Model, Phys. Rev. X **7**, 031020 (2017).

[29] C. Kittel, *Quantum Theory of Solids*, 2nd ed. (John Willey and Sons, 1986).

[30] Z.-X. Liu, Y. Zhou, and T.-K. Ng, Fermionic theory for quantum antiferromagnets with spin $S > \frac{1}{2}$, Phys. Rev. B **82**, 144422 (2010).

[31] C. Lacroix, P. Mendels, and F. Mila, *Introduction to Frustrated Magnetism*, 1st ed. (Springer, 2010).

[32] S. Liang, B.Doucot, and P. W. Anderson, Some new variational Resonating-Valence-Bond-type wave functions for the spin-1/2 antiferromagnetic Heisenberg model on a square lattice, Phys. Rev. Lett. **61**, 365 (1988).

[33] J. Hubbard, Electron correlations in narrow energy bands, Proc. Roy. Soc. A **276**, 238–257 (1963).

[34] L. Balents, Spin liquids in frustrated magnets, Nature Review Physics **464**, 10.1038/nature08917 (2010).

[35] H. Takagi, T. Takayama, G. Jackeli, G. Khaliullin, and S. E. Nagler, Concept and realization of kitaev quantum spin liquids, Nature **1**, 10.1038/s42254-019-0038-2 (2019).

[36] N. D. Mermin and H. Wagner, Absence of Ferromagnetism or Antiferromagnetism in One- or Two-Dimensional Isotropic Heisenberg Models, Phys. Rev. Lett. **17** (1966).

[37] E. Lieb and D. Mattis, Ordering energy levels of interacting spin systems, Journal of Mathematical Physics **3**, 749–751 (1962).

[38] W. Marshall, Antiferromagnetism, Proc. R. Soc. London Ser. A **232**, 48 (1955).

[39] S. Sachdev, Quantum magnetism and criticality, Nature Physics **4**, 173–185 (2008).

[40] R. Coldea, S. M. Hayden, G. Aeppli, T. G. Perring, C. D. Frost, T. E. Mason, S.-W. Cheong, and Z. Fisk, Spin Waves and Electronic Interactions in $LaCuO_4$, Phys. Rev. Lett. **86**, 5377–5380 (2001).

[41] A. Altland and B. Simons, *Condensed Matter Field Theory*, 2nd ed. (Cambrige University Press, 2010).

[42] M. J. de Oliveira, Ground-state properties of the spin-1/2 antiferromagnetic heisenberg chain obtained by use of a monte carlo method, Phys. Rev. B **48**, 6141–6143 (1993).

[43] E. Lieb, T. Schultz, and D. C. Mattis, Two Soluble Models of an Antiferromagnetic Chain, Annu. Phys. **16**, 407–466 (1961).

[44] K. Wierschem and P. Sengupta, Quenching the Haldane gap in spin-1 Heisenberg antiferromagnets, Phys. Rev. Lett. **112**, 247203 (2014).

[45] M. Greiter and S. Rachel, Valence bond solids for SU(N) spin chains: Exact models, spinon confinement and the Haldane gap, Phys. Rev. B **75**, 184441 (2007).

[46] I. Affleck, T. Kenedy, E. H.Lieb, and H. Tasaki, Valence bond ground states in isotropic quantum antiferromagnets, Commun. Math. Phys. **11**, 477–528 (1988).

[47] I. Affleck, T. Kenedy, E. H.Lieb, and H. Tasaki, Rigorous results on valence-bond ground states in antiferromagnets, Phys. Rev. Lett. **59**, 799–802 (1987).

[48] U. Schollwöck, T. Jolicoeur, and T. Garel, Onset of incommensurability at the valence-bond-solid point in the S=1 quantum spin chain, Phys. Rev. B **53**, 3304 (2007).

[49] A. Läuchli, G. Schmid, and S. Trebst, Spin nematics correlations in bilinear-biquadratic $s = 1$ spin chains, Phys. Rev. B **74**, 144426 (2006).

[50] S. Moudgalya, S. Rachel, B. A. Bernevig, and N. Regnalt, Exact excited states of nonintegrable models, Phys. Rev. B **98**, 235155 (2018).

[51] S. Yang, L. Lehman, D. Poilblanc, K. V. Acoleyen, F. Verstraete, J. I. Cirac, and N. Schuch, Edge Theories in Projected Entangled Pair State Models, Phys. Rev. Lett. **112**, 036402 (2014).

[52] N. Niggemann, A. Klümper, and J. Zittartz, Quantum phase transition in spin-3/2 systems on the hexagonal lattice – optimum ground state approach, Z. Phys. B **104**, 103–110 (1997).

[53] N. Niggemann, A. Klümper, and J. Zittartz, Ground state phase diagram of a spin-2 antiferromagnet on the square lattice, Eur. Phys. J. B **13**, 15–19 (2005).

[54] C.-Y. Huang, M. A. Wagner, and T.-C. Wei, Emergence of XY-like in deformed spin-3/2 AKLT systems, Phys. Rev. B **94**, 165130 (2016).

[55] N. Pomata, C.-Y. Huang, and T.-C. Wei, Phase transition of a two-dimensional deformed Affleck-Kennedy-Lieb-Tasaki model, Phys. Rev. B **98**, 014432 (2018).

[56] T.-C. Wei, I. Affleck, and R. Raussendorf, Affleck-Kennedy-Lieb-Tasaki state on a honeycomb lattice is a universal quantum computational resourse, Phys. Rev. Lett. **106**, 070501 (2011).

[57] D. T. Stephen, D.-S. Wang, A. Prakash, T.-C. Wei, and R. Raussendorf, Computational power of symmetry-protected topological phases, Phys. Rev. Lett. **119**, 010504 (2017).

[58] R. E. Prange and S. M. Girvin, *The Quantum Hall Effect*, 1st ed. (Springer-Verlag, 1987).

[59] J. B. Marston and I. Affleck, Large-n limit of the hubbard-heisenberg model, Phys. Rev. B **39**, 11538–11558 (1989).

[60] D. P. Arovas, A. Auerbach, and F. D. M. Haldane, Extended Heisenberg model of antiferromagnetism: analogies to the fractional quantum Hall effect, Phys. Rev. Lett. **60**, 531 (1988).

[61] J. Sólyom, *Fundamentals of the Physics of Solids*, Vol. 3 (Springer, 2010).

[62] M. A. Nielsen and I. L. Chuang, *Quantum Computation and Quantum Information*, 1st ed. (Cambridge University Press, 2010).

[63] A. W. Sandvik, Ground State Projection of Quantum Spin Systems in the Valence-Bond Basis, Phys. Rev. Lett. **95**, 207203 (2005).

[64] K. S. D. Beach and A. W. Sandvik, Some formal results for the valence bond basis, Nucl. Phys. B **750**, 142–178 (2006).

[65] J. Zang, H.-C. Jiang, Z.-Y. Weng, and S.-C. Zhang, Topological quantum phase transition in an $S = 2$ spin chain, Phys. Rev. B **81**, 224430 (2010).

[66] H.-C. Jiang, S. Rachel, Z.-Y. Weng, S.-C. Zhang, and Z. Wang, Critical theory of the topological quantum phase transition in an $S = 2$ spin chain, Phys. Rev. B **82**, 220403 (2010).

[67] W. Guo, N. Pomata, and T.-C. Wei, Nonzero spectral gap in several uniformly spin-2 and hybrid spin-1 and spin-2 AKLT models, Phys. Rev. Research **3**, 013255 (2021).

[68] J. W. Negele and H. Orland, *Quantum Many-Particle Systems*, 1st ed. (Westview, 1988).

[69] W.-M. Zhang, D. H. Feng, and R. Gilmore, Coherent states: Theory and some applications, Rev. Mod. Phys. **62**, 867–927 (1990).

[70] I. Affleck, Quantum spin chains and the haldane gap, Journal of Physics: Condensed Matter **1**, 3047–3072 (1989).

[71] F. D. M. Haldane, Exact jastrow-gutzwiller resonating-valence-bond ground state of the spin-$\frac{1}{2}$ antiferromagnetic heisenberg chain with $1/r^2$ exchange, Phys. Rev. Lett. **60**, 635–638 (1988).

[72] K. S. D. Beach, Master equation approach to computing RVB bond amplitudes, Phys. Rev. B **79**, 224431 (2009).

APPENDICES

APPENDIX A

FORMATION OF SPIN VALUE

The electron is a spin-half quantum object which points upward or downward. However, there are several systems which include the spin values $S = 1, 3/2, 2$, etc. We observe this in several systemswhich include transition and rare-earth elements. The formation of spins higher than 1/2 are defined by three Hunds' rules in solid state physics. For transition and rare-earth elements, they include d and f orbitals where several electron levels are partly filled [1].

Hund's First Rule Out of the many states one can form by placing n electrons into the $2(2\ell + 1)$ levels of the partially filled shell, those with"*lowest energy*" have the largest total spin S that is consistent with the exclusion principle. To see what that value is, one notes that the largest value S can have is equal to the largest magnitude that S_z can have. If $n \leq 2\ell + 1$, all electrons can have parallel spins without multiple occupation of any one-electron level in the shell, by assigning them levels with different values of ℓ_z. The second and third Hund rules are similar to the first one, except the apply to the angular momentum and total spin of the system.

In Table. A.1, the filling of electrons in the orbital levels maximize the number of single electrons with spin-down. In the d-shell, the value of spin-S can range from 0, 1/2, to 5/2. In the f-shell, the value of S spin can be 0, 1/2 to 7/2. From these principles, there are many compounds which will have total effective spin S larger than spin $S = 1/2$ of the electron.

Table A.1: The filling electrons in d- and f-shell elements [1].

GROUND STATES OF IONS WITH PARTIALLY FILLED *d*- OR *f*-SHELLS, AS CONSTRUCTED FROM HUND'S RULES[a]

d-shell ($l = 2$)										
n	$l_z = 2,$	$1,$	$0,$	$-1,$	-2	S	$L = \lvert\Sigma l_z\rvert$	J		SYMBOL
1	↓					1/2	2	3/2	$J = \lvert L - S\rvert$	$^2D_{3/2}$
2	↓	↓				1	3	2		$^3F_2$
3	↓	↓	↓			3/2	3	3/2		$^4F_{3/2}$
4	↓	↓	↓	↓		2	2	0		$^5D_0$
5	↓	↓	↓	↓	↓	5/2	0	5/2		$^6S_{5/2}$
6	↕	↑	↑	↑	↑	2	2	4	$J = L + S$	$^5D_4$
7	↕	↕	↑	↑	↑	3/2	3	9/2		$^4F_{9/2}$
8	↕	↕	↕	↑	↑	1	3	4		$^3F_4$
9	↕	↕	↕	↕	↑	1/2	2	5/2		$^2D_{5/2}$
10	↕	↕	↕	↕	↕	0	0	0		$^1S_0$

f-shell ($l = 3$)											
n	$l_z = 3,$	$2,$	$1,$	$0, -1, -2, -3$				S	$L = \lvert\Sigma l_z\rvert$	J	
1	↓							1/2	3	5/2	$^2F_{5/2}$
2	↓	↓						1	5	4	$^3H_4$
3	↓	↓	↓					3/2	6	9/2	$^4I_{9/2}$
4	↓	↓	↓	↓				2	6	4	$^5I_4$
5	↓	↓	↓	↓	↓			5/2	5	5/2	$^6H_{5/2}$
6	↓	↓	↓	↓	↓	↓		3	3	0	$^7F_0$
7	↓	↓	↓	↓	↓	↓	↓	7/2	0	7/2	$^8S_{7/2}$
8	↕	↑	↑	↑	↑	↑	↑	3	3	6	$^7F_6$
9	↕	↕	↑	↑	↑	↑	↑	5/2	5	15/2	$^6H_{15/2}$
10	↕	↕	↕	↑	↑	↑	↑	2	6	8	$^5I_8$
11	↕	↕	↕	↕	↑	↑	↑	3/2	6	15/2	$^4I_{15/2}$
12	↕	↕	↕	↕	↕	↑	↑	1	5	6	$^3H_6$
13	↕	↕	↕	↕	↕	↕	↑	1/2	3	7/2	$^2F_{7/2}$
14	↕	↕	↕	↕	↕	↕	↕	0	0	0	$^1S_0$

[a] ↑ = spin $\frac{1}{2}$; ↓ = spin $-\frac{1}{2}$.

Spin

APPENDIX B

FOURIER TRANSFORM OF SINGLET OPERATOR IN MOMENTUM SPACE

Derive the commutation relation We start from the commutation relation:

$$\begin{aligned}\left[\chi_{\mathbf{q}}, \chi^{\dagger}_{\mathbf{q}'}\right] &= \frac{1}{8S^2}\sum_{\mu,\nu}\sum_{\alpha,\beta}\left[\left(a^{\alpha}_{\mathbf{q}}b^{\beta}_{-\mathbf{q}} - b^{\alpha}_{\mathbf{q}}a^{\beta}_{-\mathbf{q}}\right), \left(a^{\mu\dagger}_{\mathbf{q}'}b^{\nu\dagger}_{-\mathbf{q}'} - b^{\mu\dagger}_{\mathbf{q}'}a^{\nu\dagger}_{-\mathbf{q}'}\right)\right] \\ &= \frac{1}{8S^2}\sum_{\mu,\nu}\sum_{\alpha,\beta}\left\{\left[a^{\alpha}_{\mathbf{q}}b^{\beta}_{-\mathbf{q}}, a^{\mu\dagger}_{\mathbf{q}'}b^{\nu\dagger}_{-\mathbf{q}'}\right] + \left[b^{\alpha}_{\mathbf{q}}a^{\beta}_{-\mathbf{q}}, b^{\mu\dagger}_{\mathbf{q}'}a^{\nu\dagger}_{-\mathbf{q}'}\right] - \left[a^{\alpha}_{\mathbf{q}}b^{\beta}_{-\mathbf{q}}, b^{\mu\dagger}_{\mathbf{q}'}a^{\nu\dagger}_{-\mathbf{q}'}\right] - \left[b^{\alpha}_{\mathbf{q}}a^{\beta}_{-\mathbf{q}}, a^{\mu\dagger}_{\mathbf{q}'}b^{\nu\dagger}_{-\mathbf{q}'}\right]\right\}.\end{aligned} \tag{B.1}$$

Here, each term in Eq. (B.1) is derived following: First term:

$$\begin{aligned}\left[a^{\alpha}_{\mathbf{q}}b^{\beta}_{-\mathbf{q}}, a^{\mu\dagger}_{\mathbf{q}'}b^{\nu\dagger}_{-\mathbf{q}'}\right] &= a^{\alpha}_{\mathbf{q}}b^{\beta}_{-\mathbf{q}}a^{\mu\dagger}_{\mathbf{q}'}b^{\nu\dagger}_{-\mathbf{q}'} - a^{\mu\dagger}_{\mathbf{q}'}b^{\nu\dagger}_{-\mathbf{q}'}a^{\alpha}_{\mathbf{q}}b^{\beta}_{-\mathbf{q}} \\ &= \left(\delta_{\mathbf{q},\mathbf{q}'}\delta^{\alpha\mu} + a^{\mu\dagger}_{\mathbf{q}'}a^{\alpha}_{\mathbf{q}}\right)\left(\delta_{-\mathbf{q},-\mathbf{q}'}\delta^{\beta\nu} + b^{\nu\dagger}_{-\mathbf{q}'}b^{\beta}_{-\mathbf{q}}\right) - a^{\alpha}_{\mathbf{q}}b^{\beta}_{-\mathbf{q}}a^{\alpha}_{\mathbf{q}}b^{\beta}_{-\mathbf{q}} \\ &= \delta_{\mathbf{q},\mathbf{q}'}\delta_{-\mathbf{q},-\mathbf{q}'}\delta^{\alpha\mu}\delta^{\beta\nu} + \delta_{-\mathbf{q},-\mathbf{q}'}\delta^{\beta\nu}a^{\mu\dagger}_{\mathbf{q}'}a^{\alpha}_{\mathbf{q}} + \delta_{\mathbf{q},\mathbf{q}'}\delta^{\alpha\mu}b^{\nu\dagger}_{-\mathbf{q}'}b^{\beta}_{-\mathbf{q}}.\end{aligned} \tag{B.2}$$

Second term:

$$\begin{aligned}\left[b^{\alpha}_{\mathbf{q}}a^{\beta}_{-\mathbf{q}}, b^{\mu\dagger}_{\mathbf{q}'}a^{\nu\dagger}_{-\mathbf{q}'}\right] &= b^{\alpha}_{\mathbf{q}}a^{\beta}_{-\mathbf{q}}b^{\mu\dagger}_{\mathbf{q}'}a^{\nu\dagger}_{-\mathbf{q}'} - b^{\mu\dagger}_{\mathbf{q}'}a^{\nu\dagger}_{-\mathbf{q}'}b^{\alpha}_{\mathbf{q}}a^{\beta}_{-\mathbf{q}} \\ &= \left(\delta_{\mathbf{q},\mathbf{q}'}\delta^{\alpha\mu} + b^{\mu\dagger}_{\mathbf{q}'}b^{\alpha}_{\mathbf{q}}\right)\left(\delta_{-\vec{q},-\vec{q}'}\delta^{\beta\nu} + a^{\nu\dagger}_{-\mathbf{q}'}a^{\beta}_{-\mathbf{q}}\right) - b^{\alpha}_{\mathbf{q}}a^{\beta}_{-\mathbf{q}}b^{\alpha}_{\mathbf{q}}a^{\beta}_{-\mathbf{q}} \\ &= \delta_{\mathbf{q},\mathbf{q}'}\delta_{-\mathbf{q},-\mathbf{q}'}\delta^{\alpha\mu}\delta^{\beta\nu} + \delta_{-\mathbf{q},-\mathbf{q}'}\delta^{\beta\nu}b^{\mu\dagger}_{\mathbf{q}'}b^{\alpha}_{\mathbf{q}} + \delta_{\mathbf{q},\mathbf{q}'}\delta^{\alpha\mu}a^{\nu\dagger}_{-\mathbf{q}'}a^{\beta}_{-\mathbf{q}}.\end{aligned} \tag{B.3}$$

Third term:

$$\begin{aligned}\left[a^{\alpha}_{\mathbf{q}}b^{\beta}_{-\mathbf{q}}, b^{\mu\dagger}_{\mathbf{q}'}a^{\nu\dagger}_{-\mathbf{q}'}\right] &= a^{\alpha}_{\mathbf{q}}b^{\beta}_{-\mathbf{q}}b^{\mu\dagger}_{\mathbf{q}'}a^{\nu\dagger}_{-\mathbf{q}'} - b^{\mu\dagger}_{\mathbf{q}'}a^{\nu\dagger}_{-\mathbf{q}'}a^{\alpha}_{\mathbf{q}}b^{\beta}_{-\mathbf{q}} \\ &= \left(\delta_{-\mathbf{q},\mathbf{q}'}\delta^{\beta\mu} + b^{\mu\dagger}_{\mathbf{q}'}b^{\beta}_{\mathbf{q}}\right)\left(\delta_{\mathbf{q},-\mathbf{q}'}\delta^{\alpha\nu} + a^{\nu\dagger}_{-\mathbf{q}'}a^{\alpha}_{-\mathbf{q}}\right) - b^{\mu\dagger}_{\mathbf{q}'}a^{\nu\dagger}_{-\mathbf{q}'}a^{\alpha}_{\mathbf{q}}b^{\beta}_{-\mathbf{q}} \\ &= \delta_{-\mathbf{q},\mathbf{q}'}\delta_{\mathbf{q},-\mathbf{q}'}\delta^{\alpha\nu}\delta^{\beta\mu} + \delta_{-\mathbf{q},\mathbf{q}'}\delta^{\beta\mu}a^{\nu\dagger}_{-\mathbf{q}'}a^{\alpha}_{\mathbf{q}} + \delta_{\mathbf{q},-\mathbf{q}'}\delta^{\alpha\nu}b^{\mu\dagger}_{\mathbf{q}'}b^{\beta}_{-\mathbf{q}}.\end{aligned} \tag{B.4}$$

Fourth term:

$$\begin{aligned}\left[b^{\alpha}_{\mathbf{q}}a^{\beta}_{-\mathbf{q}}, a^{\mu\dagger}_{\mathbf{q}'}b^{\nu\dagger}_{-\mathbf{q}'}\right] &= b^{\alpha}_{\mathbf{q}}a^{\beta}_{-\mathbf{q}}a^{\mu\dagger}_{\mathbf{q}'}b^{\nu\dagger}_{-\mathbf{q}'} - a^{\mu\dagger}_{\mathbf{q}'}b^{\nu\dagger}_{-\mathbf{q}'}b^{\alpha}_{\mathbf{q}}a^{\beta}_{-\mathbf{q}} \\ &= \left(\delta_{-\mathbf{q},\mathbf{q}'}\delta^{\beta\mu} + a^{\mu\dagger}_{\mathbf{q}'}b^{\beta}_{\mathbf{q}}\right)\left(\delta_{\mathbf{q},-\mathbf{q}'}\delta^{\alpha\nu} + b^{\nu\dagger}_{-\mathbf{q}'}b^{\alpha}_{-\mathbf{q}}\right) - a^{\mu\dagger}_{\mathbf{q}'}b^{\nu\dagger}_{-\mathbf{q}'}b^{\alpha}_{\mathbf{q}}a^{\beta}_{-\mathbf{q}} \\ &= \delta_{-\mathbf{q},\mathbf{q}'}\delta_{\mathbf{q},-\mathbf{q}'}\delta^{\alpha\nu}\delta^{\beta\mu} + \delta_{-\mathbf{q},\mathbf{q}'}\delta^{\beta\mu}b^{\nu\dagger}_{-\mathbf{q}'}b^{\alpha}_{\mathbf{q}} + \delta_{\mathbf{q},-\mathbf{q}'}\delta^{\alpha\nu}a^{\mu\dagger}_{\mathbf{q}'}a^{\beta}_{-\mathbf{q}}.\end{aligned} \tag{B.5}$$

$$\begin{aligned}\left[\chi_{\mathbf{q}}, \chi^{\dagger}_{\mathbf{q}'}\right] &= \frac{1}{8S^2}\sum_{\mu,\nu}\sum_{\alpha,\beta}\Bigg\{2\delta_{\mathbf{q},\mathbf{q}'}\delta^{\alpha\mu}\delta^{\beta\nu} + \delta_{\mathbf{q},\mathbf{q}'}\Big[\delta^{\alpha\mu}\left(a^{\nu\dagger}_{-\mathbf{q}'}a^{\beta}_{-\mathbf{q}} + b^{\nu\dagger}_{-\mathbf{q}'}b^{\beta}_{-\mathbf{q}}\right) + \delta^{\beta\nu}\left(a^{\mu\dagger}_{\mathbf{q}'}a^{\alpha}_{\mathbf{q}} + b^{\mu\dagger}_{\mathbf{q}'}b^{\alpha}_{\mathbf{q}}\right)\Big] \\ &\quad - 2\delta_{\mathbf{q},-\mathbf{q}'}\delta^{\beta\mu}\delta^{\alpha\nu} - \delta_{\mathbf{q},-\mathbf{q}'}\Big[\delta^{\beta\mu}\left(a^{\nu\dagger}_{-\mathbf{q}'}a^{\alpha}_{\mathbf{q}} + b^{\nu\dagger}_{-\mathbf{q}'}b^{\alpha}_{\mathbf{q}}\right) + \delta^{\alpha\nu}\left(a^{\mu\dagger}_{\mathbf{q}'}a^{\beta}_{-\mathbf{q}} + b^{\mu\dagger}_{\mathbf{q}'}b^{\beta}_{-\mathbf{q}}\right)\Big]\Bigg\} \\ &= \left(\delta_{\mathbf{q},\mathbf{q}'} - \delta_{\mathbf{q},-\mathbf{q}'}\right) + \frac{1}{4S}\Bigg\{\delta_{\mathbf{q},\mathbf{q}'}\Big[\sum_{\nu,\beta}\left(a^{\nu\dagger}_{-\mathbf{q}}a^{\beta}_{-\mathbf{q}'} + b^{\nu\dagger}_{-\mathbf{q}}b^{\beta}_{-\mathbf{q}'}\right) + \sum_{\mu,\alpha}\left(a^{\mu\dagger}_{\mathbf{q}'}a^{\alpha}_{\mathbf{q}} + b^{\mu\dagger}_{\mathbf{q}'}b^{\alpha}_{\mathbf{q}}\right)\Big] \\ &\quad - \delta_{\mathbf{q},-\mathbf{q}'}\Big[\sum_{\nu,\alpha}\left(a^{\nu\dagger}_{-\mathbf{q}'}a^{\alpha}_{\mathbf{q}} + b^{\nu\dagger}_{-\mathbf{q}'}b^{\alpha}_{\mathbf{q}}\right) + \sum_{\mu,\beta}\left(a^{\mu\dagger}_{\mathbf{q}'}a^{\beta}_{-\mathbf{q}} + b^{\mu\dagger}_{\mathbf{q}'}b^{\beta}_{-\mathbf{q}}\right)\Big]\Bigg\}\end{aligned} \tag{B.6}$$

$$\left[\chi_{\mathbf{q}}, \chi^{\dagger}_{\mathbf{q}'}\right] = \left(\delta_{\mathbf{q},\mathbf{q}'} - \delta_{\mathbf{q},-\mathbf{q}'}\right) + \frac{1}{2}\Big[\delta_{\mathbf{q},\mathbf{q}'}(T_{\mathbf{q}',\mathbf{q}} + T_{-\mathbf{q}',-\mathbf{q}}) - \delta_{\mathbf{q},-\mathbf{q}'}(T_{\mathbf{q}',-\mathbf{q}} + T_{-\mathbf{q}',\mathbf{q}})\Big]. \tag{B.7}$$

The Fourier transforms of the biquadratic term using the same equations for the Heisenberg term:

$$\hat{H}_{\text{biq}} = B(\alpha_1,\alpha_2)\sum_i\left[(\bar{\chi}^{\dagger}_{i,1})^2(\bar{\chi}_{i,1})^2 + (\bar{\chi}^{\dagger}_{i,2})^2(\bar{\chi}_{i,2})^2\right] \tag{B.8}$$

$$= \frac{B(\alpha_1,\alpha_2)}{N^4}\Big[\sum_{\mathbf{q}_1,\mathbf{q}_2,\mathbf{q}_3,\mathbf{q}_4}\bar{\chi}^{\dagger}_{\mathbf{q}_1}\bar{\chi}^{\dagger}_{\mathbf{q}_2}\bar{\chi}_{\mathbf{q}_3}\bar{\chi}_{\mathbf{q}_4}\sum_i e^{i\mathbf{r}_i\cdot(\mathbf{q}_1+\mathbf{q}_2-\mathbf{q}_3-\mathbf{q}_4)} \tag{B.9}$$

$$+ \sum_{\mathbf{q}'_1,\mathbf{q}'_2,\mathbf{q}'_3,\mathbf{q}'_4}\bar{\chi}^{\dagger}_{\mathbf{q}'_1}\bar{\chi}^{\dagger}_{\mathbf{q}'_2}\bar{\chi}_{\mathbf{q}'_3}\bar{\chi}_{\mathbf{q}'_4}\sum_i e^{i\mathbf{r}_i\cdot(\mathbf{q}'_1+\mathbf{q}'_2-\mathbf{q}'_3-\mathbf{q}'_4)}\Big] \tag{B.10}$$

$$= \frac{B(\alpha_1,\alpha_2)}{N^3}\Big[\sum_{\mathbf{q}_1,\mathbf{q}_2,\mathbf{q}_3,\mathbf{q}_4}\bar{\chi}^{\dagger}_{\mathbf{q}_1}\bar{\chi}^{\dagger}_{\mathbf{q}_2}\bar{\chi}_{\mathbf{q}_3}\bar{\chi}_{\mathbf{q}_4}\delta(\mathbf{q}_1+\mathbf{q}_2-\mathbf{q}_3-\mathbf{q}_4) \tag{B.11}$$

$$+ \sum_{\mathbf{q}'_1,\mathbf{q}'_2,\mathbf{q}'_3,\mathbf{q}'_4}\bar{\chi}^{\dagger}_{\mathbf{q}'_1}\bar{\chi}^{\dagger}_{\mathbf{q}'_2}\bar{\chi}_{\mathbf{q}'_3}\bar{\chi}_{\mathbf{q}'_4}\delta(\mathbf{q}'_1+\mathbf{q}'_2-\mathbf{q}'_3-\mathbf{q}'_4)\Big]. \tag{B.12}$$

$$\hat{H}_{\mathrm{bi}} = \frac{B(\alpha_1,\alpha_2)}{N^7}\Big[\sum_{\mathbf{q}_1,\mathbf{q}_2,\mathbf{q}_3,\mathbf{q}_4} \sum_{\mathbf{k}_1,\mathbf{k}_2,\mathbf{k}_3,\mathbf{k}_4} e^{-i(\mathbf{q}_1+\mathbf{q}_2-\mathbf{q}_3-\mathbf{q}_4)\cdot\tau_{\mathrm{B}}}\delta(\mathbf{q}_1+\mathbf{q}_2-\mathbf{q}_3-\mathbf{q}_4)e^{-i(\mathbf{k}_1+\mathbf{k}_2-\mathbf{k}_3-\mathbf{k}_4)\cdot\tau_{\mathrm{B}}}$$
$$\chi^\dagger_{\mathbf{k}_1}\chi^\dagger_{\mathbf{k}_2}\chi_{\mathbf{k}_3}\chi_{\mathbf{k}_4} + \sum_{\mathbf{q}'_1,\mathbf{q}'_2,\mathbf{q}'_3,\mathbf{q}'_4} \sum_{\mathbf{k}'_1,\mathbf{k}'_2,\mathbf{k}'_3,\mathbf{k}'_4} e^{-i(\mathbf{q}'_1+\mathbf{q}'_2-\mathbf{q}'_3-\mathbf{q}'_4)\cdot\tau_{\mathrm{B}}}\delta(\mathbf{q}'_1+\mathbf{q}'_2-\mathbf{q}'_3-\mathbf{q}'_4)e^{i(\mathbf{k}'_1+\mathbf{k}'_2-\mathbf{k}'_3-\mathbf{k}'_4)\cdot\tau_{\mathrm{B}}}$$
$$\chi^\dagger_{\mathbf{k}'_1}\chi^\dagger_{\mathbf{k}'_2}\chi_{\mathbf{k}'_3}\chi_{\mathbf{k}'_4}\Big]$$
$$= \frac{B(\alpha_1,\alpha_2)}{N^4}\Big[\sum_{\mathbf{k}_1,\mathbf{k}_2,\mathbf{k}_3,\mathbf{k}_4} \chi^\dagger_{\mathbf{k}_1}\chi^\dagger_{\mathbf{k}_2}\chi_{\mathbf{k}_3}\chi_{\mathbf{k}_4}e^{-i(\mathbf{k}_1+\mathbf{k}_2-\mathbf{k}_3-\mathbf{k}_4)\cdot\tau_{\mathrm{B}}} + \sum_{\mathbf{k}'_1,\mathbf{k}'_2,\mathbf{k}'_3,\mathbf{k}'_4} \chi^\dagger_{\mathbf{k}'_1}\chi^\dagger_{\mathbf{k}'_2}\chi_{\mathbf{k}'_3}\chi_{\mathbf{k}'_4}e^{i(\mathbf{k}'_1+\mathbf{k}'_2-\mathbf{k}'_3-\mathbf{k}'_4)\cdot\tau_{\mathrm{B}}}\Big]. \tag{B.13}$$

So, the biquadratic Hamiltonian with $\mathbf{Q}_1 = \mathbf{k}_1 - \mathbf{k}_3$ and $\mathbf{Q}_2 = \mathbf{k}_2 - \mathbf{k}_4$ is:

$$\hat{H}_{\mathrm{bi}} = \frac{2B(\alpha_1,\alpha_2)}{N^4}\cos\left[(\mathbf{Q}_1+\mathbf{Q}_2)\cdot\tau_{\mathrm{B}}\right]\chi^\dagger_{\mathbf{k}_1}\chi^\dagger_{\mathbf{k}_2}\chi_{\mathbf{k}_1+\mathbf{Q}_1}\chi_{\mathbf{k}_2+\mathbf{Q}_2}. \tag{B.14}$$

Now, we obtain the Fourier representation of the spin-1 AKLT Hamiltonian with the combination of Eq. (3.27) and Eq. (B.14):

$$\hat{H} = \frac{2A(\alpha_1,\alpha_2)}{N^2}\sum_{\mathbf{k},\mathbf{Q}}\cos(\mathbf{Q}\cdot\tau_{\mathrm{B}})\chi^\dagger_{\mathbf{k}}\chi_{\mathbf{k}+\mathbf{Q}}$$
$$+ \frac{2B(\alpha_1,\alpha_2)}{N^4}\sum_{\mathbf{k}_1,\mathbf{k}_2,\mathbf{Q}_1,\mathbf{Q}_2}\cos\left[(\mathbf{Q}_1+\mathbf{Q}_2)\cdot\tau_{\mathrm{B}}\right]\chi^\dagger_{\mathbf{k}_1}\chi^\dagger_{\mathbf{k}_2}\chi_{\mathbf{k}_1+\mathbf{Q}_1}\chi_{\mathbf{k}_2+\mathbf{Q}_2}. \tag{B.15}$$

VITA

HUU T. DO

Education

University of Mississippi, Oxford, MS, USA.

- **Ph.D.** in Physics, Department of Physics and Astronomy, August, 2021.
- **M.S.** in Physics, Department of Physics and Astronomy, 2017.

Hanoi University of Science and Technology, Hanoi, Vietnam. 2013.

- **B.S.** in Materials Science and Engineering.

Academic Employment

Teaching Assistant 2016 – 2020

The University of Mississippi, Oxford, MS, USA

Research Assistant 2009 – 2014

Institute of Materials Science, Vietnam Academy of Science and Technology, Hanoi, Vietnam

Published articles

3. **Huu T. Do**, Khagendra Adhikari, and K. S. D. Beach, "*Effective interactions between local hopping modulations on the square lattice*", arXiv:1904.03220 (Revised at PRB).

2. **Huu T. Do**, Nguyen Hai yen, Pham Thi Thanh, Nguyen Thi Mai, Tran Dang Thanh, The-Long Phan, Seong Cho Yu and Nguyen Huy Dan,, "*Magnetic, magnetocaloric and critical properties of* $Ni_{50-x}Cu_xMn_{37}Sn_{13}$ *rapidly quenched ribbons* ", *J. Alloys. Comp.* **662**, 535-540, 2015.

1. Huy Dan Nguyen, **Huu T. Do**, Hai Yen Nguyen, Thi Thanh Pham, Huu Duc Nguyen, Thi Nguyet Nga Nguyen, Dang Thanh Tran, "*Influence of fabrication conditions on giant magnetocaloric effect on Ni-Mn-Sn ribbons*", *Adv. Nat. Sci. :Nanosci. Nanotechnol.* **4**, 025011, 2013.

Selected Conference Presentations

3. **Huu T. Do** and Kevin SD Beach, *"Effective interactions between local hoping modulations on the square lattices"*, APS March Meeting 2018, Los Angeles, California, USA, March 5-9.

2. Huy Dan Nguyen, **Huu T. Do**, Hai Yen Nguyen, Thi Thanh Pham and Dang Thanh Tran, *"Magnetocaloric effect and critical behavior in Fe-Gd-Zr melt-spun ribbons"*, The 7th International Workshop on Advanced Materials Science and Nanotechnology (IWAMSN2014) - Halong, Vietnam, Nov. 2-6, 2014)

1. N. H. Dan, **Huu T. Do**, Hai Yen Nguyen, Thi Thanh Pham, Huu Duc Nguyen, Thi Nguyet Nga Nguyen, Dang Thanh Tran, The Long Phan and Seong Cho Yu, *"Influence of fabrication conditions on giant magnetocaloric effect of Ni-Mn-Sn ribbons"*, The 6th International Workshop on Advanced Materials Science and Nanotechnology (IWAMSN2012) - Halong, Vietnam (Oct. 30 - Nov. 2, 2012)